NON-INVASIVE DIAGNOSIS OF OSTEOARTHRITIS USING VIBROARTHROGRAPHY APPROACH

FARSHAD GOLSHAN

FACULTY OF ENGINEREENG
UNIVERSITY OF MALAYA
KUALA LUMPUR

2018

NON-INVASIVE DIAGNOSIS OF OSTEOARTHRITIS USING VIBROARTHROGRAPHY APPROACH

FARSHAD GOLSHAN

DISSERTATION SUBMITTED IN FULFILMENT OF THE REQUIREMENTS FOR THE DEGREE OF MASTER OF ENGINEREEING

DEPARTMENT OF BIOMEDICAL ENGINEERING
FACULTY OF ENGINEERING
UNIVERSITY OF MALAYA
KUALA LUMPUR

2018

UNIVERSITY OF MALAYA

ORIGINAL LITERARY WORK DECLARATION

Name of Candidate: Farshad Golshan

Matric No: KGA150100

Name of Degree: Master of Engineering

Title of Project Paper/Research Report/Dissertation/Thesis ("this Work"):

NON-INVASIVE DIAGNOSIS OF OSTEOARTHRITIS USING VIBROARTHROGRAPHY APPROACH

Field of Study: Biomedical Engineering

I do solemnly and sincerely declare that:

(1) I am the sole author/writer of this Work;
(2) This Work is original;
(3) Any use of any work in which copyright exists was done by way of fair dealing and for permitted purposes and any excerpt or extract from, or reference to or reproduction of any copyright work has been disclosed expressly and sufficiently and the title of the Work and its authorship have been acknowledged in this Work;
(4) I do not have any actual knowledge, nor do I ought reasonably to know that the making of this work constitutes an infringement of any copyright work;
(5) I hereby assign all and every rights in the copyright to this Work to the University of Malaya ("UM"), who henceforth shall be owner of the copyright in this Work and that any reproduction or use in any form or by any means whatsoever is prohibited without the written consent of UM having been first had and obtained;
(6) I am fully aware that if in the course of making this Work I have infringed any copyright whether intentionally or otherwise, I may be subject to legal action or any other action as may be determined by UM.

Candidate's Signature Date:

Subscribed and solemnly declared before,

Witness's Signature Date:

Name:

Designation:

ABSTRACT

Osteoarthritis (OA) is one of the most common type of disease among elderly and athletes. Although OA is widely known by doctors and researchers, the current diagnosis methods available for detection of OA are either expensive and invasive or very inconvenient for an average person. Early detection of osteoarthritis is of utmost importance due to its progressive nature. If OA is left unintended, it can lead to major issues for the patients such as joint bone deformity and infuriating joint pain. This study focuses on the development of a much more suitable method for easy and efficient early diagnosis of osteoarthritis. The previous studies done on non-invasive detection of OA have proven that use of Vibroarthrography (VAG) technique can indeed provide clear results on detecting the difference between OA and healthy knee's Vibroarthrography signals produced from vibration and acoustic emission of the knee joint while performing an action. To continue the advancement in the Field of non-invasive diagnosis of OA, current proposed researched began tasting on different types of already existing sensors (mainly piezo element, ultrasound sensor and accelerometer) for detection of vibration and acoustic emission of the knee non-invasively. The results of the sensors testing showed that the accelerometer is able to produce much better results compared to other selected sensors. To evaluate and develop a suitable testing method for detection of OA on the knee, a data logging tool was developed to remove the noise from the vibration taken from the sensor and store the data. Tests were done on healthy subjects as well as UMMC patients with the supervision of physicians. The final outcome shows satisfactory results with 95% classification accuracy in differentiating OA knee from healthy knee. This study also discovered major difference between left and right knee VAG differences for both OA and healthy subjects which may provide more answers about the main cause of OA and method of preventing it.

ABSTRAK

Sakit sendi atau Osteoarthritis (OA) ialah penyakit yang biasa di kalangan warga emas dan atlet. Walaupun OA dikenali secara luas oleh doktor dan pakar-pakar penyelidik, kaedah diagnosis semasa yang sedia ada untuk pengesanan OA sama ada mahal dan invasif atau sangat menyulitkan untuk orang biasa. Pengesanan awal OA adalah yang paling penting kerana sifatnya yang progresif. Jika OA dibiarkan begitu sahaja, OA boleh mengakibatkan kesan yang lebih besar seperti kecacatan tulang dan sendi dan kesakitan sendi yang merengsa. Kajian ini bertumpu kepada perkembangan kaedah yang lebih sesuai untuk kemudahan dan kecekapan diagnosis awal OA. Kajian-kajian lepas yang dilakukan berkenaan pengesanan OA secara tidak invasif telah membuktikan pengunaan kaedah Vibroarthrography (VAG) sememangnya mampu memberi hasil yang jelas untuk mengesan perbezaan antara isyarat Vibroarthrography OA dan lutut yang sihat yang dihasilkan dari getaran dan pelepasan akustik sendi lutut semasa melakukan tindakan. Untuk meneruskan kemajuan dalam bidang diagnosis OA yang tidak invasif, kajian semasa yang dicadangkan ini mula mencuba pelbagai jenis sensor atau alat pengesan sedia ada (terutamanya elemen piezo, sensor ultrasound dan accelerometer) untuk pengesanan getaran dan pelepasan akustik lutut yang tidak invasif. Hasil pengujian sensor menunjukkan bahawa sensor pecutan atau accelerometer dapat menghasilkan hasil yang lebih baik dibandingkan dengan sensor lain yang dipilih. Untuk menilai dan membangunkan kaedah ujian yang sesuai untuk mengesan OA pada lutut, alat logging data telah dibangunkan untuk mengeluarkan bunyi dari getaran yang diambil dari sensor dan menyimpan data. Ujian dilakukan terhadap subjek yang sihat serta pesakit UMMC dengan pengawasan doktor. Hasil akhir menunjukkan keputusan yang memuaskan dengan ketepatan klasifikasi 95% dalam membezakan lutut OA dari lutut yang sihat. Kajian ini juga menemui perbezaan utama antara perbezaan VAG lutut

kiri dan kanan untuk kedua-dua OA dan subjek yang sihat yang boleh memberikan lebih banyak jawapan mengenai penyebab utama OA dan cara mencegahnya.

ACKNOWLEDGEMENTS

I am grateful to my siblings and close friends Sattar and Deyna, who have provided me with moral and emotional support in my life. I am especially grateful to my Father and Mother who have supported me along the way and helped at every step of my studies.

I sincerely thank my supervisors Dr. Lai Khin Wee and Dr. Zulkarnain bin Jarfaar who have guided me throughout my studies and eased my studies difficulties.

A very special gratitude goes out to all down at Research Fund and also IPPP for helping and providing the funding for the work.

Thanks for all your encouragements!

TABLE OF CONTENTS

LIST OF FIGURES

LIST OF TABLES

LIST OF SYMBOLS AND ABBREVIATIONS

OA	:	Osteoarthritis
AHC	:	Average hit count of constant magnitude hit at varying frequencies
RMS	:	Root Mean Square
FFT	:	Fast furrier transform
SFT	:	Short time Fourier transform
VG	:	Vibrography
VAG	:	Vibroarthrography
f	:	Frequency
POC	:	Point-Of-Care
GND	:	Ground voltage level
ACC	:	Accelerometer
GYR	:	Gyroscope
r	:	Angular rotation speed rad/sec
t	:	Time duration
AI	:	Artificial Intelligent
sAGEs	:	skin advanced glycation endproducts
JSN		Joint space narrowing
TKA	:	Total Knee Arthroplasty
KLG	:	KELLGREN-LAWRENCE GRADING for OA Grading
AE	:	Acoustic emission
Vp	:	Peak amplitude of signal
Tr	:	Rise time of the signal from the start to peak amplitude
KNN	:	K nearest neighbour algorithm
FF	:	Form factor

IGpA	:	Industrial Grade piezo based accelerometer
US	:	Ultrasound sensor
IDE	:	Integrated development environment
SOC	:	System on the cheap
I/O	:	General purpose microcontroller pin with Input and output capability
PSD	:	Power Spectrum Density
FMH	:	Number points across the frequency domain pass the magnitude limit
TFMH	:	Time-frequency magnitude hits across time domain
SPRA	:	Significant Point Recognition Algorithm
MHC	:	Magnitude Hit Count
SPRA	:	Significant Position Recognition Algorithm
RMS	:	Root Mean Square
STFT	:	Short Time Fourier Transform

LIST OF APPENDICES

CHAPTER 1: INTRODUCTION

1.1 BACKGROUND TO THE STUDY

Knee joint is the largest and one of the strongest bone structure in the human body, enabling the body to have essential roles in horizontal and vertical movement directions while supporting the body's weight along with hip joint which consists of complex musculoskeletal soft tissue structures within the joint and its surrounding (Kauffman & Bolton, 2007). There are three main compartments of knee joint: medial and lateral, tibiofemoral and patellofemoral where the knee joint is located between the femur and tibia as shown in Figure 1.1 (Gray, 2000). Knee joint functions of flexing and extending which are essential to many everyday activities including walking, running, sitting, and standing (Callaghan, 2003). Hence, the knee joint is vulnerable to both acute injuries and the development of many types of arthritis such as osteoarthritis (OA). However, previous studies could never prove the exact factor that causes OA. Weight, age, knee injury, genetics, repetitive actions such as climbing stairs, and weak muscles may arguably be the primary cause of knee OA (Hinterwimmer et al., 2004).

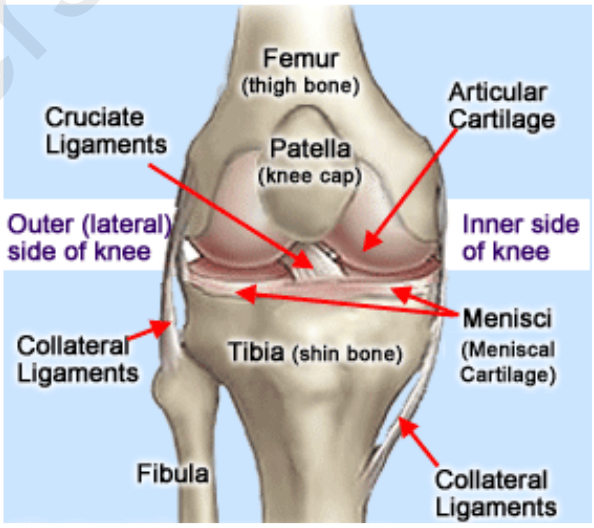

Figure 1.1: Anatomy of human knee joint (source: http://www.bigkneepain.com)

Osteoarthritis (OA) is a common musculoskeletal disorder and its prevalence is predicted to rise significantly in the future as the population ages. In the United States, knee OA currently affects about 40% of people aged over 75 years, while hip OA affects about 10% of the same age group. Meanwhile, the prevalence of OA affects about 10-20% of the adult population. In all populations studied so far, the prevalence of knee OA is higher than that of hip OA, especially in Asian population. The most common form of OA in Malaysia is knee OA (Veerapen, Wigley & Valkenburg, 2007).

Current existing OA treatment methods are divided into two stages based on the severity of the OA, namely, the early stages where the bone deformity is insignificant, and the advanced stages where joint deformity is substantial with a low chance of recovery. Treatment methods in early stages are OA medications, lifestyle modifications, and physiotherapy. Meanwhile, the treatment of advanced stages of OA is rather painful with low chances of success. The most common and widely used method of treatment for severe OA is total knee replacement (TKR) which requires removing the bone structure around the knee joint and replacing it with titanium alloy (Rabenda et al., 2007). Although all the existing methods are able to give patients the mobility, the damage done is irreversible and none of the methods is able to reform the knee structure back to its original form (Cooper et al., 2000). Due to lack of permanent solutions to treat OA, early diagnosis of OA and treatment are of utmost importance.

The majority of OA patients are treated in primary care, but recent studies indicate that this care needs to be improved. Most patients with OA who are assessed and treated within primary care settings seemed to perceive the severity of OA differently to their doctors (Atlas & Deyo, 2001). Furthermore, OA of the knee is often neglected by doctors until the disease progresses to severe stages, mainly because the development of OA is invariably assumed to be a part of the 'normal' aging process (Shark, Chen, &

Goodacre, 2011). A more reliable, cost effective and efficient method (point of care approach) assessable for both doctors and patients, especially in urban areas, is needed to educate doctors, patients, and the general public about the progressive effects of OA on the body.

Although OA is very common among elderly people, the current diagnostic methods are inconvenient, time-consuming, expensive, invasive and in most cases, painful. Currently, the most common methods used in diagnosing OA are imaging diagnosis tools which consist of magnetic resonance imaging (MRI) (Wakefield et al., 2003), x-ray (Kellgren & Lawrence, 1957), and ultrasonography (Tehranzadeh, Ashikyan, & Dascalos, 2003). The x-ray diagnosis is performed by capturing two static pictures of the patient's internal structure of the knee in two different directions, namely, side view and sky top view. The x-ray images are then assessed by doctors to indicate the narrowing of joint spaces for the possibility or severity of OA (Kellgren & Lawrence, 1957). However, this method has certain limitations as the doctor cannot view the deformity of the knee joints. The MRI and ultrasound can provide relatively clearer images of articular cartilage degeneration (Wang, Huang, Saarakkala, & Zheng, 2010). MRI is able to provide relatively more data as well as 3D anatomic information (Roemer, Van Holsbeeck, & Genant, 2005). Other than the non-invasive imaging diagnosis, an invasive diagnosis method called joint aspiration is also used in certain clinic and hospitals. The joint aspiration is performed by extracting the fluid between the knee joints and performing chemical analyses in lab. The chemical compound indicates whether the OA is present or not (Ferri, 2016).

A healthy knee joint's articular cartilage surface is smooth and lubricated allowing for frictionless and smooth movement of the knee while performing fast actions. Due to wear and tear, this smooth surface will degenerate causing direct friction on the knee

joint cartilage surface. The direct friction will eventually damage the bone surface and eventually the human body will respond to the damaged joint bone by reinforcing the bone structure with thicker layers of bone in which more friction will be applied to the joint as shown in Figure 1.2. This causes a chain reaction which speeds up the progression of OA (Davis et al., 2017).

Figure 1.2: Uneven surface of knee OA (source: http://physioworks.com.au)

The OA knee's uneven surface produces abnormal vibration and acoustic emission which are relative to healthy knees. These vibrations and acoustic emissions can be captured using accurate vibrations and acoustic sensors (Cooper et al., 2000).

1.2 PROBLEM STATEMENT

OA is a very common disease among elderly people. Its rapid progress affects patients' mobility and lifestyle. The early diagnosis and treatment of OA are of importance. However, the current diagnostic methods are rather inconvenient especially for a person with minor knee pain. The cost and time required for testing could force those suffering from minor knee pain to avoid any consultations with the doctor.

X-ray scans will increase the risk of cancer because of exposure to radiation. When the selected test method is chosen by the physician, several similar tests will be administered throughout the treatment to track the treatment progress on the knee.

Selecting the X-ray scan as a diagnosis tool will expose the patient to excessive radiation which can contribute to major side effects such as an increased risk of cancer (Berrington & Darby, 2004). Due to side effects of radiation, doctors would prefer the use of other alternative imaging methods. Ultrasonography is an alternative to the X-ray scan; however, it is largely avoided by doctors due to poor visual representation and lack of reliability (Abraham, et al., 2011). Recent studies exploring the possibility of using artificial intelligence (AI) in diagnosis of OA have used the ultrasound to increase the detection accuracy (Faisal et al., 2017). Magnetic resonance imaging (MRI) provides a much more accurate visual representation of the cartilage structure. However, the cost of the test and facility required for the MRI OA diagnosis make this option not suitable for majority of patients especially in urban areas. These non-invasive methods primarily rely on the visual testing and are highly subjective. The most reliable OA testing currently available is joint aspiration which is not recommended by doctors due to its side effects which include infection. A cheap, non-invasive, and portable knee OA diagnosis tool is needed for an early diagnosis of OA to help both doctors and patients as well as to track the progress of OA throughout the treatment.

1.3 AIM OF THE STUDY

This research is focused on the development of a non-invasive diagnostic kit using the point-of-care approach (POC). This includes appropriate sensors for non-invasive detection of OA on the knee and a system to record the sensor data for analyses. The novelty of this study emanates from the signal processing method used and motion gesture recognition tool that have been created. The signal processing was done in time and frequency domains by creating the motion gesture recognition tool and feeding the rotation speed ratio obtained by this tool into the magnitude analysis algorithm. The magnitude analysis algorithm used short-time Fourier Transform (STFT) to analyse the specific magnitude of the signal at a unique range limit specified by the sit-stand-sit test

speed ratio. By using this method, both speed and vibration of the knee could be analysed by a highly reliable system in analysing and tracking the progress of the OA.

1.4 OBJECTIVES OF THE STUDY

- To perform testing on different types of VAG sensors and selection of suitable sensors for non-invasive detection of VAG signals.
- To develop a data logging tool for capturing the knee signals of OA and healthy subjects and creating a database containing knee VAG signals.
- To create signal analysis algorithms to detect and classify the OA.

1.5 THESIS STRUCTURE

This thesis follows the conventional format which contains five chapters, namely, introduction, literature review, methodology, results and discussion as well as conclusion.

The literature review chapter is divided into two sections: medical research and engineering. The methodology chapter describes procedures of testing the capability of the sensors and evaluation of the sensor performance. After the sensor selection elaboration, the construction process of the hardware to record the knee data as well as the method of the testing on subjects are comprehensively discussed. In the results and discussion chapter, a detailed analysis of data captured from the data logger construction is explained and the results of the data after signal processing are also presented followed by an explanation of the raw collected data. In the discussion chapter as well, the programming of both microcontroller and MATLAB for signal processing is also clarified in detail.

CHAPTER 2: LITERATURE REVIEW

2.1 MEDICAL RESEARCH

2.1.1 Causes and prevalence of knee arthritis

The number of people in the USA suffering from arthritis is expected to increase from 40 million in 1995 which was equivalent to 15% of the population, to 59 million which is equivalent to 18% of the population by 2020 (Song et al., 2017). This figure is closely related to the average age of USA citizens since age is one of the key factors in the prevalence of OA (Zhang & Jordan, 2010). Figure 2.1 shows the median age growth of the USA population from 1960 to 2015. There was a steady growth in average age from 28.1 years old in year 1970 to 37.8 years old in year 2015. This is positively correlated with an increase in the prevalence of OA.

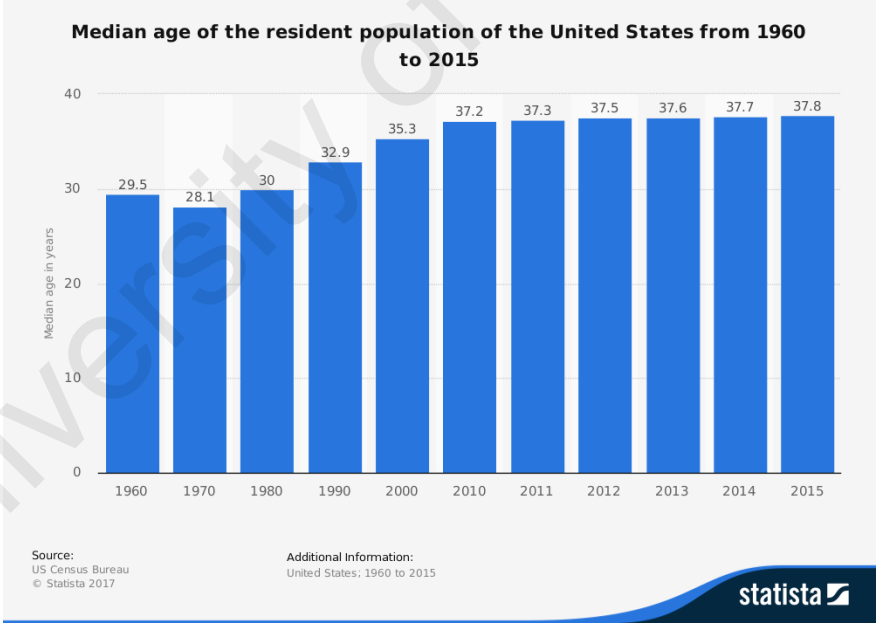

Figure 2.1: Steady growth of median age of USA from 1960 to 2015 (Source: Statista)

There are many other risk factors other than age as the primary cause of OA. The most notable cause is gender. A recent study showed that symptomatic knee OA can

occur in 10% of men and 13% of women aged 60 years and above (Zhang & Jordan, 2010). The study also suggested that progress of OA at early stages was much higher in men compared to women. Study conducted by Eaton et al. (2017) provided statistics of OA progress differences in men by 7%, 16% and 17.7% while for women by 11.4%, 14.4% and 8.4% in terms of hip OA, patella-femur OA, and tibia-femur OA, respectively. Although skin advanced glycation endproducts (sAGEs) is independent of age and BMI, it is associated with knee joint space narrowing (JSN) in men. However, this does not occur in women.

The third influential factor contributing to the prevalence of OA is genetics or more specifically race. A study in 2016 performed tests by comparing the prevalence of OA between whites and non-whites. The study involved 1915 participants (50% OA patients). It was found that among men, 2.0 % of whites and 1.9% non-whites were at risk of total knee arthroplasty (TKA). Meanwhile, among women, 2.2% of whites and 1.0% of non-whites were suffering from severe OA and required TKA (Collins, Deshpande, Katz, & Losina, 2016). Considering the test results, it could be estimated that non-whites were 30% less likely to acquire OA in late ages compared to whites.

Considering these factors and comparing them to Malaysian statistics, the overall figure on how likely are Malaysians to suffer from OA in the future can be estimated. Figure 2.2 shows the median age of Malaysians until the year 2020. As can be observed, there has been a rapid increase in the median age, indicating that the number of OA patients will rapidly increase as well, due to its correlation with age.

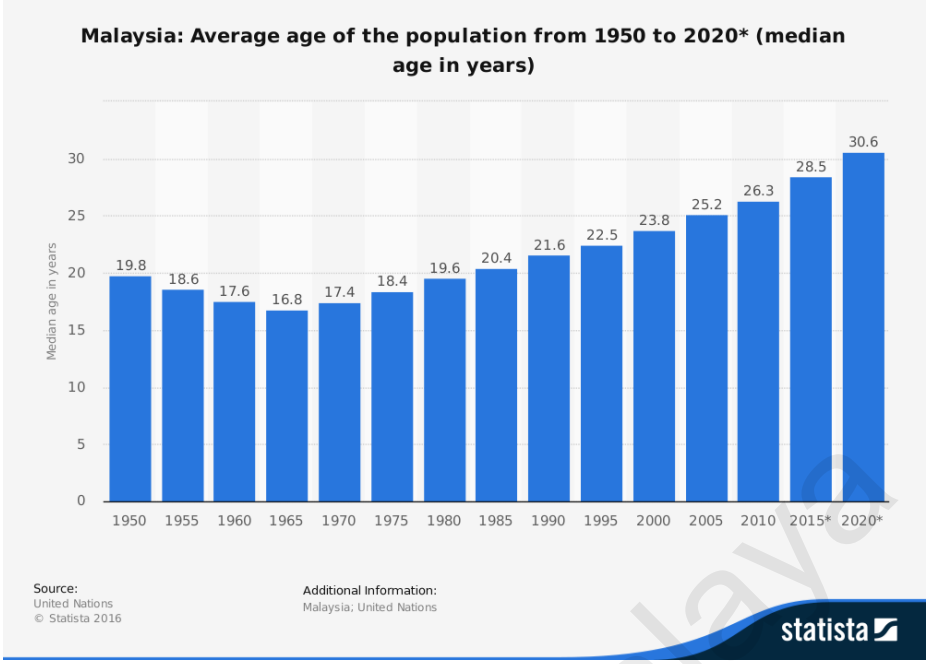

Figure 2.2: Median age of Malaysians until year 2020 (source: Statista)

The second main factor of OA, weight, has shown a rapid increase as well. Based on the study done by Ismail in 2002 on a group of 1000 participant, about 24% of men and 21% women were obese in Malaysia (Ismail et al., 2002). When combined with the rapid increase of median age, it is assumed that the number of elders suffering from OA will rapidly increase in future.

OA is often considered as a common old age disease. However, knee OA can occur in younger adults as well. In a population aged from 35 to 54, about 5% showed signs of knee OA and from this 5%, almost all of them suffered knee injuries. The most common risk factor of OA in young adults is considered to be joint injury (Buckwalter, 2003). Simple knee injuries in younger adults such as falling on the knee might increase the risk of rapid development of radiographic and/or symptomatic osteoarthritis. A study has shown that knee injuries at the mean age of 22 years old could substantially increase the risk of knee OA with a relative risk of 5.17% (Gelber et al., 2000).

2.1.2 Types and symptoms of knee arthritis

Knee arthritis (KA) is divided into two main categories, namely, primary KA and secondary KA (Suszynski, 2016) depending on how it occurs. Primary KA occurs naturally due to wear and tear or genetics and starts developing around the age of 55 to 60 years old which can occur over time in anyone eventually but in different severity (Abramson & Yazici, 2006). Secondary KA is caused by any unnatural factor due to lifestyle. Knee injury, obesity, inactivity, genetics, and inflammation are the main causes of secondary KA (Samson et al., 2007).

There are three types of KA that can be found in both primary and secondary KA where each can occur depending on where the damage is done to the knee.

- OSTEOARTHRITIS: It is a common form of arthritis which can be found due to degeneration of cartilage. In that area, there exist no blood vessel or nerve that can cause pain to the patient unless certain activities are carried out such as climbing the stairs (Hawker et al., 2008).
- POST-TRAUMATIC KNEE ARTHRITIS: Developed by trauma or knee injury. Due to knee joint shock, the cartilage stops regenerating. This type of KA may not show any signs for years after an incident (Hawker et al., 2008).
- RHEUMATOID ARTHRITIS: It is an immune system malfunction disease. Rheumatoid arthritis can occur when the white blood cells wrongly attack the bone joints and cause joint swelling and pain, however, it can easily be treated and does not affect the cartilage surface (Hawker et al., 2008).

Furthermore, vulnerability to one type of arthritis will lead to many other types as well due to weight distribution. The chain reaction will rapidly increase and speed up the arthritis progression. A study has shown that weight alignment can be the key factor to OA progress and the signs can be found in as early as teenagers where the weight

distribution on the left and right sides of the body is not equal (Sharma et al., 2001). The following Table 2.1 is a list that shows all the existing arthritis which may contribute to knee OA.

Table 2.1: List of all OA types (Source: http://www.arthritis.org/about-arthritis/types/)

Disease name	**Disease name**
Adult-onset Still's disease	Reflex Sympathetic Dystrophy
Ankylosing Spondylitis	Reiter's Sydrome
Back Pain	Rheumatic Fever
Behçet's Disease	Rheumatism
Bursitis	Rheumatoid Arthritis
Calcium Pyrophosphate Deposition Disease (CPPD)	Scleroderma
Carpal Tunnel Syndrome	Sjögren's Disease
Chondromalacia Patella	Spinal Stenosis
Chronic Fatigue Syndrome	Spondy loarthritis
Complex Regional Pain Syndrome	Systemic Juvenile Idiopathic Arthritis
Cryopyrin-Associated Periodic Syndromes (CAPS)	Systemic Lupus Erythematosus
Degenerative Disc Disease	Systemic Lupus Erythematosus in Children & Teens
Developmental-Dysplasia of Hip	Systemic Sclerosis
Ehlers-Danlos	Vasculitis
Familial Mediterranean Fever	Wegener's Granulomatosis
Fibromyalgia	Raynaud's Phenomenon
Fifth Disease	Reactive Arthritis
Giant Cell Arteritis	Vasculitis
Gout	Pagets
Hemochromatosis	Palindromic Rheumatism
Infectious Arthritis	Patellofemoral Pain Syndrome
Inflammatory Arthritis	Pediatric Rheumatic Diseases
Inflammatory Bowel Disease	Pediatric SLE
Juvenile Arthritis	Polymyalgia Rheumatica
Juvenile Dermatomyositis (JD)	Pseudogout
Juvenile Idiopathic Arthritis (JIA)	Psoriatic Arthritis
Juvenile Scleroderma	Temporal Arteritis
Kawasaki Disease	Tendinitis
Lupus	Mixed Connective Tissue Disease
Lupus in Children & Teens	Myositis (inc. Polymyositis, Dermatomyositis)
Lyme Disease	Osteoporosis

2.1.3 Kellgren–Lawrence Grading

The Kellgren–Lawrence grading (KLG) is a gold standard evaluation of the OA severity for many hospitals and studies. This method mainly focuses on the x-ray imaging of the knee where skyline photos of both left and right knees will be evaluated (Schiphof, Boers, & Bierma-Zeinstra, 2008). The narrowing of the joint space is the main defining factor of OA severity based on JSN. The severity of the knee is divided into 5 grades (from grade 0 to grade 4) as the grade increases, the joint narrowing space decreases and the bone deformity around tibia and femur will increase (Kellgren & Lawrence, 1957).

The following is the grading system defined by Kellgren and Lawrence (1957). The present study employed this method of OA grading to categorize the data gathered;

- Grade 0: none (definite absence of OA)
- Grade 1: doubtful (doubtful narrowing of joint space and possible osteophyte)
- Grade 2: minimal (definite osteophytes and possible narrowing of joint space)
- Grade 3: moderate (moderate osteophytes, definite narrowing of joints space, some sclerosis and possible deformity of bone contour)
- Grade 4: severe (Large osteophytes, marked narrowing of joint space, severe sclerosis and definite deformity of bone contour).

Figure 2.3 is the skyline x-ray captured image of grade 3 left and right knees of an OA patient taken at the University Malaya Medical Centre (UMMC). The joint deformity of the OA knee can be clearly seen on the tip of each joint as it has been marked in Figure 2.3.

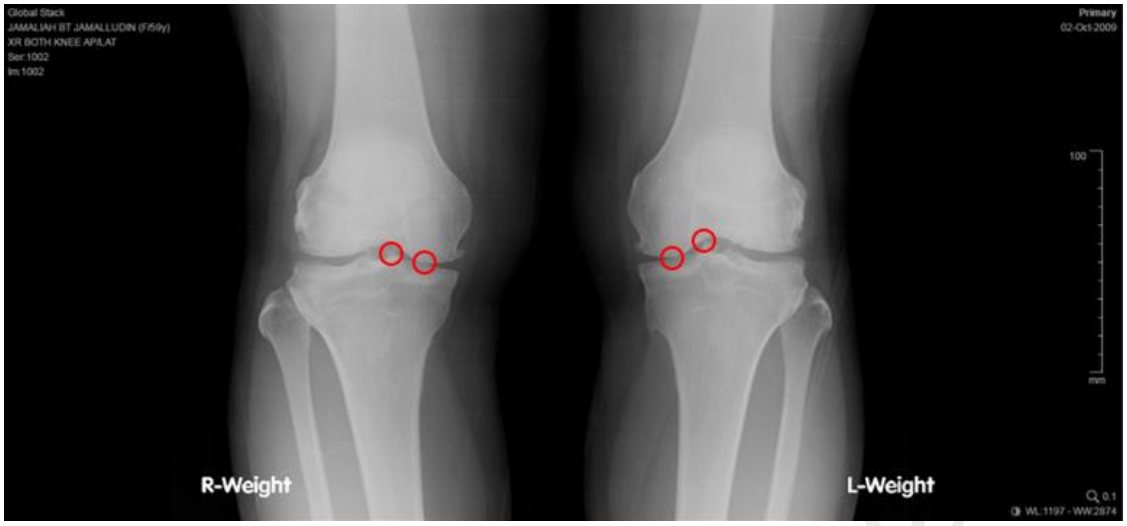

Figure 2.3: X-ray photo capture of grade 3 knee OA patient

2.2 ENGINEERING RESEARCH

2.2.1 Vibrography

Vibrography is a method of detection and visualization of vibration and acoustic emission produced from a mechanical structure and has been used for years in industry to detect faulty in complex machineries and motors (Peng & Chu, 2004). The principle of vibrography lies in detection of vibration and acoustic emission produced by motor gears grinding and friction produced form motion of machinery using highly sensitive sensors, which are then compared with the results of the ideal signal (i.e., the gold standard); while signal frequencies and amplitude differences contribute in the detection. By simply placing the sensors on the body of the machinery, the vibration or the acoustic emission in a specific area can be detected; hence, troubleshooting can be performed (Baydar & Ball, 2003).

Monitoring the machinery condition is essential for maintaining as well as work efficiency in factories. The main sensors used for condition monitoring of the machinery are accelerometer and microphones for the detection of vibration. The recorded vibration signals produced usually are within the audible frequency, mostly less than 20 kHz (Baydar & Ball, 2001)

Several studies have been conducted on the measurement of vibration signals within audible range for the diagnosis of rolling element bearing. A research conducted by Tanaka and Choudhury (1999) evaluated the vibration produced by bearing, then created a cascade filtering for the removal of noise to prepare for simple signal processing. Another study performed the feature extraction on audible vibration signals for the detection of localised defects such as cracks and spalls on rolling surface, and disrupted defects such as surface irregularities (Choudhury & Tandon, 1998). The properties of the machine used for testing had a close resemblance to knee joint surface fraction and poor lubrication, hence hinting at the possibility of using these methods to detect knee joint malfunctioning such as OA. Figure 2.4 shows the comparison of vibrography signals captured by different machineries (Al-Ghamd & Mba, 2006). As shown in Figure 2.4, the vibration produced by the machine bearing was a non-linear multilayer signal. These two characteristics promoted the use of time-frequency signal analysis method for signal feature extraction. Figure 2.5 shows the vibrography tool used in industry for capturing and data logging of the vibration and acoustic emission.

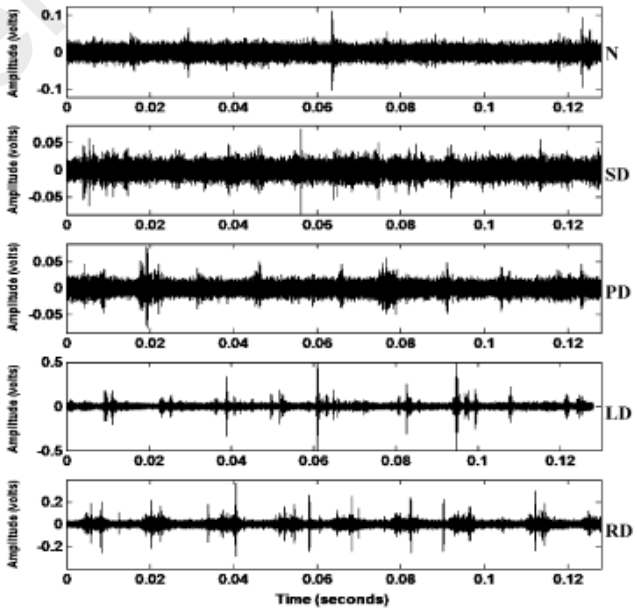

Figure 2.4: Vibrography signal comparison between different machinery (Al-Ghamd & Mba, 2006)

Figure 2.5: UNI-T UT315 Vibrography tester and data logger

2.2.2 Acoustic emission

Acoustic emission (AE) is categorized as a vibrograph signal and unlike vibration, AE can occur at frequencies higher than 20 KHz which are called elastic waves. In machineries, AE usually is produced by under pressure gears and can be captured using piezo-electric materials (Park et al., 2012).

AE is an alternative method used in studies for detection and evaluation of cracks in gears. The main application for AE condition monitoring is related to diagnosis and prediction of bearing surfaces (Hemelrijck, Busse, Solodov, & Anastasopoulos, 2008) as well as machinery gears (Tan, Irving, & Mba, 2007). Major developments have been done in the diagnosis of bearing defects using AE, the experiments done by Choudhury and Tandon have been extended to investigate the severity as well as size of the damage to the bearing (Choudhury & Tandon, 2000). Abovementioned was accomplished by comparing both AE and audible vibration in a variety of speeds on load bearings. By analysing the findings of AE and vibration, AE could identify an early fault diagnosis of bearing defects for small fractures compared to vibration diagnosis. A subsequent study performed similar tests and analysed the signals obtained from vibration and

spectrometric sensors in time, frequency and time-frequency and compared the findings. The results of the tests showed that AE signals were able to identify local fault progressions in terms of gear crack, damage of tooth and localised wear with high accuracy (87.7%) (Tehranzadeh et al., 2003).

There are many studies that have delved into the AE performance on health monitoring aerospace structures (Hemelrijck et al., 2008), damage progression monitoring for composite laminates (Richards, 2008), chatter vibration and AE respond in identification of tool wear (Scruby, 1987), aluminium alloy fatigue growth monitoring (Mascaro et al., 2009) and reinforced concrete tolerance analysis and quality evaluation of shotcrete (Prior et al., 2010). The signal analysis methods used for feature extractions of AE are as follows:

- AE waveform features
- Time reverse modelling method
- Mixed time-frequency analysis
- Multivariate statistics AE

AE based biomedical engineering field assessments showed promising results in monitoring bone conditions. In a study, a minor bone failure was investigated by applying load in specific intervals to the bone to generate AE. The results showed that AE signals collected could identify fractures and sensitive damages to the bone. In the same study, a further capability of AE to predict small bone fractures in early stage was investigated. The results of the experiment showed that the use of AE sensors was a viable tool in detecting the small bone fractures. Also, a passive experiment method used AE to detect acrylic bone cement failure on the hip joint (Trebacz & Zdunek, 2006). Feature extraction methods of AE signals are mainly focused on the signal

magnitude, duration and rise time. Duration of the rise time on AE signals was positively correlated to fatigue related AE. AE has also been found useful to be applied in the anterior cruciate ligament damage monitoring. The results of AE signal peak amplitude (V_p) and rise time (T_r) of the collected AE signals had a positive correlation with the matrix deformation, fibre fracture and deboning in which these tests were done on the fibre composite materials. The low V_p and short T_r corresponded to the matrix deformation while high V_p and long T_r corresponded to the fibre fracture (Wierzcholski, 2006).

All the mentioned studies were only performed on small groups of test subjects. This was due to the unreliability of the tests. The human bones by nature reflect different types of acoustic emotions due to the variety of bone structures and density. The muscle mass also plays a big role in the magnitude of AE reflection. Due to a large number of controlled parameters needed to be taken into account, the reliability of AE use in detecting OA seems less attractive for the currently available technology.

2.2.3 Vibroarthrography

Similar to mechanical gears, the human knee joint too is a complex structure which can perform complex mechanical motions in its own range of motion (ROM) (Figure 2.6). The cartilage is placed at the tip of the three-knee joint bone structure which plays a major role in a smooth and frictionless movement between the knee joints. However, due to wear and tear of the cartilage which is caused by weak muscles and too much pressure or knee injury, the cartilage is progressively worn out to an extent in which the bones become completely exposed (Veerapen, Wigley, & Valkenburg, 2007).

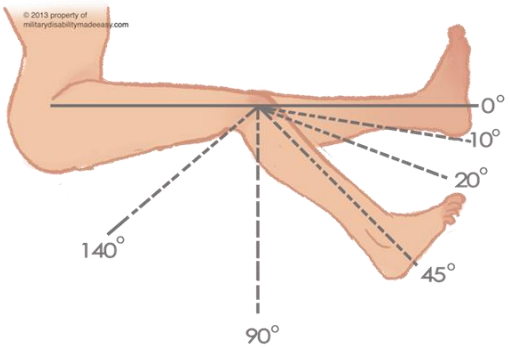

Figure 2.6: Knee range of motion (Source: http://www.militarydisabilitymadeeasy.com)

The earliest study investigating the possibility of non-invasive detection of OA belongs to S. Krishnan (1997) which was inspired by the traditional method used by doctors to evaluate the health of knee joint. Without relying on the sensors to detect OA in early 1800s, doctors would use their hands to determine the severity of OA. This was done by placing the palm on mid patella followed by flexing and extending leg (Krishnan, Rangayyan, Bell, Frank, & Ladly, 1997). By sensing the vibration, the severity was determined. However, this was discouraged as it was unreliable due to presence of human error. This method is still being used by doctors but for different purposes. After injecting the lubricant materials into the knee joint space of OA patient, the doctor will perform the hand diagnosis to ensure the flex and extend are performed more fluently relative to prior injection. The injection contains a gel-like mixture made of a substance called hyaluronan (pronounced hy-al-u-ROE-nan) that comes from chicken combs, used as a temporary solution in cases of severe OA (KLG grade 3 and above) (Callaghan, 2003). Hyaluronan is a natural substance found in the body and is present in a very high amount between joints. The body's own hyaluronan acts like a lubricant and shock absorber in the joint and is needed for the joint to work properly. However, due to unknown reasons, hyaluronan reproduction stops in elderly thus causing wear and tear in the knee.

When the knee bone surface is exposed or performing an action, OA knees would produce abnormal vibrations and acoustic emissions relative to the vibrations and acoustic emissions of normal knees (Shark et al., 2011). The uneven surface of the patella, tibia and femur carry a unique characteristic which can be taken advantage of by using vibrography techniques. Vibrography is done through detection and comparison of the vibration and echoes reflected in the bone structure of the OA knee, while the knee is performing a motion. This technique is also termed as Vibroarthrography (VAG).

Many studies in the past evaluated the possibility of non-invasive diagnosis of knee pathology and articular cartilage breakdown using VAG signals. Based on Krishan's year 2000 findings, VAG signals should follow specific characteristics (Krishnan, Rangayyan, Bell, & Frank, 2000). The characteristics are as follows:

- VAG signals are non-stationary similar to all bio signals. This is due to uneven and non-linear surface of knee cartilage and due to angular movement while the knee is in motion from one angular position (point of time) to another during articulation of the joint.
- The surface of the healthy knee's cartilage is smooth and lubricated. However, in OA knees, the VAG signal generated from frictions between articular cartilage surfaces is different in amplitude (V_p) and frequency from a healthy knee. Identifying and specifying the frequency bandwidth, unique for OA knees may help in the identification of OA non-invasively.
- The VAG signal is of multicomponent signal. Vibration produced by the knee may reside from many sources and produce several frequencies from several sources.

- In case of recording the vibration on the surface of the knee, the signals produced at different frequencies would require them passing through multiple layers of tissue. This would create multiple-energy components at different frequencies at a specific point of knee bend.
- Recording knee vibration from skin surface is bound to many background noises and filtering is required for noise removal.

Due to these characteristics, many tests were administered and analysed in the frequency domain for a better identification of the noise produced and feature extraction (Rangayyan, Krishnan, Bell, Frank, & Ladly, 1997). Most studies conducted on detection of OA using VAG signals mainly focused on acoustic emissions produced by knees while bending. The signal analysis of such waveforms however, produced unreliable readings as the signal might contain disturbance due to reflected emissions from skin structure (Mascaro et al., 2009).

To measure emissions produced by knees, extensive and highly accurate devices are required to filter and analyse the data. However, depending on each type of knee structure, the corresponding filters may differ. To overcome such problem, dynamic and complex machine learning techniques are used. However, the machine learning techniques are considered to be impractical for developing a standalone diagnosis tool due to the requirements of large learning group and high computer processing power to analyse the data.

A study was conducted on the signal analysis based on vibration, by performing filtering using K Nearest Neighbour (KNN) algorithm and form factor (FF) to ignore the vibration produced by muscles (Liu et al., 2014). In other studies, adaptive segmentation method to segment non-stationary VAG signals was executed to perform the feature extraction (Krishnan et al., 2000). Methods such as recursive least squares

(RLS) algorithm would then normally be applied to the signal after segmentation. Conversion of segmented signals to frequency domain using fast Fourier transform (FFT) is essential due to the variance of knee bend in time domain. The frequency domain hence provides more information about the signal characteristics (Rangayyan et al., 1997).

The method of modelling by linear prediction was used in adaptive segmentation and para magnetization of vibrating signals (Umapathy & Krishnan, 2006). Non-invasive techniques to localize sound or vibroarthrography (VAG) signal sources in human knee joints of the patients who subsequently underwent arthroscopy and cadavers with arthroscopically created lesions, obtained by stimulation with fingertip over mid patella and swinging movement of leg were analysed for the time delays using cross-correlation function for source localization (Rangayyan & Yunfeng, 2008). An adaptive segmentation method was developed to segment the non-stationary VAG signals. The least square modelling method was used to reduce the number of data samples to a few model parameters (Umapathy & Krishnan, 2006).

VAG signals are obtained by applying logistic and discriminant algorithms. An adaptive time frequency distribution was constructed by a minimum cross entropy optimization of the time frequency distributions obtained by matching pursuit decomposition algorithm. Parameters of VAG signals namely energy, energy spread, frequency and frequency spread were extended from adaptive TFD. Denoising methods such as wavelets and wavelet packets and matching pursuit (MP) were used (McCoy, McCrea, Beverland, Kernohan, & Mollan, 1987).

2.2.4 Signal analysis method

As explained in the previous section, based on past studies done on both vibrography and VAG signals, analyses as well as feature extraction done in the frequency and

mixed time-frequency domains are of the utmost importance. This was due to multicomponent nature of the signals. The use of classic feature extraction methods such as Fourier transform tended to provide insufficient detail about signal properties because of the non-stationary nature of bio signals. The non-stationary nature of the signals however, would provide more information if signals were analysed using the newly developed methods such as time-frequency transformation and wavelet transformation which have been widely used in medical fields by providing both time and frequency dimensions in one plot (Tamil, Kamarudin, Salleh, & Tamil, 2008).

Time-frequency transformation (TFT) was developed to aid in analyses of non-stationary signals specifically for bio-signals such as heart and EEG signals (Cohen, 1995). However, few years after TFT, other alternative methods were used to overcome the Fourier transformation limitations. There was a need to monitor the existing signals at different time periods since Fourier transformation was only able to provide general information of the existing frequencies throughout the finite time interval. One of the alternatives to TFT was time periodic transformation (TPT) and it was obtained by performing the fast Fourier transform (FFT) on specific time intervals. This method had major limitations because of its complexity and overlapping, if the time window was not large enough. To monitor all the changes in the frequency domain, the time periods recorded must have had overlapped which would affect the reading accuracy greatly. A short-term Fourier transformation (STFT) was an alternative method created based on the periodic Fourier transformation. Equation 2.1 shows that the FFT is commonly used for frequency domain transformation. Where f represents the frequency domain and usually is denoted by capital letter symbol of the analog signal counterpart (in this case x(t) is converted to X(f).

$$X(f) = \int_{-\infty}^{\infty} x(t).e^{-2j\pi ft}\,dt \qquad (2.1)$$

The Fourier transform was created by assuming that all the existing signals were a form of sinusoidal signals at different frequencies combined hence Equation 2.1 was derived from Equation 2.2 (Polikar, 2007).

$$e^{-2j\pi ft} = Cos(2\pi ft) + j.Sin(2\pi ft) \qquad (2.2)$$

For a better understanding of the capability of the FFT and other signal transformations, a mixed signal which consisted of 5, 10, 20, and 50 Hz at different periods of time was created using MATLAB as shown in Figure 2.7. Figure 2.8 shows the same signal in frequency domain. Clearly, from these two figures, even though in time domain (Figure 2.7) the increase in frequency was applied as time progressed, while the frequency domain (figure 2.8) was only able to show the general frequencies distributed throughout the signal and not able to pinpoint when changes to frequency had accrued.

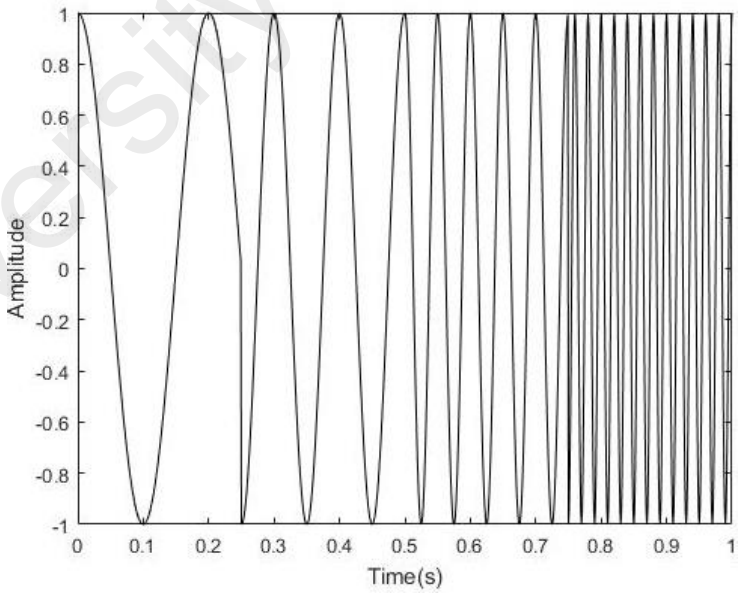

Figure 2.7: Signal contain 5, 10, 20, 50Hz frequency

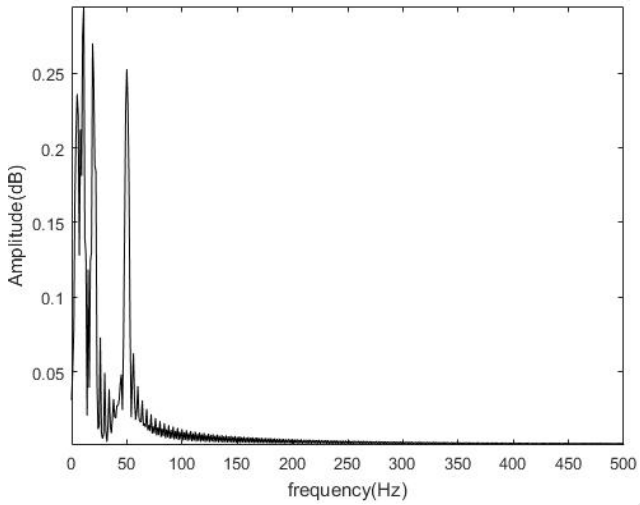

Figure 2.8: FFT of the mixed signal

Short term Fourier transform (STFT) was developed to compensate for the issues with TPT and FFT by providing a third-time dimension to the plot. The STFT followed Equation 2.3 where the signals were separated in the specific time period while the signal amplitudes were analysed in Gaussian waveform (Polikar, 2007). The ω represents time interval while t-t' is its range. Figure 2.9 shows the STFT done on the signal in Figure 2.7.

$$STFT_x^{\omega}(t,f) = \int_t [x(t).\omega^*(t-t')].e^{-2j\pi ft}dt \qquad (2.3)$$

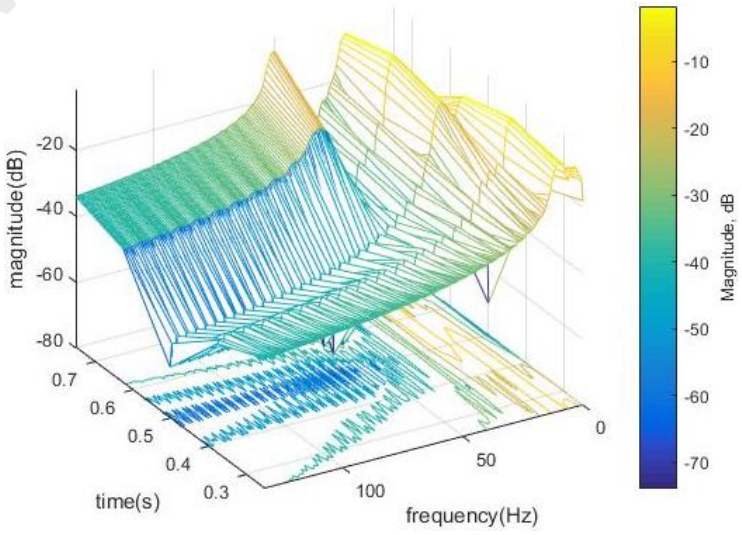

Figure 2.9: STFT of the mixed signal

As can be seen in Figure 2.9, STFT could provide clear information about the time period where a specific frequency was applied in the time line by providing three-dimensional graph of time, frequency, and frequency magnitude.

It should be noted that the resolution of the signals was directly affected by the duration and frequency that can vary greatly. A high frequency signal would provide greater magnitude resolution for accurate reading but because of shorter time window, the time resolution was affected hence provided lesser accurate reading. This can also be applied to lower frequency signals but in the reverse effect.

2.2.5 Research gap

The single database used in most of vibrography studies previously explained, were based on vibration VAG samples taken from Krishnan's research exclusively (Krishnan et al., 1997). The database was developed using the industrial grade piezo based accelerometer (IGpA) produced in 1970. Despite it being an outdated technology, the database was used in recent years to construct effective non-invasive VAG screening techniques. Present study has revised Krishnan's study by utilising a recent microelectromechanical system (MEMs) based capacitive accelerometers technology and performing modifications to the data acquisition method compared to previous studies. This present study has evaluated the feasibility of using such sensors and explored the possibility of creating a portable non-invasive OA diagnosis tool. MEMs accelerometers have certain advantages over industrial grade piezo accelerometers as follows:

- Cost: Mass production of MEMs for commercial use has lowered the cost per item compared to limited production of their counterparts, enabling the construction of low cost diagnostic kits that would be used by consumers and doctors especially in rural areas.

- Power consumption: MEMs capacitive accelerometers operate at relatively low power (3.5v/0.1μA); such characteristic allows them to work with microcontrollers and ARM based processors in creating standalone kits without requiring separate power supply. In case of IGAs, to provide high accuracy results, consuming a large amount of power is required which can only be provided by external power supply (more than 12v to operate).

- Accuracy: Despite providing highly accurate data, IGAs are limited to single axis due to their use in motor diagnosis tools. However, MEMs accelerometers can provide 3-axes (x, y, and z) of data simultaneously establishing new insight to evaluation and analysis of knee vibration.

- Noise: The data provided by IGAs are highly contaminated with noise due to high sensitivity nature of such devices as well as analog to digital conversion (ADC) hardware flows. To remove the noise, many complex filtering techniques are used which require powerful computing power to calculate, such as local discriminant bases algorithm (Umapathy & Krishnan, 2006). Lower accuracy of the MEMs accelerometers can carry much less noise contamination and hence simplifies the filtering techniques. All MEMs capacitive accelerometers are built as a part of system on chip (SoC), allowing on chip ADC and enhanced signal stabilization to facilitate the processing of the data by micro controller.

CHAPTER 3: METHODOLOGY

This chapter will firstly focus on identifying suitable sensors for VAG signal capturing and selecting the best option by performing tests on them. The selected sensors were then compiled with a specially designed data logger for data acquisition. The method of data acquisition will also be addressed in this chapter. The following progress flowchart in Figure 3.1 explains the flow of the methodology performed for the first and second prototypes created for this study.

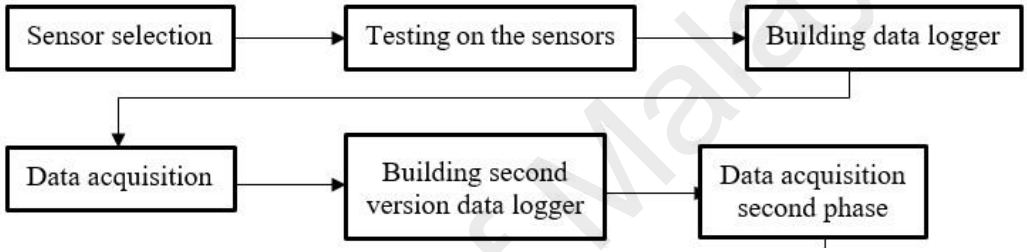

Figure 3.1: Flow process of the methodology

As can be seen from Figure 3.1, the data logger was built in two different versions. In version 1 of the data logger, after the analysis of collected data, it was found that there were many issues with the prototype and data logger. These issues had led to the construction of the second version of the prototype for data collection. Further details on the issues and problems faced in the first version will be explained in Section 3.4.

3.1 MICROCONTROLLER

Microcontroller is a vital part of present study as the purpose of the microcontroller was to capture the data produced by the sensor and make them available on the computer for later analysis. In some occasions, the sensor data would also be manipulated for a more reliable and simple analysis. Arduino Mega 2560 (Figure 3.2) was selected to perform the data logging process. Critical specification of this microcontroller is provided in

Table 3.1 while the microcontroller (AT-mega 2650) datasheet is provided in Appendix A.

Figure 3.2: Arduino Mega 2560

Table 3.1: Characteristics of the Arduino mega

Microcontroller	**ATmega2560**
Operating Voltage	5v
Digital I/O Pins	54
Analog Input Pins	16
Flash Memory	256KB
SRAM	8 KB
Clock Speed	16 MHz
ADC sampling rate	125KHz

The fast clock rate, large number of pins as well as high ADC sampling rate make this microcontroller a better choice compared to other options. One major advantage of Arduino is the use of Arduino IDE (Integrated Development Environment). Arduino IDE is an open source modified C++ programming language which is suitable to use for both novices as well as experts to create extensive programs. The open source nature of this programming language also will create possibilities of many free libraries readily available on the internet for many different situations.

AT-mega 2560 contains several IC to IC communication ports. The followings are the communication ports available on it:

- ICSP communication port.
- I2C communication port.
- Wire communication port.
- 4x Serial communication ports RS-232.

3.2 SOFTWARE PRODUCTS

Three types of software were used in creating the data logger, analysing the sensors, and signal processing. Arduino IDE was used in programming the Arduino Mega to collect and store the data from the sensor. Meanwhile, Processing is a software that was used in testing and visualising the sensor outputs and MATLAB was used in performing signal analysis and feature extraction.

Arduino IDE and Processing have been created from the same programming engine and perform in a similar way. Because of this, the programming on both platforms were very similar. Processing software functions closely with JAVA to provide the visual representation of what has been programmed. Processing is most often used to convert the programming command to simple animations. This feature has been used on robotics and microcontrollers to visualise the action taken and is done by capturing the serial output of the microcontroller. Arduino IDE however is strictly for AT-mega microcontroller programming. Both Processing and Arduino IDE can be modified using different types of libraries provided by other users to utilise their functionalities in specific ways. The open source nature of these software products allows for unlimited modification by anyone.

3.3 SENSOR SELECTION

Sensor selection is limited to the vibration and acoustic emission sensors to capture VAG signals. The sensors selected for testing were LV-MAXSONAR-EZ-D ultrasonic

sensor, 4 mm piezoelectric element, ADXL345 accelerometer, and MPU6050 gyro/accelerometer. Testing on the sensors were performed in different environments to evaluate the performance and effectiveness of the sensor in detection of VAG signals.

3.3.1 Piezoelectric element

Piezoelectric in industry is a vital diagnosis and sensory equipment due to its many applications, mainly used for faulty machinery troubleshooting. Piezoelectric is made of crystal structure where minor changes to the structure will cause the disk to produce current (PIPiezoTechonology, 2014).

Piezo element sensor has been used for years for detection of vibration in many different applications. By placing the piezo disk on the body of the machinery, the vibration produced by machinery will affect the current output of the sensor and by plotting the output signal, the vibration can be visualised. The amount of voltage produced will determine the amount of pressure on the piezo disk. In theory, this characteristic can be used to detect the rough surface of articular cartilage in testing. The piezo element is also capable of detecting acoustic emission signals produced at very high frequencies. The detection frequency range depends on the thickness of the piezo element. The friction in the knee joint may produce acoustic emissions that can be detected by piezo element, however, in this study this feature was ignored as to focus strictly on vibration of the knee.

To test the viability of piezo element to detect VAG signals, it was directly connected to the Arduino Mega's analog port and its signal was converted to digital. The sensor itself was attached to the mid patella and tested by flexing and extending the knee. The analog signals usually vary at very small scales (1 to 100 μv) and can easily get overwhelmed by signal interferences (noise) from surroundings; in this case, majority of noise was produced by muscle vibration. The muscles produced vibration as

well as acoustic emission signals which could indirectly affect the signal output of the piezo element. Hence, to avoid data corruption, active signal filtering circuit was used to nullify the noise and improve the signal quality. The sensors were mounted on the adjustable knee band to ensure their steadiness during the leg movements and to avoid unintended noise from piezo movement.

The data were attained from two different methods. The first method used serial monitoring to read the data outputs of the signal. These raw data were then transferred to the spreadsheet software and compared to the raw signals while piezo element was ideal. Figure 3.3 shows the samples of data taken.

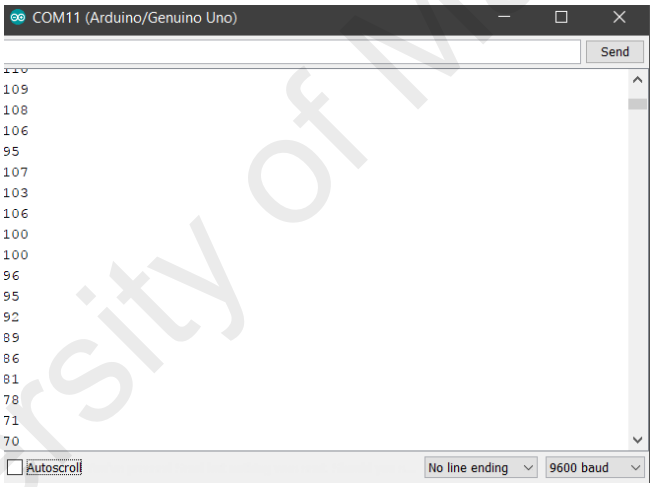

Figure 3.3: Sample of the accelerometer row data recorded from Arduino mega COM port

The second data recording method was done by creating a visual diagram based on the raw input data. The software that was used is called Processing. Samples of data taken using Processing can be seen in Figure 3.4.

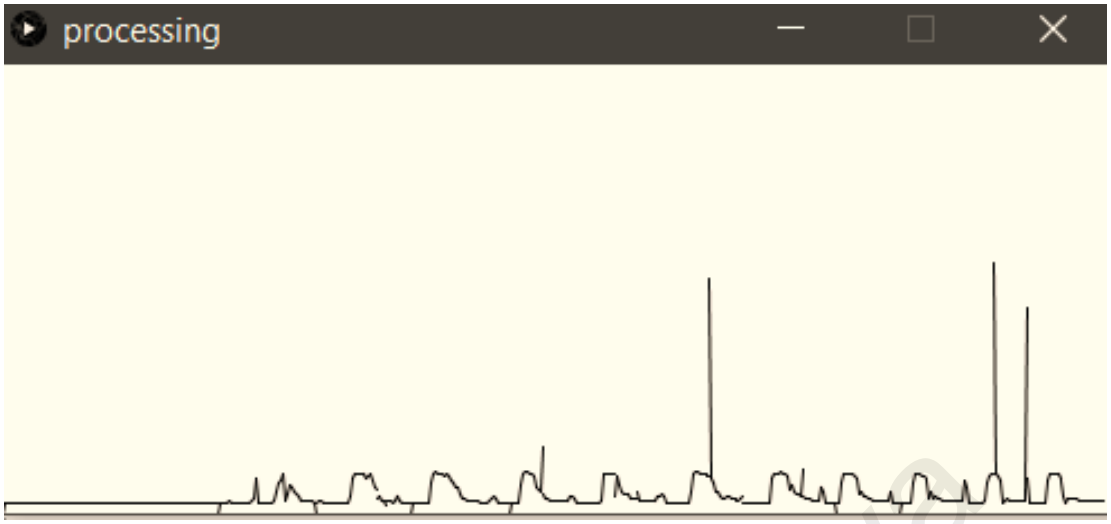

Figure 3.4: Samples of piezo vibration visuals data using processing software

Piezo element only requires two connections, ground (input) and analog (output). When the element is pressed, the crystal structure will produce small amount of electricity relative to the ground. Hardware connection was performed by connecting the output of the element to the pin A0 and read the collected data. Figure 3.5 shows the circuit diagram of the connected piezo element for testing. The software that was used to show the circuit diagram is called Proteus8 which was employed in this present study to demonstrate circuit designs.

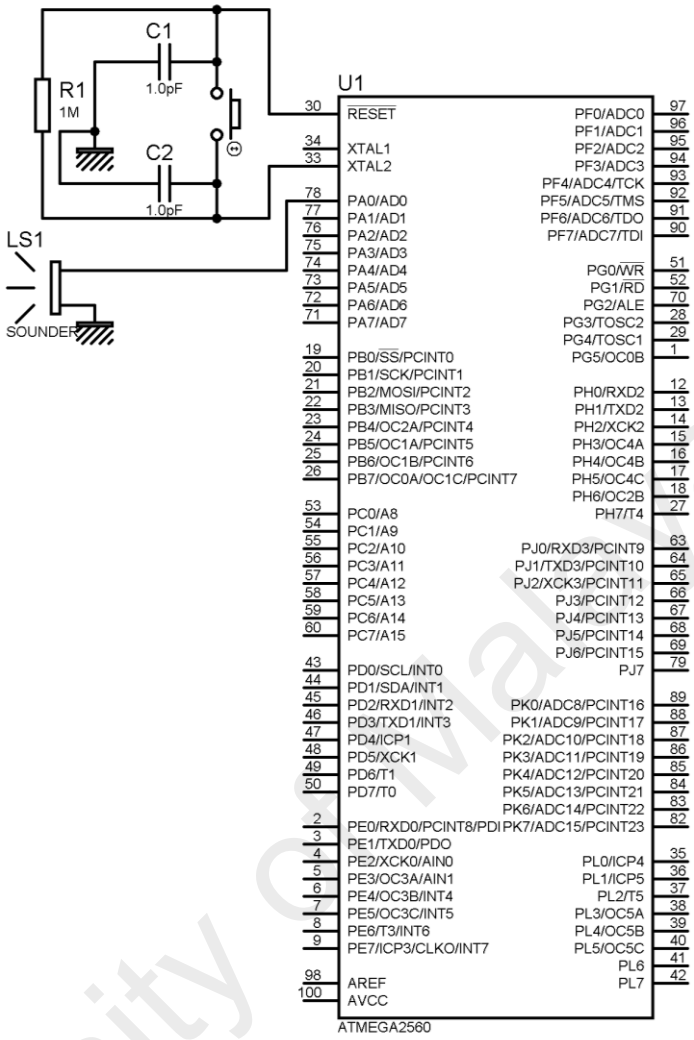

Figure 3.5: Circuit diagram of connection of piezo element to the AtTMEGA2560 microcontroller

The programming for testing piezo element on Arduino was very simple and did not require complex coding. The programming can be found in Appendix B Section 1.1 and the processing programming used to show Figure 3.4 is provided in Appendix B Section 1.2. It should be noted that, the signals collected from piezo element were shown on computer through USB serial terminal which is the default way of communication on Arduino. The processing software simply collected the values obtained from the terminal and visualised them based on the programming written in the processing software. Figure 3.6 and Figure 3.7 show the flowcharts of the programming of the Processing and Arduino respectively.

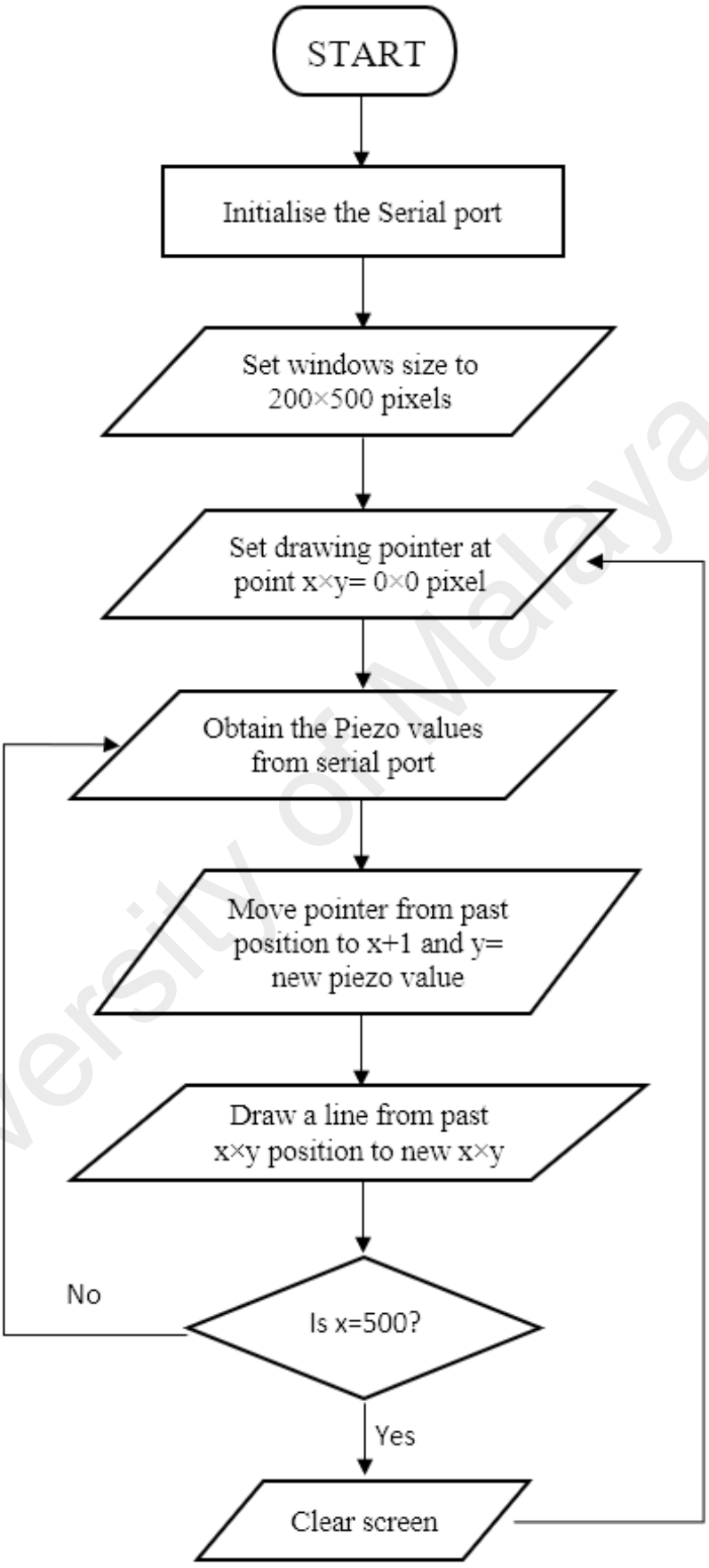

Figure 3.6: Flowchart of processing programming for Piezo element testing

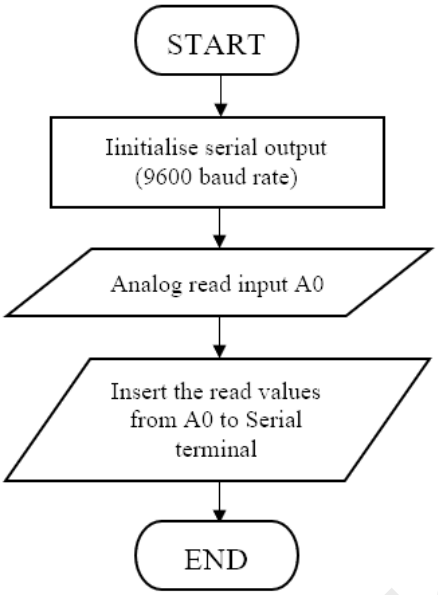

Figure 3.7: Flowchart of Arduino programming for piezo element testing

Use of piezo element had few major flaws:

1. Durability of the sensor: Piezo disks were very fragile and put too much pressure on the sensor which could lead to disk breakage. The sensor could only be placed on top of the patella for good reading which was not possible due to bending of the knee containing many angular movements which applied directional force to the sensor.

2. Calibration: Since the sensor relied heavily on the pressure applied to the crystal structure, outside force might have affected the results obtained. While the size of the knee varied from subject to subject, the affected pressure on the sensor would vary as well and might cause problem in analysing the data.

3. Noise: The sensor produced current and a very low amplitude which was highly susceptible to internal and external noises. Decode and filtering of such signal could be very challenging and required a much stronger data logging system.

3.3.2 Ultrasound sensor

Ultrasound sensors (US sensors) are mainly used in distance measurements. The basic structure of US sensor is of very thin piezoelectric disc. Depending on the thickness of the piezoelectric and the voltage applied to it, the sound waves sent can vary. US sensor will send a sound wave much higher than the hearing range (more than 23 Khz). The wave will then hit the object and reflect back to the sensor. By calculating the time taken for the US to hit the object and reflect, the distance can be determined. In theory, the uneven surface cartilage would reflect the US differently at different time intervals and this variance can be used to detect the abnormalities.

The LV-MAXSONAR-EZ-D sensor (Figure 3.8) was selected for testing due to its high accuracy. The specification of this sensor can be observed in Appendix A, Section 2. The programming for US sensor was similar to piezo element due to their similar analog output. The only difference was the output voltage which could vary dramatically depending on the distance of the object.

Figure 3.8: LV-MAXSONAR-EZ-D ultrasound sensor

Basic properties of this sensor are provided in Table 3.2 which were taken from the datasheet's essential information to build the testing prototype.

Table 3.2: Important US sensor specifications

Description	Value
Operating voltage	2.2v – 5.5v
Sampling rate	20 Hz
Voltage per distance scale	Vcc/512/inch
Minimum distance for reliable reading	16 inches from sensor
Inputs	Vcc, PW, BW, RX
Output	GND, TX, AN

Figure 3.9 shows the data collected from a serial port on the computer and Figure 3.10 shows the visualised analog signal obtained from a serial port using a processing software. It should be noted that the programming code used for the software was the same coding used for testing the piezo element.

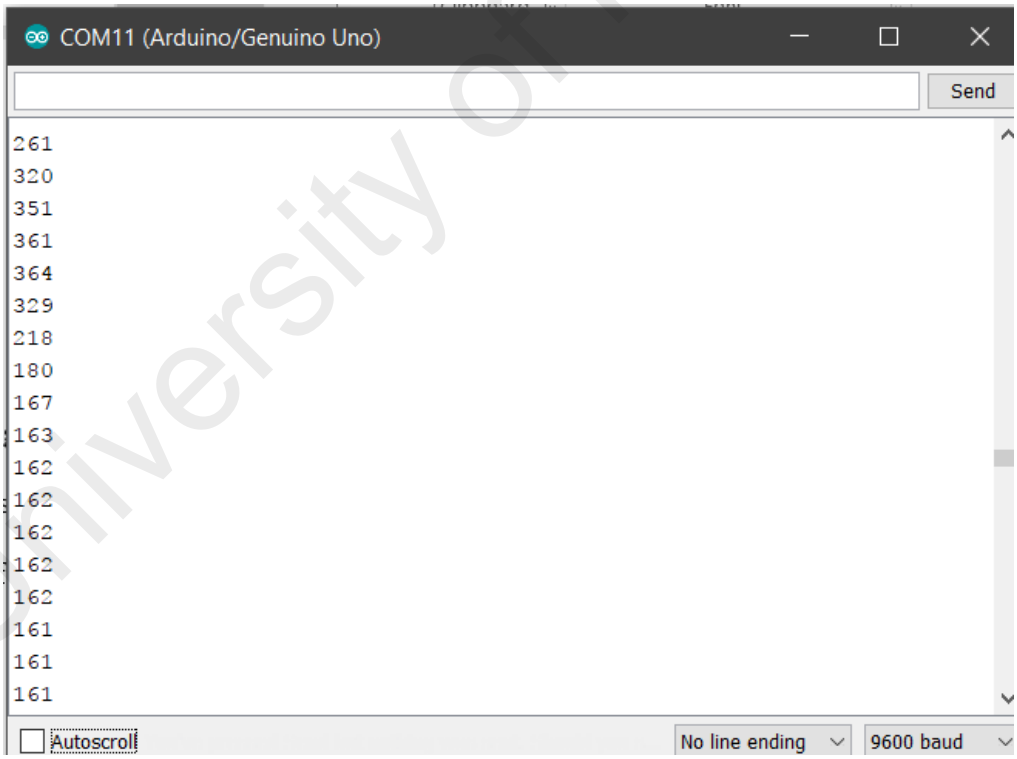

Figure 3.9: Serial input values of the US sensor

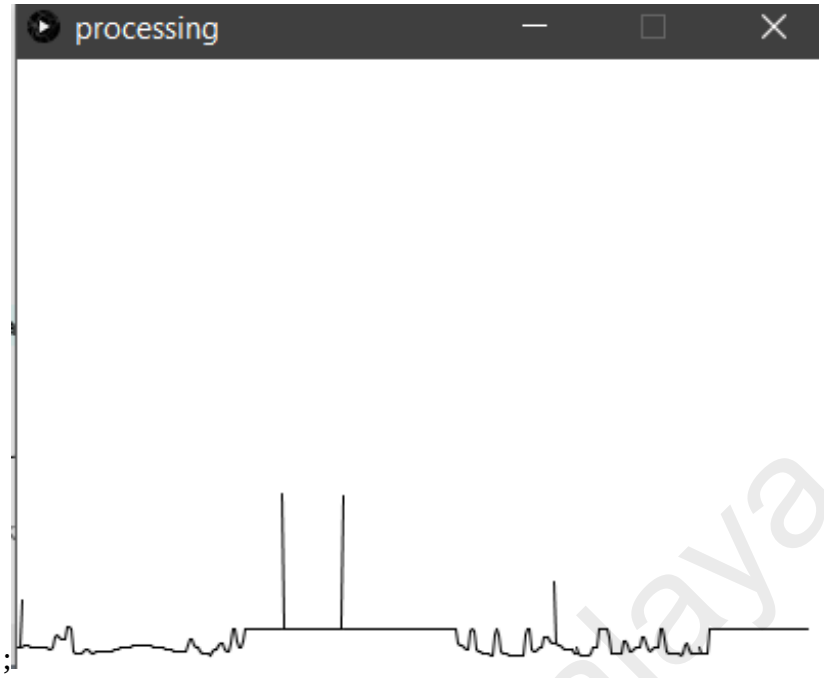

Figure 3.10: Visualisation of the US sensor analog output

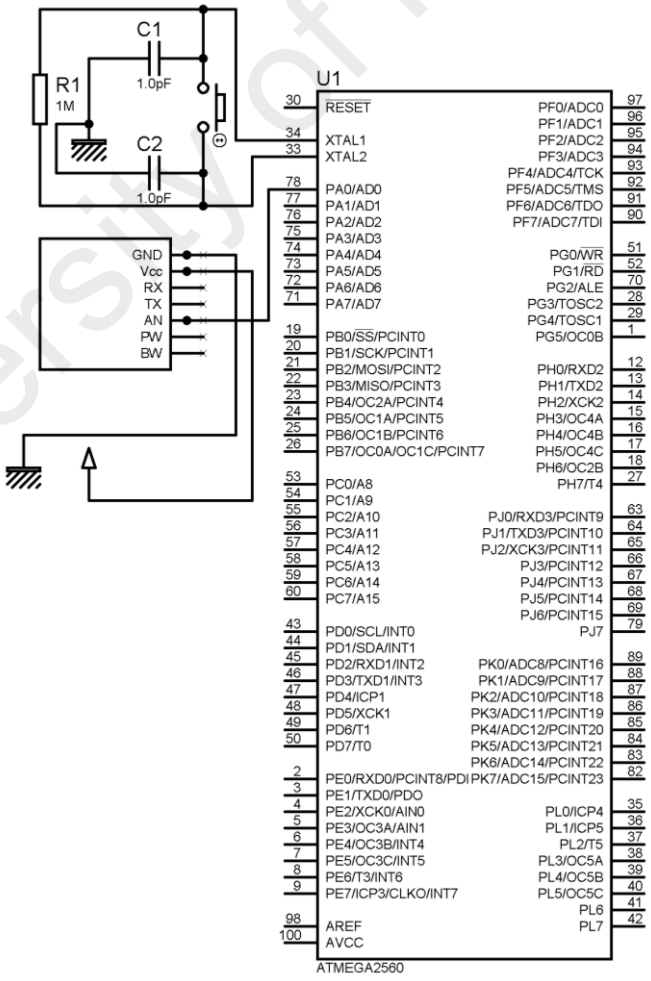

Figure 3.11: Circuit diagram of Ultrasound sensor connections

Figure 3.11 above shows the circuit diagram of the US sensor connected to the microcontroller. This US sensor contains 7 pins however, only 3 pins were used for the testing, the other pins were designated for wire communication between the microcontroller and sensor. The use of wire communication might lower the noise in the signal however, the sampling rate of the data would drop significantly due to a number of clock cycles needed to convert the bytes back to decimals. One major issue with using US sensor is sensitivity range. Even though this sensor can provide highly accurate data, the reliability and accuracy of the sensor will fall off if it is used in less than 15 cm (6 inches) from the target. Due to this issue, after a few tests, this method was rejected as it did not provide any acceptable results.

3.3.3 MEMS accelerometer

Two types of accelerometers were mainly focused in this study, MPU6050 and ADXL345. Both sensors are highly accurate and power efficient and are used in smart phones as well as other low power hand-held devices. However, each has its own unique property which needs to be evaluated and analysed. This study mainly focuses on accelerometers as they are the primary sensor required for detecting vibrations.

ADXL 345 could provide 3-axis accelerometer digital signals which could be obtained from the I_2C outputs pins (Figure 3.12). The analog values could be obtained and converted using ADXL345 built-in ADC or an external 10-bit ADCs. However, the ADXL345 on its own can support 10-bit sensitivity so a built-in ADC would suffice. After the conversion of the analog signals, I_2C protocol conversion sequence could be used to convert the row values to angel values. After obtaining the raw decimal values, converting them to actual angular change values might not be necessary since in this study, the same raw data would be obtained from all subjects and tested relative to each

other. This also allowed for lesser programming lines and faster data logging. Datasheet and necessary information about ADXL345 are provided in Appendix A, Section 3.1.

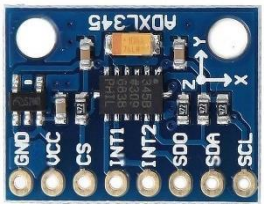

Figure 3.12: ADXL345 3-axis accelerometer

MPU6050 is a more popular option as it contains 6-axis mixed accelerometer and gyro with built in signal stabilization and ADC (16 bit) as shown in Figure 3.13. This allows for more stable signal output while avoiding any noise from outside sources, since the signals will be converted right after it is produced. Although MPU6050 has many features, it can only be connected to a microcontroller through I_2C connection, similar to ADXL345. Detailed specifications are provided in Appendix A, Section 3.2.

Figure 3.13: MPU6050 6-axis accelerometer, gyro

MPU6050 uses relatively lower voltage for power efficiency at 2.25 to 3.3 volts and to use this sensor on Arduino, voltage regulator is required to step down the input voltage from 5.5 volts generated from Arduino to 3.3 volts. This can easily be done by selecting a suitable PCB which contains voltage regulator for the MPU6050 to mount on. MPU6050 system on a chip (SoC) has contained preinstalled firmware to allow for special functionalities. The functions are as follows:

- BlurFree™ which is used for software or hardware image stabilization on phones and professional cameras
- MotionCommand™ for gesture system control
- InstantGesture™ gesture recognition
- Toys
- Wearable sensors for health, fitness and sports

Adding such features to the sensor is only possible via Digital Motion Processing™ engine built around the sensor. This engine is able to use all existing sensors (accelerometer, gyroscope and temperature) on the SOC (system on the cheap) to create a virtual 3D environment and by detecting the direction and intensity of the vibration, as well as determining the types of motion.

There are many differences between ADXL435 and MPU6050 and Table 3.3 below shows the key differences.

Table 3.3: Comparison between ADXL345 and MPU6050

Description	**ADXL345**	**MPU6050**
Communication type	I_2C	I_2C, SPI
Operating voltage	5v	3.3v
sensors	ACC	ACC, GYR, TEMP
Output resolution	10-bit resolution	16-bit resolution
Max acc output data rate	3200 Hz	4500 Hz

A test was performed on these two sensors in determining which can provide more reliable and higher speed data logging. Both sensors were connected to the same microcontroller (ATMEGA 2560) while a similar programming code was written to read the data from sensors and log them into the computer in a duration of 5 seconds. MPU6050 would require a selection of registries to be enabled for I_2C data transfer protocol while ADXL345 has a I_2C transfer protocol previously enabled through library

already available in Arduino IDE. Both sensors were connected to the microcontroller through I_2C port. After monitoring the data collection, the signals were visualised using processing software. Figure 3.14 shows the circuit diagram of the connection between the ADXL and MPU modules to the microcontroller.

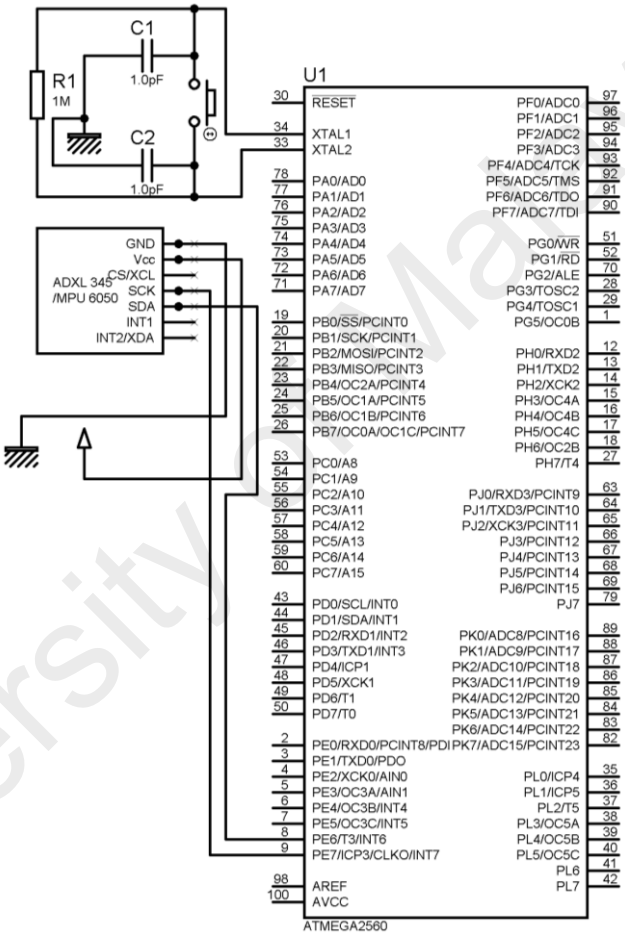

Figure 3.14: Circuit Diagram of the accelerometer sensor connected to microcontroller through I_2C connection

Arduino IDE library has a pre-existing registry map for ADXL345 that can help minimise the coding complexity even though it does not contain many registry addresses. The only two customisable parameters are the operating power and output type which can directly affect the sampling rate and output parameters respectively. Table 3.4 represents the registry value which can control the input power and clock

speed of ADXL435. For this present study, the highest clock speed was selected to get the most accurate reading. The programme coding to test the ADXL sensor is provided in Appendix B, Section 2.1.

Table 3.4: Register codes to control ADXL345 clock speed

Output Data Rate (Hz)	Bandwidth (Hz)	Rate Code	I_{DD} (μA)
3200	1600	1111	145
1600	800	1110	100
800	400	1101	145
400	200	1100	145
200	100	1011	145
100	50	1010	145
50	25	1001	100
25	12.5	1000	65
12.5	6.25	0111	55

Table 3.5: Special registry values of MPU6050 for accelerometer activation

Programming code	Value
MPU6050_I2C_MST_CTRL	0x19
MPU6050_I2C_SLV0_REG	0x1A
MPU6050_I2C_SLV0_CTRL	0x1B
MPU6050_I2C_SLV1_ADDR	0x1C
MPU6050_I2C_SLV1_REG	0x1D
MPU6050_I2C_SLV2_CTRL	0x1E
MPU6050_I2C_SLV3_ADDR	0x1F
MPU6050_I2C_SLV3_REG	0x20
MPU6050_I2C_SLV3_CTRL	0x21
MPU6050_I2C_SLV4_ADDR	0x22
MPU6050_I2C_SLV4_DO	0x23
MPU6050_I2C_SLV4_CTRL	0x24
MPU6050_I2C_SLV4_DI	0x25
MPU6050_I2C_MST_STATUS	0x26
MPU6050_INT_PIN_CFG	0x27
MPU6050_INT_ENABLE	0x28
MPU6050_INT_STATUS	0x29
MPU6050_ACCEL_XOUT_H	0x2A
MPU6050_ACCEL_XOUT_L	0x2B
MPU6050_ACCEL_YOUT_H	0x2C
MPU6050_ACCEL_YOUT_L	0x2D
MPU6050_ACCEL_ZOUT_H	0x2E
MPU6050_ACCEL_ZOUT_L	0x01

MPU6050, unlike ADXL345, does not have a built-in library in Arduino IDE. This sensor also, unlike ADXL345, has many registries which require individual configuration to use it effectively. Table 3.5 shows the registry values selected for most important registries (refer Appendix A for more details on register information). Based on the programming for both sensors, flowcharts for ADXL345 (Figure 3.15) and MPU6050 (Figure 3.16) are provided below. For higher serial communication between Arduino and computer, 15200 baud rate transfer bandwidth was selected.

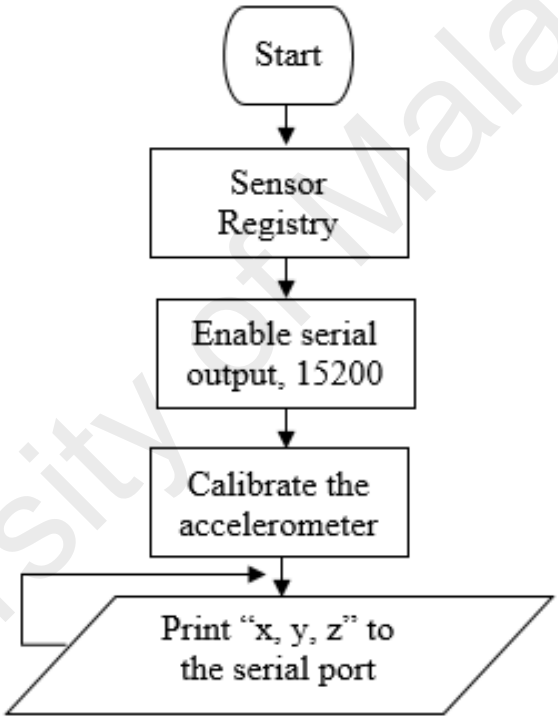

Figure 3.15: Flowchart of accelerometer testing

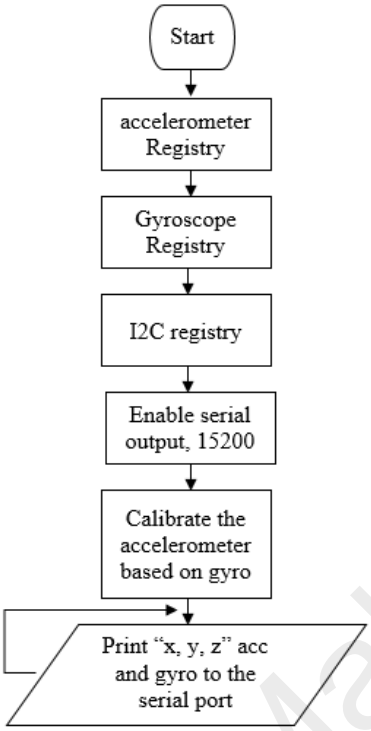

Figure 3.16: Flowchart of the MPU6050 testing programming

To test the vibration sensors, we prepared a sensitivity test by placing the sensors on a rigid table and tapped on the other far end of the table. Data captured through a serial monitor is shown in Figure 3.17 and the visualisation of the data through processing is shown in Figure 3.18.

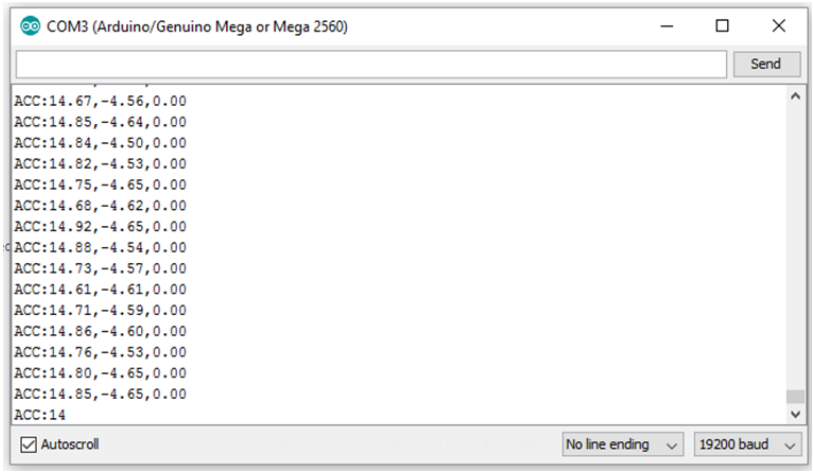

Figure 3.17: Data captured through accelerometer sensor

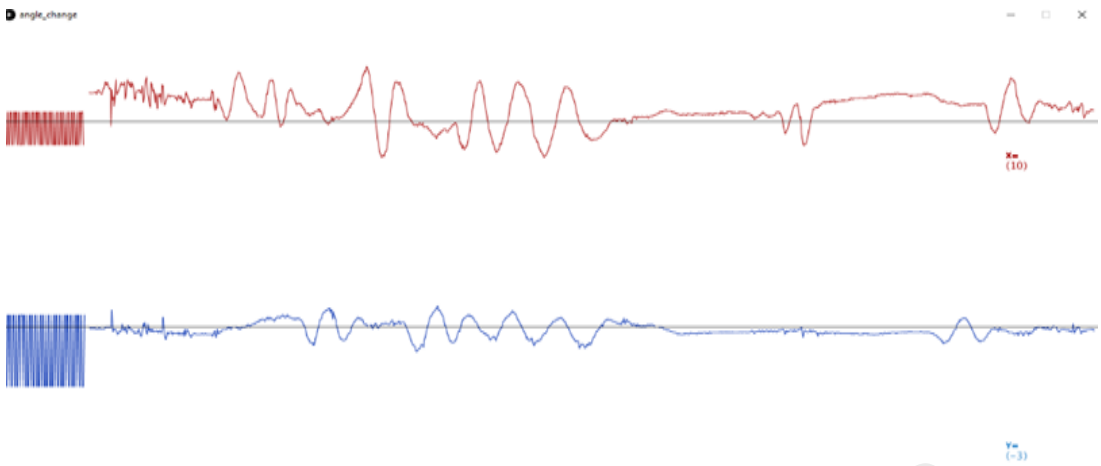

Figure 3.18: Visualised accelerometer data through processing

After tests performed on each sensor, both were able to provide close to 750 samples per second (S/sec). The goal of this study is to obtain 1000 S/sec and above in each test to avoid any possible data loss. To address the slow sampling rate, further tweaking and overclocking on the MPU6050 chip was performed and its sampling rate increased close to 1300 S/sec. However, the clock rate and sample rate of the ADXL345 remained consistent even after tweaking and overclocking on the chip which could be the results of limited functionality of the sensor. ADXL345 was designed for ultralow power use in detecting mobile phone orientation and its use for precise vibration detection is not practical. On the other hand, MPU6050 contains many features such as accelerometer, gyroscope, temperature sensor, and signal conditioning. By turning off the extra provided features, the accelerometer sampling rate can be increased beyond its usual limit.

3.3.4 Selecting the most suitable sensor

Based on the usability, durability and accuracy of the sensors, MPU6050 was proven to be the best choice in building the prototype for VAG of the knee signal capture. This sensor was on for the first prototype and by monitoring its performance, further changes were done to the second prototype.

The main problem faced in performing the sensor selective test was the limitation of the Arduino's serial port communication speed to the computer. Arduino Mega uses a secondary microcontroller to add serial protocol to the data transmitted by the main controller (ATMEGA 2560) and enables it to communicate with the computer through USB. However, the clock rate of the serial port through the secondary IC was significantly lower than the main microcontroller. This would cause a technical software problem called data mudding where data must be buffered in the microcontroller's Static random-access memory (SRAM) to be transferred to the secondary IC when it is done transmitting the last data (which is only 1K byte in capacity) resulting in loss of data while they are replaced in the SRAM due to overload. This problem can be resolved by directly saving the collected data through an SD card or sending them directly through WIFI. Table 3.6 shows the differences between each sensor tested.

Table 3.6: Difference between sensors

	Sampling speed/s	**Input type**	**durability**	**Accuracy/ rating**		**Noise reduction**	**Cost (RM)**
Piezo element	2000	analog	Very bad	Good	±0.5v	NA	12
Ultra Sound	2000	analog	Very good	Very bad	±0.35v (1 to 5 meters)	NA	30
ADXL345	708	I_2C	Good	Very good	±0.43º	yes	35
MPU6050	1300	I_2C/ SPI	Good	Very good	±0.13º	yes	60

3.4 FIRST PROTOTYPE CONSTRUCTION

The first prototype was built after selecting the suitable VAG sensor. Many other decisions such as the use of SD card for data logging were made in the middle of prototype construction to solve limitations faced which will be explained briefly at the end of this chapter.

3.4.1 SD card module

ATMEGA 2560 microcontroller contains several IC to IC communication ports such as Serial Peripheral Interface (SPI) and I_2C. SPI on ATMEGA can work at clock speed of 15M Hz, a much higher speed compared to the serial port (1 Mhz at max). Higher transfer speed enables the microcontroller to use the full potential of the accelerometer sampling rate without the loss of any data. For SD card memory module as well, the only means of communication is through SPI communication. Figure 3.19 shows the name of the pins available on the SD cards.

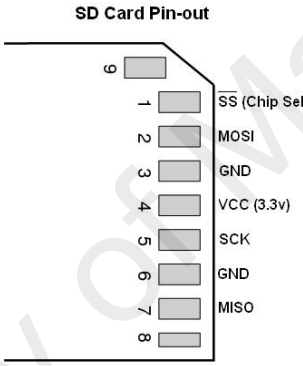

Figure 3.19: Standard SD card SPI pin-out

The speed of the SD cards can be calculated with their classification labels. SD card classification marks can be found on the SD card itself. The classes C2, C4, C6, and C10 refer to the speed of the SD card directly which are 2MB/s, 4MB/s, 6MB/s, and 10MB/s respectively and are called speed class. From 2014 onwards, new classes were introduced namely U1 and U3 which are made for 2K resolution high speed video capture as well as 720p ultra-highspeed video capture (more than 500 frames per second). The U1 and U3 represent 10MB/s and 30MB/s respectively and are classified as the ultra-high-speed class or UHS class. From 2017 onwards, a new class was introduced for the 4K & 8K 60 frame per second video capture. This class is called

video speed class and classified as V30, V60, and V90 which can store data at speed up to 90MB/s.

For this study, a C6 SD card would suffice as the microcontroller SPI port speed could not exceed 4MB/s. SD cards use a standardised 3.3v input power and for ease of use, an SD card module was used in this study to both regulate the voltage and ease SD card swap if necessary. Figure 3.20 shows the circuit diagram of the SD card connections to the microcontroller. The programming on Arduino IDE for SD card data capture was simplified using the existing SPI communication library. Simple commands such as “read” and “write” would enable the microcontroller to read or record data on the SD card. The SD card works in a similar way to filing system where a specific file with specific name and format must be created before data are written to the SD card. If the microcontroller breaks the connection with the SD card (in case of removing the SD card) before the program closes the file, all the written data will be deleted automatically. A “close file” command must be written after data capture is complete.

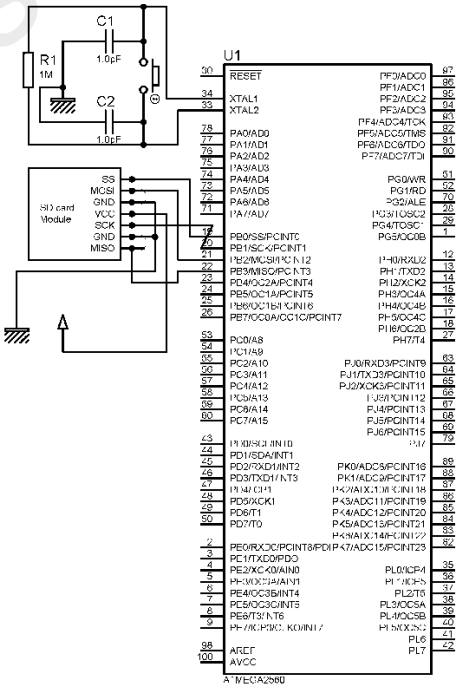

Figure 3.20: Circuit diagram of SD card module connection to the ATMEGA

3.4.2 Main circuit board construction

The data logger's main circuit board is equipped with SD card, control button, LEDs, and connection wires from the sensor to the circuit board. The passive elements were mounted on the soldering board and soldered to the board following the pin arrangement (from datasheets). The technique used to mount the solder board on top of the Arduino was inspired by the Arduino shields. Arduino shields are augments which contain several compartments that can easily be mounted on the Arduino and used seamlessly. Figure 3.21 shows the block diagram of the simplified overall circuit used to build the data logger circuit. Meanwhile, Figure 3.22 shows the actual circuit design after the circuit board was mounted on the Arduino Mega.

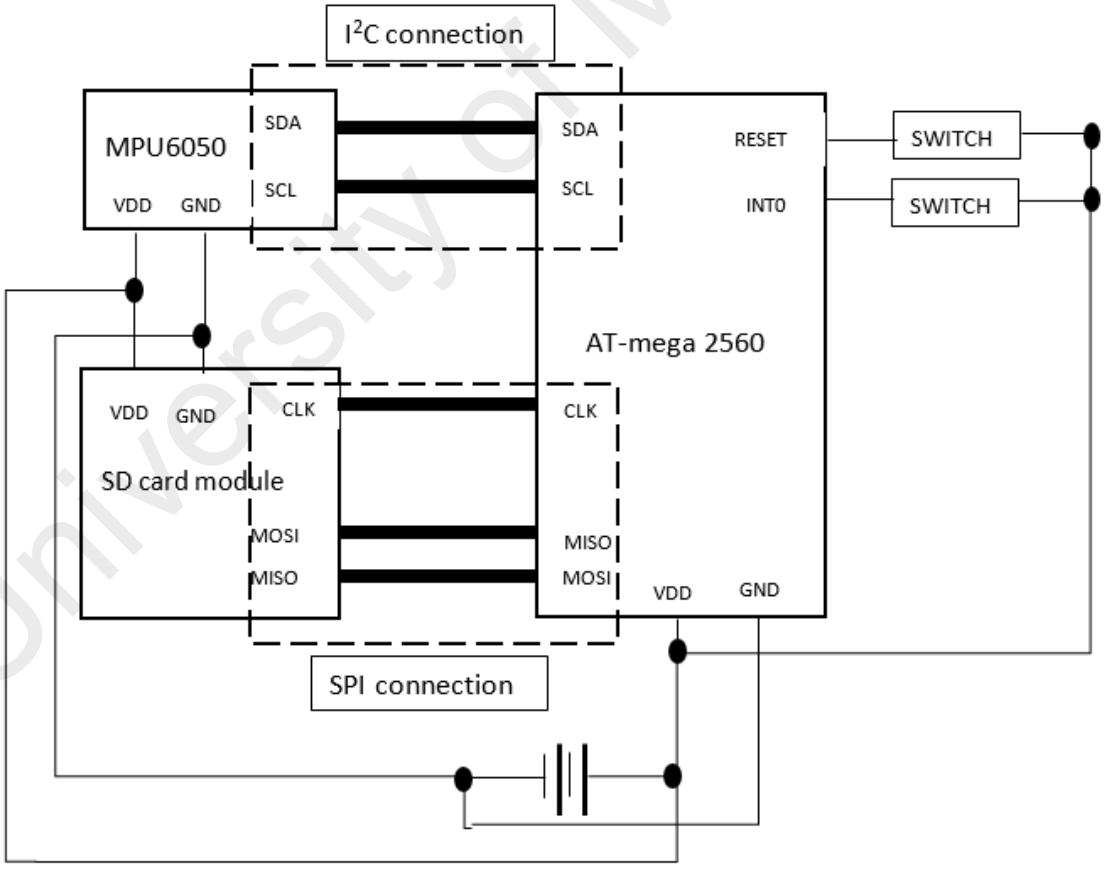

Figure 3.21: Block diagram of data logger circuit design

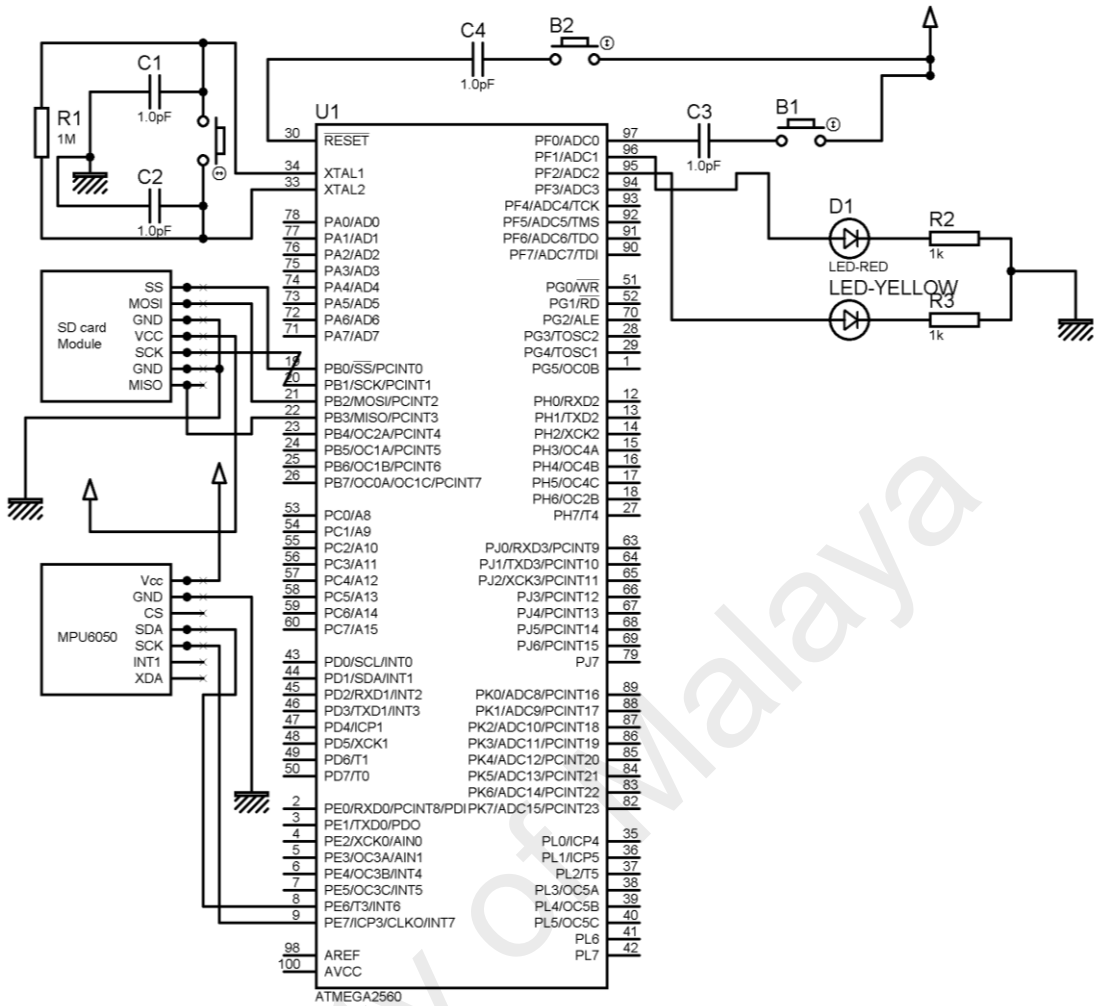

Figure 3.22: Circuit diagram of the first Data logger prototype

As shown, the circuit collected the row vibration data and stored the logged data in the SD card. Transferring data using wire serial communication directly to the computer could lead to data loss as the wire communication transfer speed is much slower (lower bit rate) than the data capturing speed from accelerometer. The Accelerometer was connected using I_2C communication system. The data acquired from the accelerometer were then stored on the SD card. The start switches on the shield, before connecting to the input of the microcontroller, was connected to a small capacitor. The capacitor would apply small delay after the button was pressed, blocking false signals to the microcontroller. AT-MEGA 2560 was the microcontroller used and is an 8-bit Atmel microcontroller which could operate at 16 MHz clock speed. The control switches were

placed to start the data recording and to restart the data recorder after the data capture was completed. Figure 3.23 shows the final soldered circuit board and Figure 3.24 shows the circuit board mounted on the Arduino Mega.

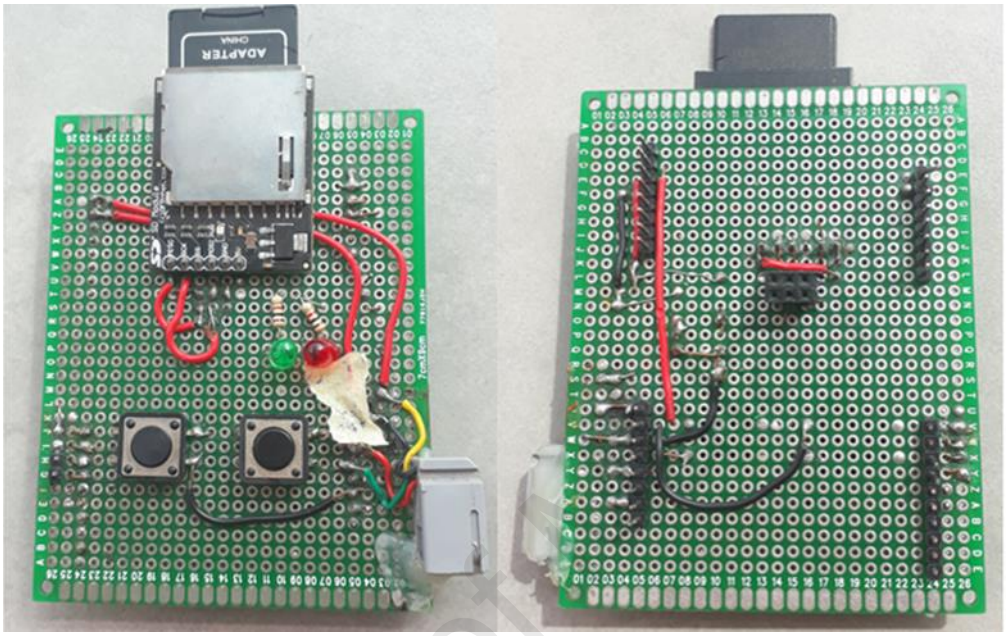

Figure 3.23: Circuit connection of the data logger parts on the solder board

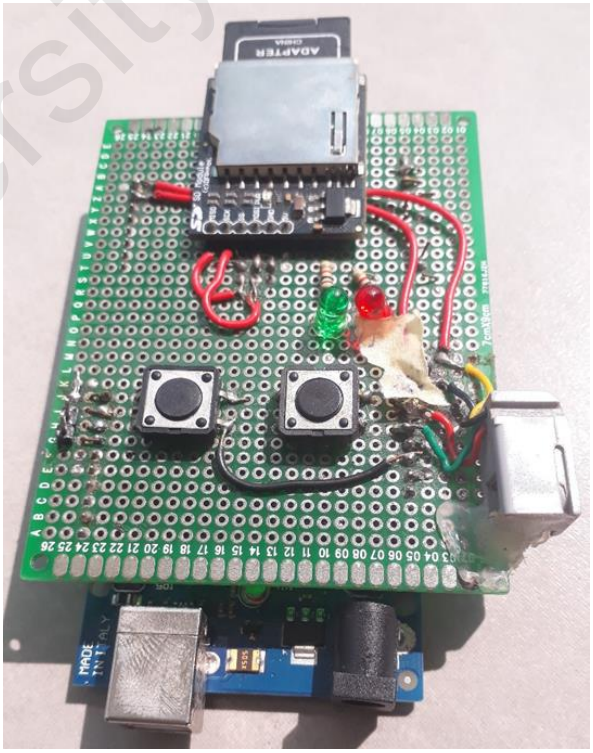

Figure 3.24: Solder board mounted on the Arduino Mega

The process of data capture on patients followed the standardised sit-stand–sit test procedure with a slight modification. This was done by adding specific resting points throughout the duration of test. In total, the test took about 7 seconds to accomplish. Figure 3.25 shows the sit-stand-sit procedure which was used for data acquisition during this research. The test procedure was as follows: before the test started, the subject should have ensured that while sitting, the feet were flat on the ground. The subject remains seated for one second after the start button had been pressed, then the subject stood up for 2 seconds and then remained in standing position for one second and continued to sit down for 2 seconds. The delay between standing up and sitting down was important as it could later be used to identify the exact time the subject performed a specific action in the test, during signal analyses.

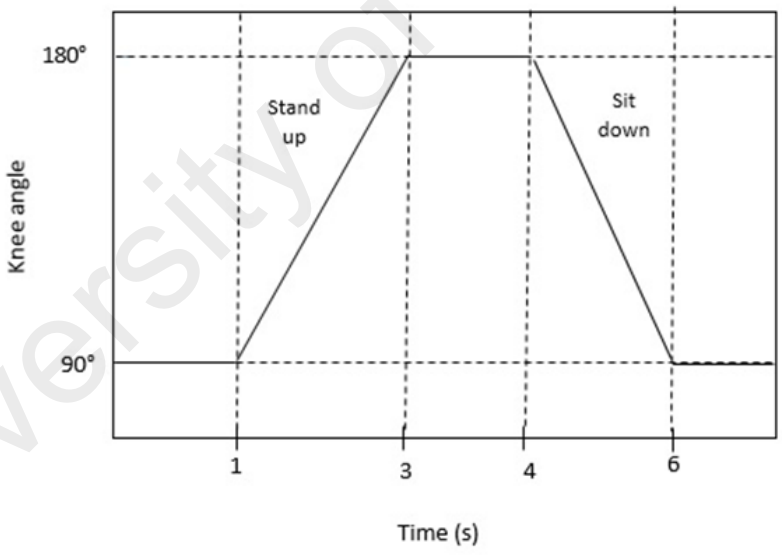

Figure 3.25: Time interval graph of sit-stand-sit test

3.4.3 First prototype programming

AT-Mega programming was modified throughout the testing to find an optimal way in recording the subject's VAG signals in a sequential manner. The final programming was done based on the LED guiding system which guided the subjects on when to stand up and sit down during data capture. The LEDs were also used for troubleshooting and

system component checking before capturing the VAG signals. The following flow chart in Figure 3.26, explains how the system checking, troubleshooting, and data capture were done. The programming code is also available in Appendix B Section 3.1. It should be noted that the programming for MPU6050 was stored in a specific library called “MPU6050.h” for easier access and faster operation. The flowchart of Arduino programming is shown in Figure 3.26.

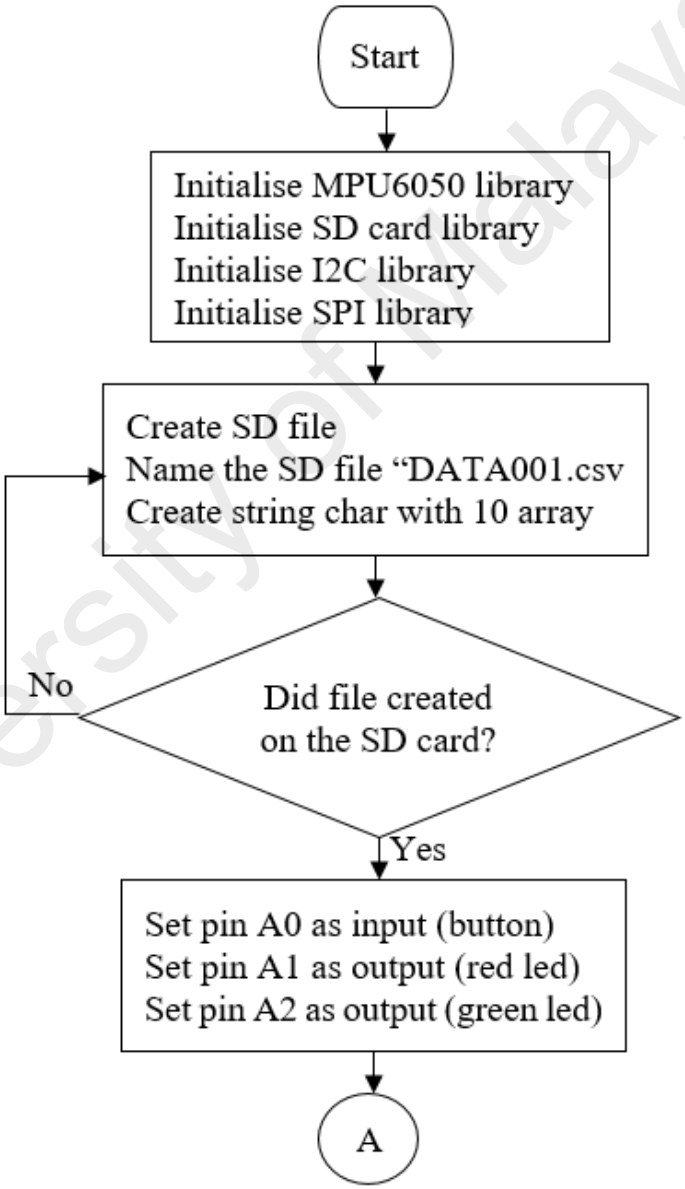

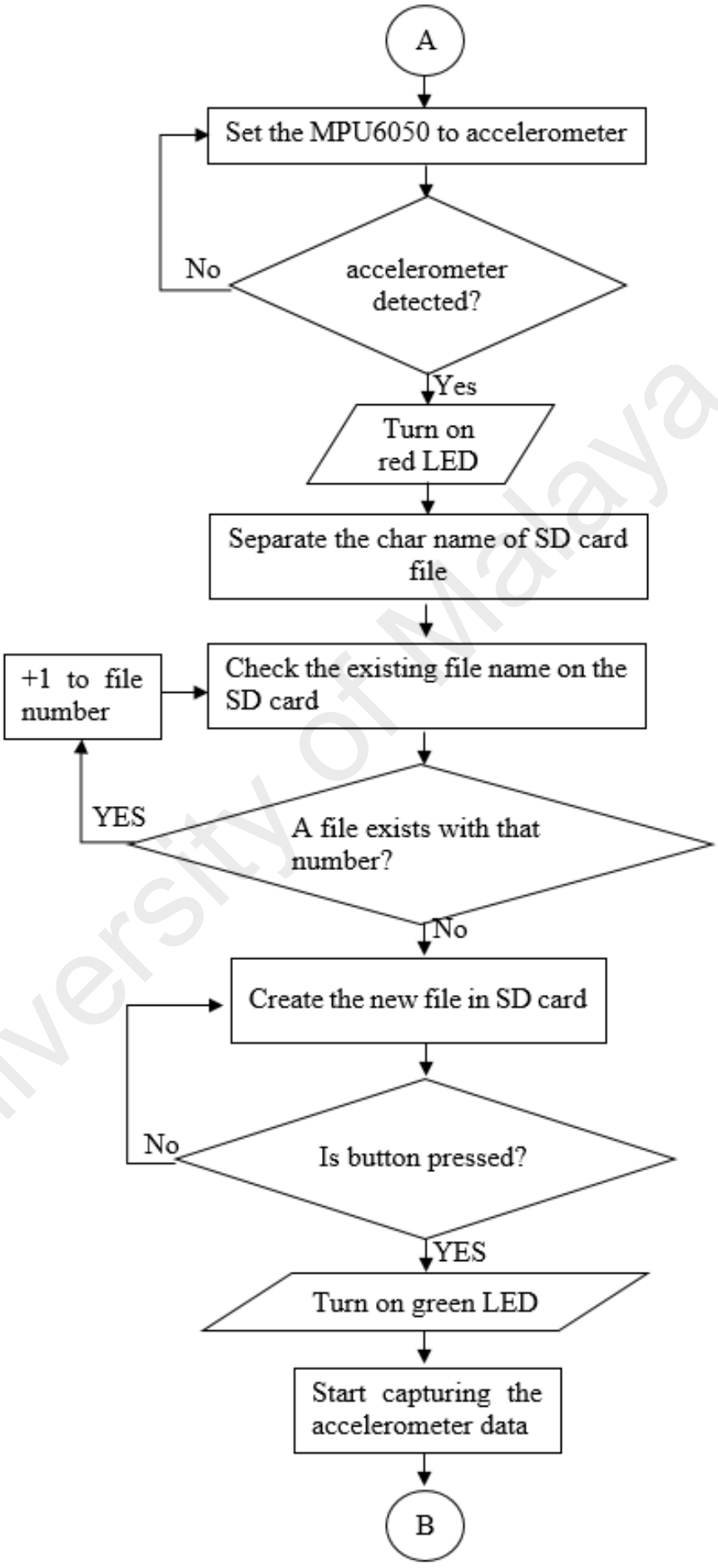

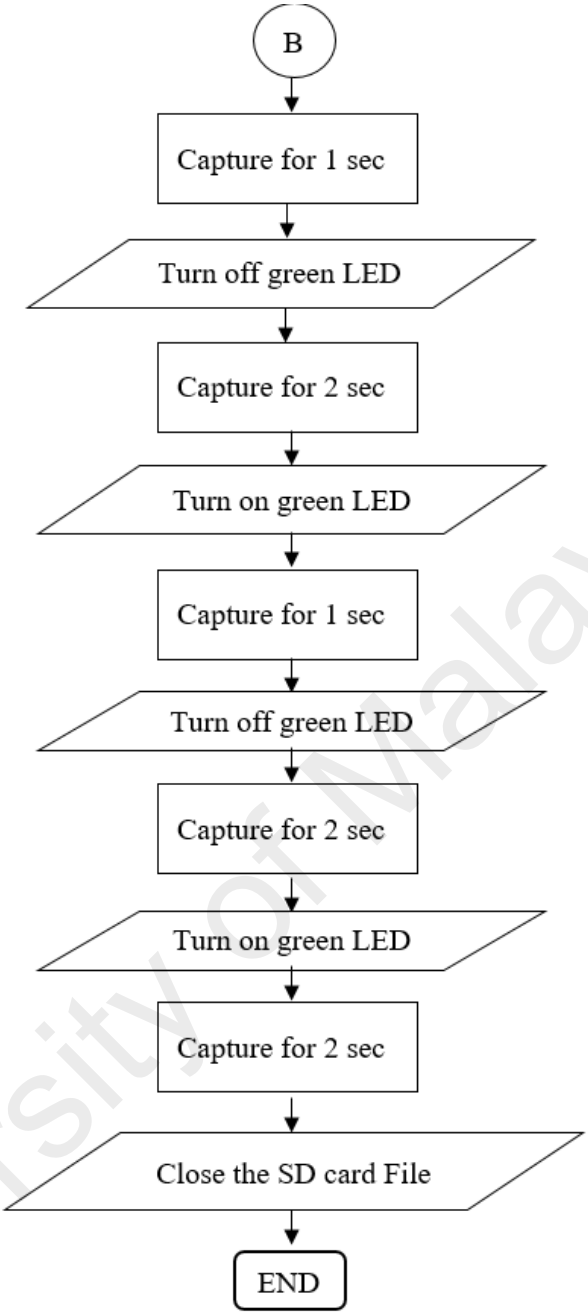

Figure 3.26: Flowchart of first VAG data logger prototype

The process of data capture based on LED guiding system (as shown in the flowchart above) was as follows: when the capture button had been pressed, the green LED turned on indicating that the subject should remain in his position (standing or sitting). When the LED turned off, the subject should by then be slowly standing up. When the LED turned on again (after two seconds) the subject should be fully standing up. After one

second, the LED turned off again and the subject should have been sitting down at the same speed he was standing up.

3.4.4 Problems faced

Many problems were faced during the construction of the prototype which were fixed while performing the first prototype data acquisition. However, the major unavoidable issues faced were the wiring of the sensor and data capture clock speed.

The MPU6050 was mounted on the knee while the subject performed the sit-stand-sit test. In the early prototype, the four wires were directly soldered to the sensor and repetitive movements of the wire could cause breakage of the solder joint and corrupt the captured data. The wire itself was over 2-meter long without signal shielding. This caused large noise in the signal especially when it was near to the hospital equipment. This problem was temporarily fixed by using noise proof audio cables with a 4 channel-audio-jack plug and header directly soldered to the sensor. After changes to the wire and connection were done, the signal noise dramatically reduced however, the connection breakdown issue was still present.

The second major issue faced was the microcontroller clock speed which had unstable clock rates when using the crystal oscillator. The uneven clock rates directly affected the data capture sequence where the total collected samples could have varied from 8000 samples per seven seconds to 10000 samples per seven seconds. This had caused many problems while performing the signal analysis due to varying frequency ranges.

3.5 SECOND PROTOTYPE CONSTRUCTION

For the first prototype after collecting and examining data, the results showed many flaws in the system mainly because of wiring connection issues. The data capture of the

second version of prototype started with added objectives based on the properties of the findings of the first version of prototype. The new objectives stated:

- Noiseless data capture
- Synced data logging clock rate between left and right knees simultaneously
- Captured the data while the subjects were moving up and down the stairs

The added objectives required a second VAG data logger working at the same time with the first data logger where each collecting VAG signals of one specific knee (either left knee or right knee). Figure 3.27 shows the overall block diagram of the new prototype.

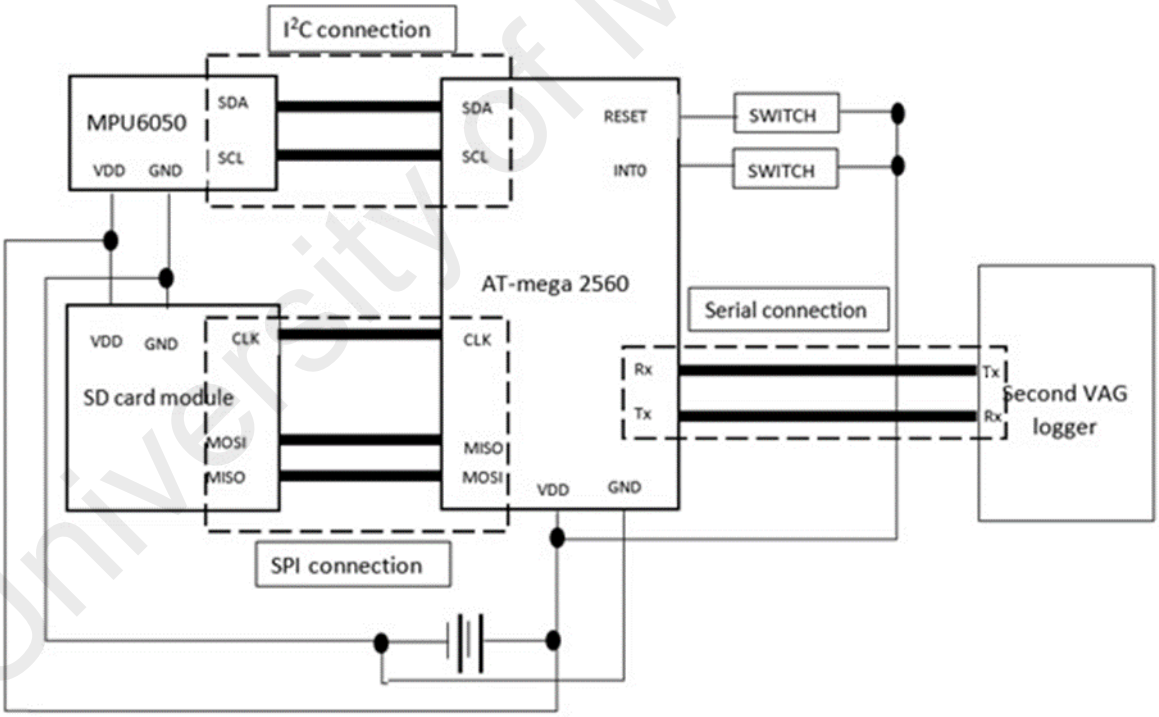

Figure 3.27: Second version prototype block diagram

Both data loggers were built similarly with minor differences. The data logger used for the first version of data acquisition was reused and named primary logger for measuring the VAG signals of the right knee specifically. Meanwhile, the new data logger named as secondary logger was appointed to the left knee specifically. The

secondary data logger contained extra LEDs as well to indicate that the connection to the primary logger had been established.

The data loggers were connected to each other through 2 digital I/O pins on the microcontrollers (pins 11 and 12). The initialisation of the SD card and MPU6050 in the programming for both data loggers were implanted similarly with added protocol for data loggers syncing behaviour to start and capture data at the same time. Capturing data while going up and down the stairs as well was performed by adding a secondary measurement method which did not rely on the time sequence that the sit-stand-sit test would require.

Portability of the prototype became of importance while performing the stair test. However, the early prototypes were only powered by the USB connection to PC. To improve portability of the prototype , the two Arduinos were connected to the dual channel Power bank via USB port.

The programming used for the second prototype was divided into three sections which are presented in the flowcharts: data logger sequencing programming as well as data capture mode selection (Figure 3.28), improved sit-stand-sit test programming (Figure 3.29), and stair test (Figure 3.30). The Arduino programming codes are available in Appendix B Section 3.2 for primary logger and Section 3.3 for secondary logger.

The first section of the programming was communication between the two data logger initiation. The method of communication establishment programming was inspired by the HTML server-client communication method. This was done by selecting two digital I/O pins where pin 11 on primary logger was selected as the transmitter pin and secondary logger was selected as the receiver pin while pin 12 was set vice versa

for both. The communication was established at the beginning of the microcontroller start up by sending and receiving communication confirmation. If the primary logger button is pressed, both data loggers would start the sit-stand-sit test at the same time and if the secondary logger button is pressed, the stair test would begin on both data loggers.

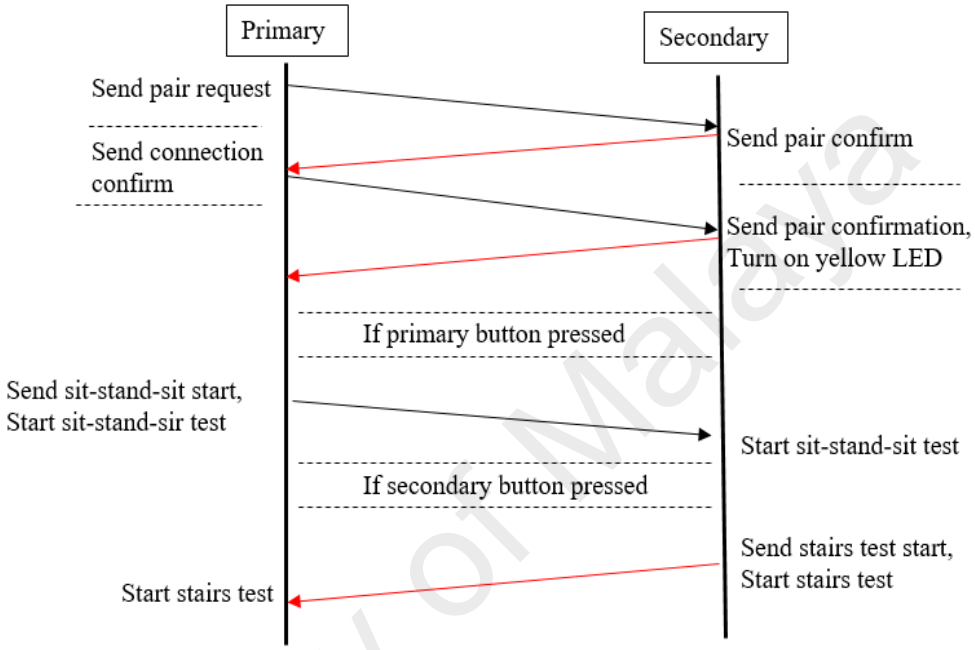

Figure 3.28: Primary and Secondary Data logger communication schematics

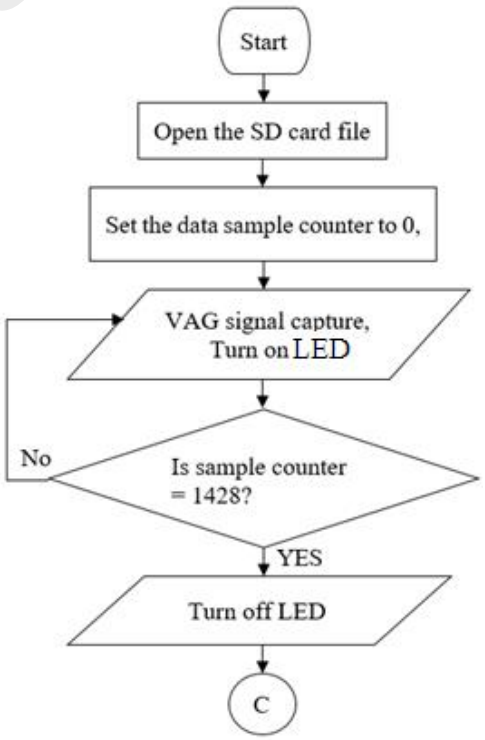

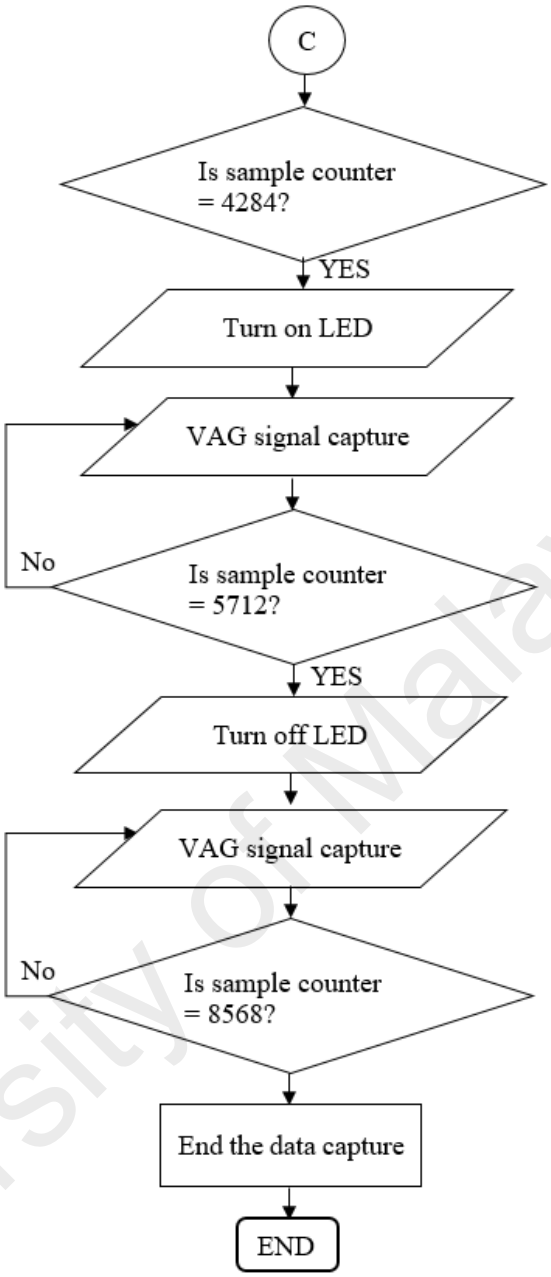

Figure 3.29: Flowchart of modified VAG data capture method

The modified data capture coding was designed to correct the clock speed issue faced in the first prototype. The issue was resolved by relying on the sampling data count instead of relying on the microcontroller clock speed. Assuming the total sample size after a complete capture in 7 seconds was 10000, each second of data captured would consist of 1429 data samples. By counting the data samples, the sit-stand-sit sequence could be accurately calculated thus, guiding the subjects to perform sit-stand-sit test

through LED guide accurately and obtained consistent 10000 sample size from all subjects.

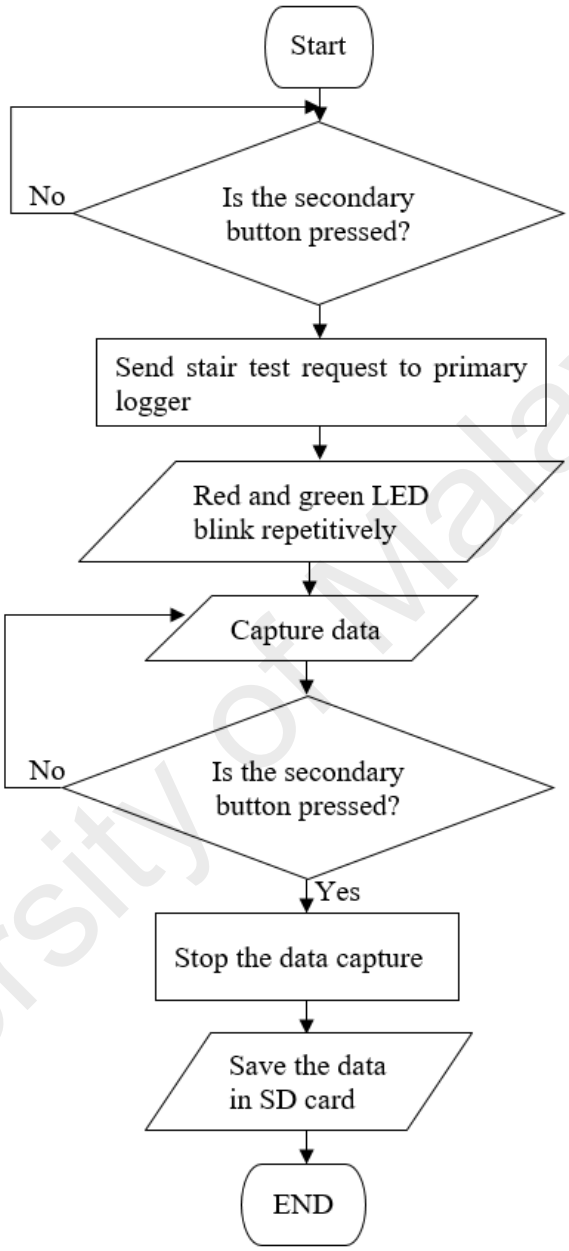

Figure 3.30: Stair test programming Flowchart

As can be seen Figure 3.30, the stair test, unlike the sit-stand-sit test did not rely on the timely sequence. After pressing the secondary data logger button, both data loggers started capturing data at the same time, while the subject was moving freely up and down the stairs. When the button was pressed again, the data capture ended.

To resolve the hardware wire connection issue faced at the first prototype, other wire connection methods such as USB, parallel port, and telephone wiring were investigated. After experimenting with different physical data connection ports and plugs, the telephone wiring and port was the most suitable option. Similarly, for MPU6050, the telephone cable is capable of carrying 4 wires and telephone wires by default are twisted inside the cable to nullify the outside noise which made them suitable for this study. The telephone cable connection port can also be mounted on top of the knee band so that it could remain motionless while knee testing is performed, ensuring no connection break would occur. Figure 3.31shows the second prototype complete with telephone wire connection.

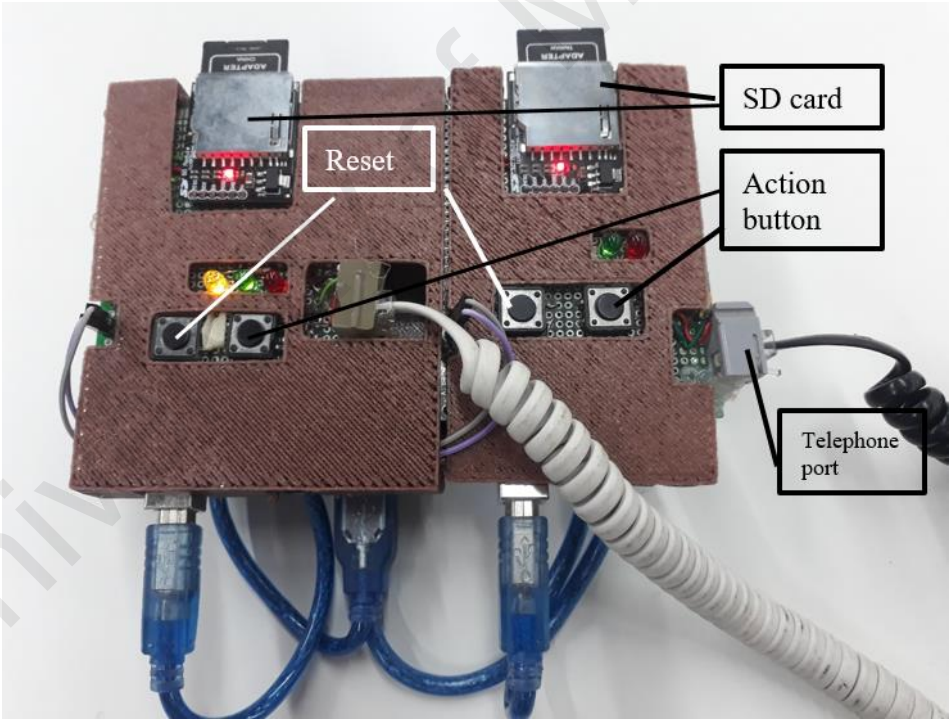

Figure 3.31: Completed second prototype data logger with telephone wire connection

3.6 SENSOR BAND

Sensor band is another essential component for capturing the VAG signals from knee joints. During the test, sensor should remain motionless on the knee while having a direct contact to the knee. Even the slightest sensor movements can corrupt the data captured and void the results. Furthermore, movements of the sensor as well may alter the hardware wire connection and produce noise or break the soldering. The following list states the properties required for the knee band:

- The sensor band should follow the safety standards. These include no direct contact between the sensor and subject's skin as well as no static electricity produced by the sensor or sensor band.

- The sensor band should be comfortable to be worn.

- The sensor band should be designed to be placed under the open patella knee support band as well as on the mid patella.

- The sensor band should have a fixed accelerometer placed at one specific position throughout the test and no noise should be produced from the movement of the accelerometer inside the sensor band.

The sensor bands for this study were created using 3D printer by using 0.18 mm soft rubber materials. Several stages were taken in creating the sensor bands where newer version of the sensor band improves on the previous version. Figure 3.32 shows the first knee band prototype used for testing the sensor and pre-hospital testing.

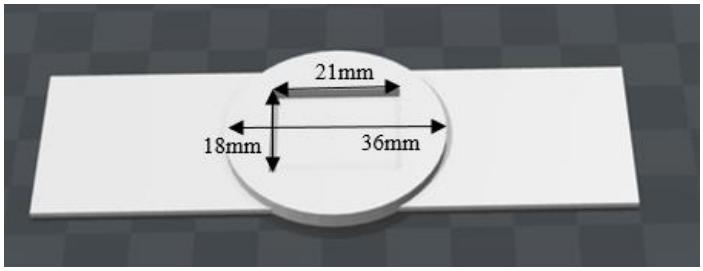

Figure 3.32: First knee sensor band prototype

The first sensor case had many issues. As shown in Figure 3.33, the sensor was glued to the sensor case with general purpose adhesive. Due to the low depth of the sensor band, while bending knee, the excessive pressure on the sensor had pushed the sensor out. The sensor case was not able to be placed properly on the knee at an extreme knee bend and moved freely. This issue was fixed by increasing the depth of the sensor pad adding more support area under the knee band.

Figure 3.33: Printed first prototype sensor band and its placement under knee band

Figure 3.34 shows the designed sensor band used for the first version of data acquisition. However, the sensor band faced issues regarding the noise produced by the sensor band itself. The thickness of the layer between the sensor and knee was found to be large which could not allow all the vibration to be transferred to the sensor.

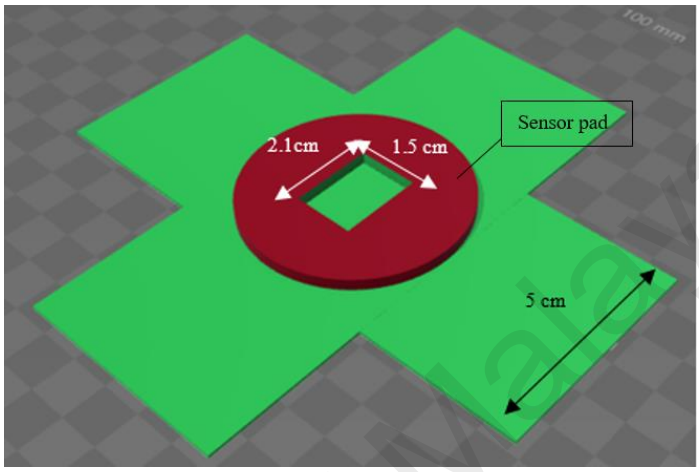

Figure 3.34: First prototype datalogger VAG testing sensor band 3D design

The second data acquisition from the data logger addressed all the issues and the newly designed sensor band had fixed the problems faced. To resolve the sensor band noise, arches around the sensor pad were risen significantly and the thickness of sensor pad where it touched the skin was lowered to 0.05 mm from 0.8 mm. Figure 3.35 shows the final 3D design of second data logger sensor band and Figure 3.36 shows the method of wearing the knee band.

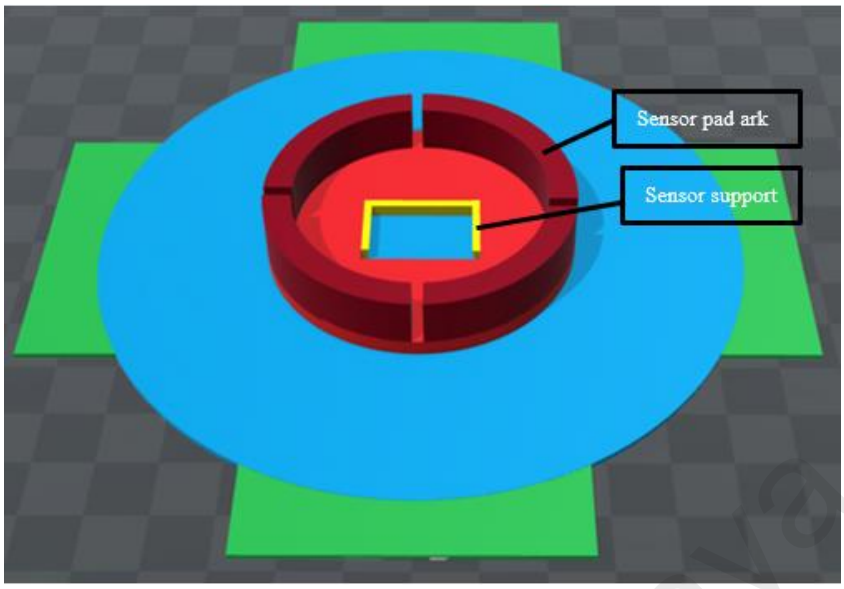

Figure 3.35: 3D design of the second version datalogger sensor band

Figure 3.36: Method of wearing the knee band equipped with sensor band

3.7 DATA ACQUISITION

Data acquisition was performed collaboratively with the Department of Sports Medicine, University of Malaya Medical Centre (UMMC). The form of medical ethics was submitted to the UMMC review board. After the review board approved the terms and conditions and granted to perform data acquisition on OA patients in UMMC as well as those with healthy knees was granted (Medical Ethics Number: 20165-19). The letter of approval can be found in Appendix C, Section 1. In the first data acquisition, 32 male and female subjects aged between 20 to 53 years old without any history of knee injuries or pain and 14 male and female patients aged 45 to 82 without any restrictions imposed on the types of knee pathology were selected (total of 46 subjects and 46 sample of data). In the second data acquisition, a total of 10 OA patients aged from 45 to 75 years old and 16 subjects with healthy knees aged between 18 to 30 years old participated in the study and a total of 64 knees were examined (left and right knees). The first 24 knees' data were selected as the control group and the remaining as the testing group. The requirements for subject selection were, their ability to stand up and sit down without the need of any support and for OA subjects, they should have a K-L grading of 2 and above approved by designated physicians using the previously captured x-ray images of the knee. Consent forms were given to the subjects before performing the test in order to inform the subjects about the test purposes and the dangers that may involve. This form is available in Appendix C, Section 2. Healthy subjects were ensured that they had no symptoms of knee OA and no history of orthopaedic or neuromuscular disease.

The sensor band was placed under the knee support band then placed on both left and right knees' mid patella. Based on studies done on VAG signals (Chu, 1978), mid patella can provide the least amount of noise produced by leg muscles during the test. After the knee band placement, the subjects were asked to perform the sit-stand-sit test

as explained in Section 3.4. Table 3.7 shows the list of patients' ages and their OA grading in the first version of data acquisition and Table 3.8 shows the testing group's OA grading in the second version of data acquisition. It should be noted that the second version of data acquisition was done on both knees of the subjects so, there were two knee samples were obtained from each subject.

The stair test was done only on few subjects in the second version of data acquisition. Many issues were faced to perform the stair test including portability and left and right knee synchronisation. Figure 3.37 shows the stairs used to perform the stair test on the patients. Due to the many issues faced with this method, a further signal analysis was avoided.

Figure 3.37: Stair test path performed at the second version of data acquisition

Table 3.7: List of subjects age and KLG grade at first data acquisition version

Subject No.	AGE	KLG	Subject No.	AGE	KLG	Subject No.	AGE	KLG
1	23	0	**21**	23	0	**41**	63	3
2	24	0	**22**	23	0	**42**	61	3
3	26	0	**23**	25	0	**43**	74	2
4	26	0	**24**	25	0	**44**	82	2
5	23	0	**25**	21	0	**45**	81	2
6	23	0	**26**	21	0	**46**	66	2
7	54	0	**27**	24	0			
8	23	0	**28**	24	0			
9	23	0	**29**	25	0			
10	23	0	**30**	25	0			
11	23	0	**31**	24	0			
12	23	0	**32**	24	0			
13	23	0	**33**	60	2			
14	24	0	**34**	53	2			
15	24	0	**35**	55	4			
16	21	0	**36**	67	4			
17	21	0	**37**	69	2			
18	22	0	**38**	66	2			
19	23	0	**39**	65	4			
20	23	0	**40**	75	4			

Table 3.8: Subjects KLG grading at the second version of data acquisition

Subject No.	KLG	Subject No.	KLG
1	2	**21**	0
2	2	**22**	0
3	3	**23**	0
4	3	**24**	0
5	3	**25**	0
6	2	**26**	0
7	2	**27**	0
8	2	**28**	0
9	2	**29**	0
10	2	**30**	0
11	3	**31**	0
12	3	**32**	0
13	4	**33**	0
14	4	**34**	0
15	2	**35**	0
16	2	**36**	0
17	3	**37**	0
18	3	**38**	0
19	4	**39**	0
20	4	**40**	0

3.7.1 Signal analysis method

For a better illustration of signal processing algorithm and method, which will be explained in detail in chapter 4, a flowchart was prepared and is shown in Figure 3.38. The flowchart was made in two sections after data collection in the MATLAB. The right section of flowchart represents the first version of data acquisition and the left side represents the second version of data acquisition.

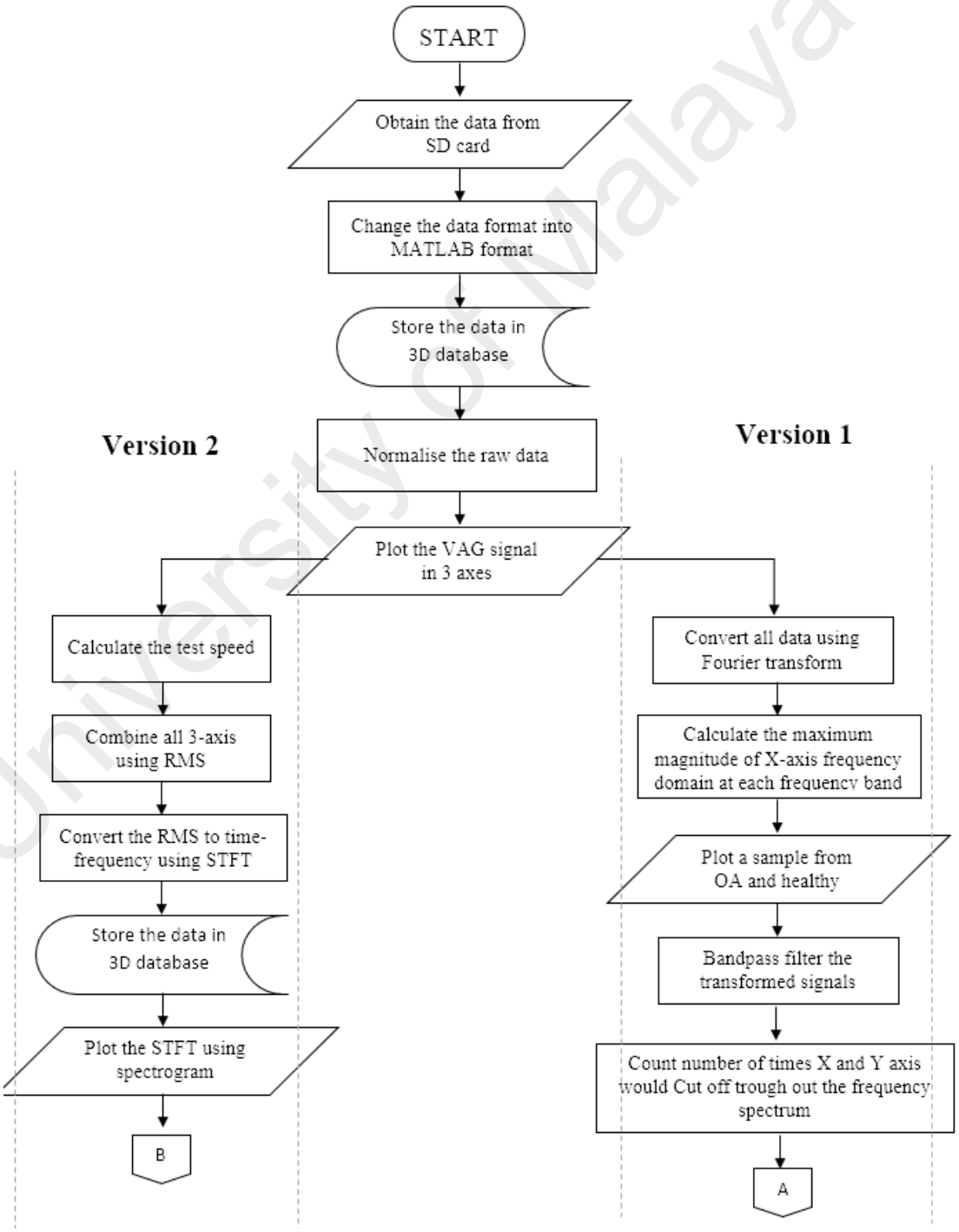

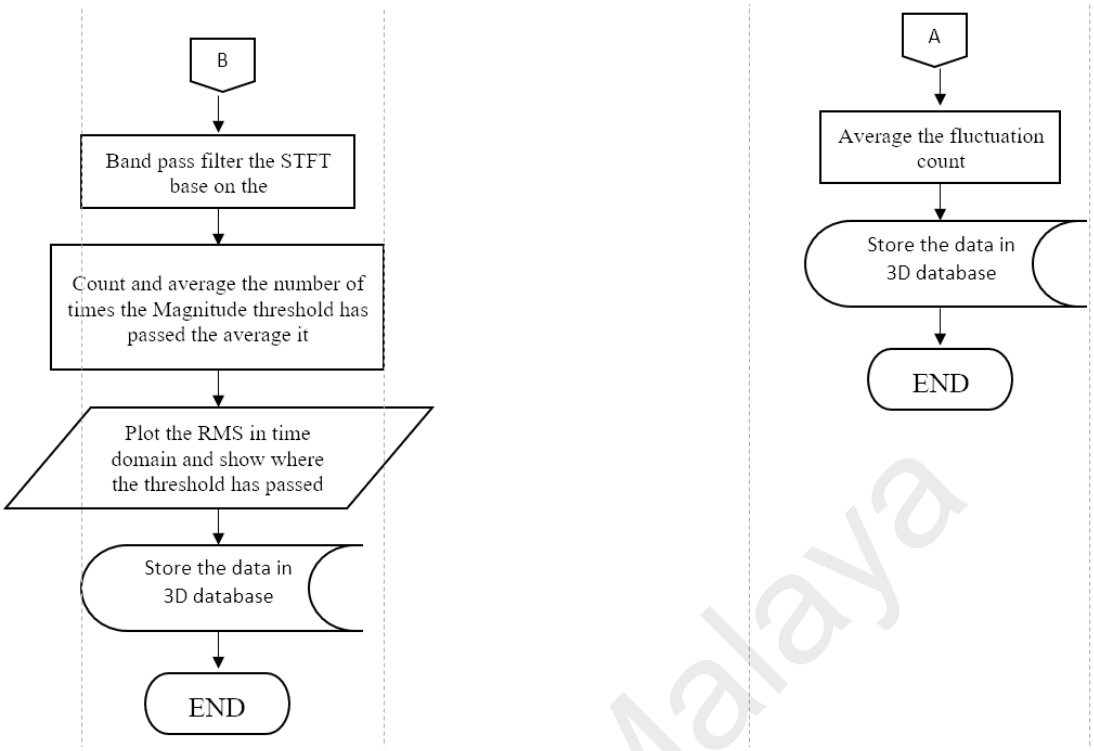

Figure 3.38: Flowchart of signal processing and algorithm for version 1 and version 2 of data acquisition

3.8 MATLAB PROGRAMMING

3.8.1 First data acquisition version

The MATLAB programming of the first prototype was divided into five sections. In this chapter, the flowchart of the programming and the detailed instruction of the programming are explained. The following is the list of the programming sections:

1. Data collection
2. Normalization
3. Band Pass filtering
4. Fast Fourier Transform
5. Frequency magnitude hit count

3.8.1.1 Data collection

A unique approach was taken to collect and store all the data in one database. Creating a singular database was beneficial for a collective data collection as well as speeding up the MATLAB signal processing. A 3D database was used to store all three axes of the VAG signals of all subjects and the modified signals through signal processing. Figure 3.39 shows the guideline of each axis of the 3D database. The y-axis stored data specifically for x, y, and z axes vibration values in registries y1, y2, and y3 respectively. The x-axis stored the data specific to the subject number and the z-axis would store all the VAG signals as well as modified data. The directory z1 held the original data while z2, z3, and z4 held the normalized signal, filtered signal, and FFT signal respectively. Figure 3.40 shows the flowchart of the MATLAB database creation.

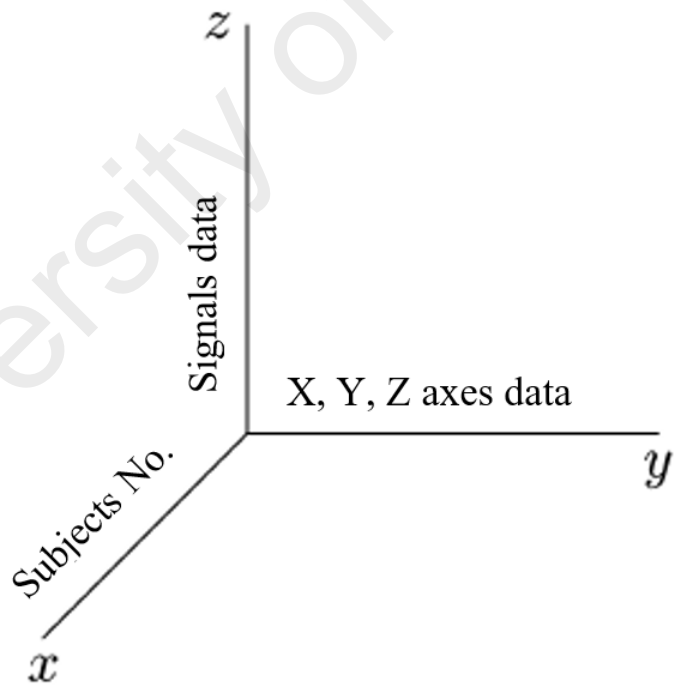

Figure 3.39: 3D database mapping for storing VAG signals

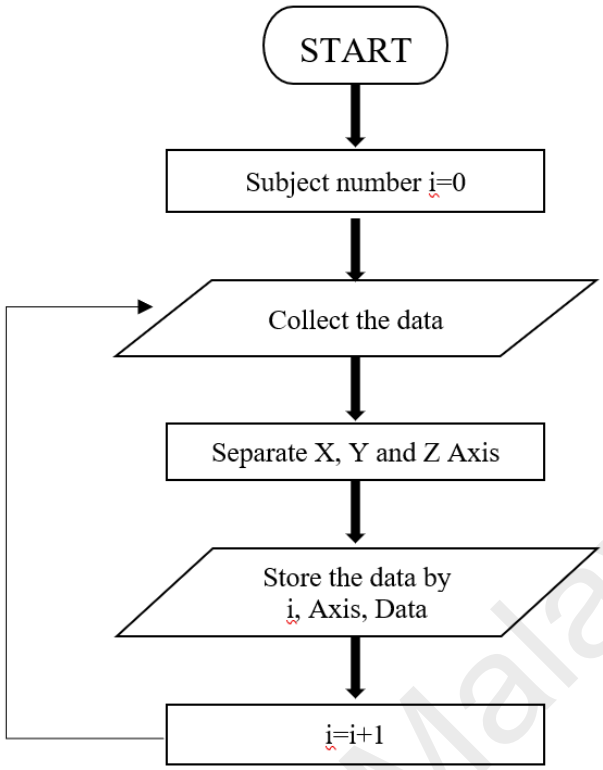

Figure 3.40: Flow chart of data collection MATLAB programming

3.8.1.2 Normalization

Normalization was done based on the initial starting point of data. The magnitude range of the signal however, was not normalized in between 0 to 1 (standard normalization method). This was due to the presence of sparks in the signals indicating sudden motions. The maximum amplitude of each subject differed as well because of the knee range of motion deference. A sample of the raw VAG signal can be seen in Figure 3.41.

Normalization was done based on the first 100 sample data. By averaging the first 100 samples and subtracting them from the total signal, the normalization can be done as shown in Equation 3.1. The normalized plot is shown in Figure 3.42 and MATLAB programming followed Equation 3.1 as well and the flowchart of the programming is shown in Figure 3.43.

$$x_{new}(n) = x(n) - \left(\sum_{p=1}^{100} x(p)\right) \Big/ 100 \qquad (3.1)$$

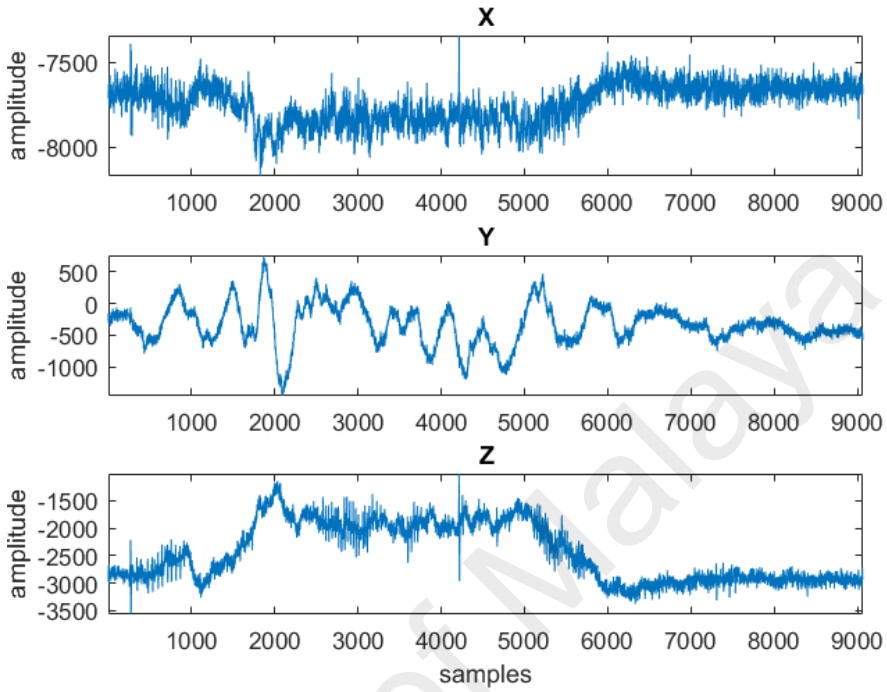

Figure 3.41. Sample Raw data of the knee VAG signal

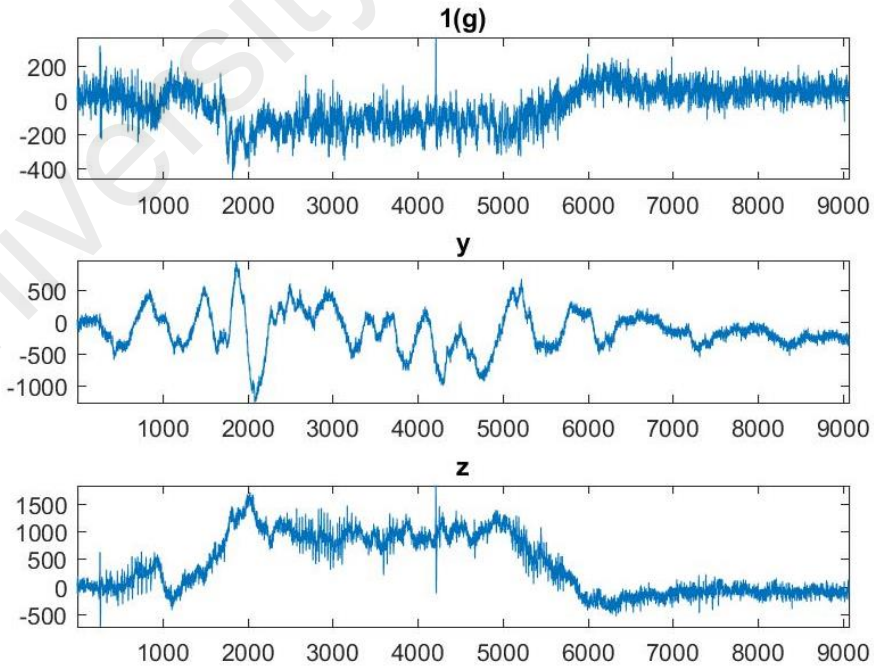

Figure 3.42: Normalised VAG signals

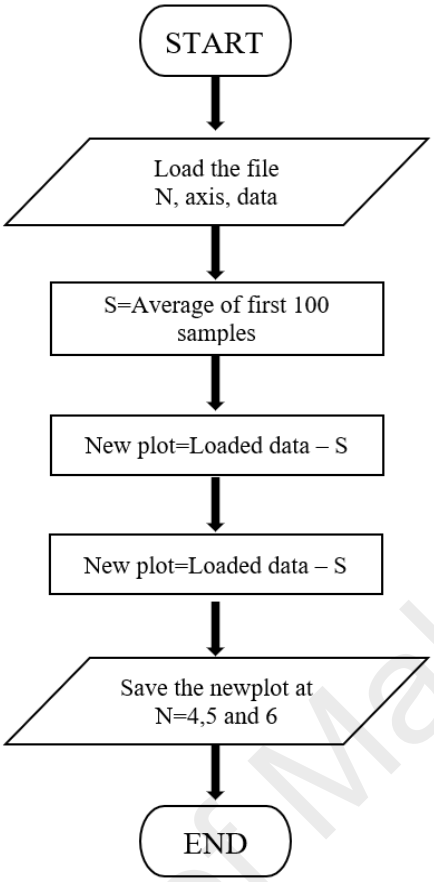

Figure 3.43: MATLAB programming Flowchart of the signal Normalization

3.8.1.3 Band-pass filtering

As it is explained in Section 4.1, the most significant difference between OA and healthy knee was found in the frequency domain between 4 to 30 Hz. To analyse the signal in that specific frequency range, band pass filtering is required. Band pass filtering in MATLAB was done by first performing the low pass filter at 30 Hz then the high pass filter at 4 Hz for the previously filtered signals.

There are two main types of digital signal filtering methods used in signal processing, finite impulse respond (FIR) and infinite impulse respond (IIR). However, the FIR filtering method provides more advantages compared to IIR and is more widely used. In this study as well, FIR filtering was used to filter out all VAG signals.

The MATLAB filtering programming operates via two functions. The first function will calculate the filter coefficient, which is done through "c= fir1(n, wn,'type')" command. Where “n” is the order of the filter and “type” is either “high” for high pass or “low” for low pass. The higher the order number is, the lower the noise from the filter will be. The second function will perform the signal filtering by “filter (c, 1, f)” command, where “c” is the filter coefficient explained earlier and “f” is the actual signal. The following Figure 3.44 shows the filter signals previously shown in Figure 3.42. The MATLAB programming flowchart is shown in Figure 3.45.

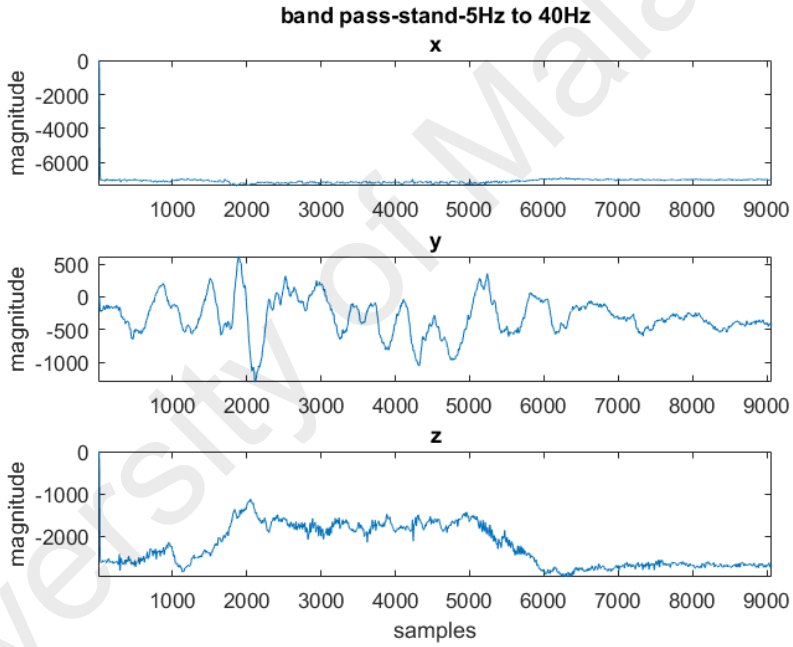

Figure 3.44: Bandpass filtered VAG signal

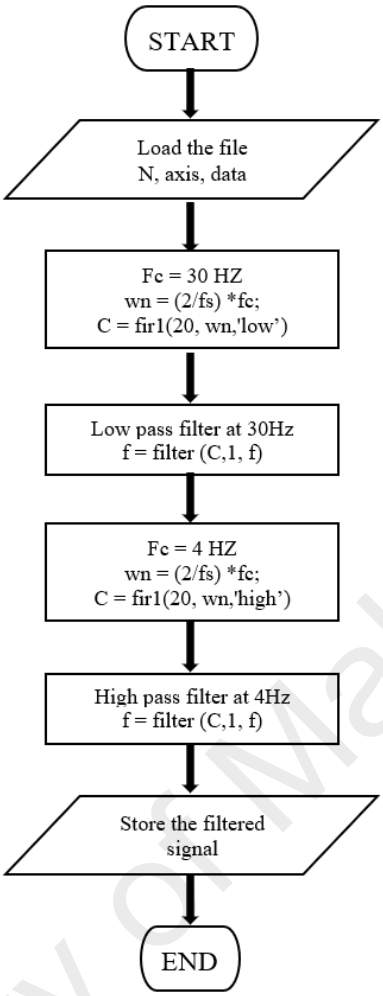

Figure 3.45: Flowchart of the Band pass filter MATLAB programming

3.8.1.4 Fast Fourier Transform

FFT can be performed automatically in MATLAB programming using "fft(f(x))" command. However, it can also produce complex values where real values are actual representation of frequencies present in the signal. FFT signal as well is symmetrical which means the negative half of the FFT can be removed without loss of features in the signals.

In MATLAB programming as well, similar steps were taken to remove the imaginary section and negative half of the FFT signals. Figures 4.6 and 4.7 in Section 4.1 show the FFT after band pass filtration and normalization while Figure 3.46 shows the flowchart of the MATLAB programming.

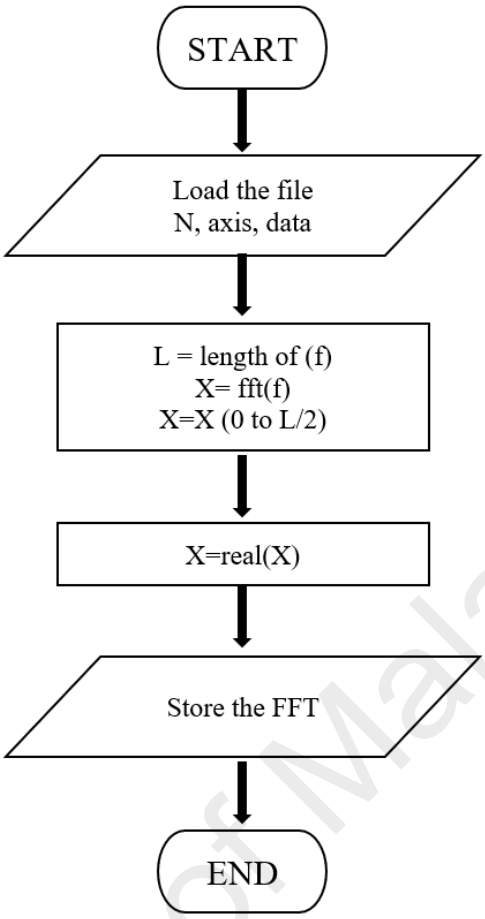

Figure 3.46: MATLAB programming for FFT on filtered VAG signal

3.8.1.5 Frequency magnitude hit count

The frequency magnitude hit count (FMH) count was done by setting a limit on the frequency magnitude in the frequency domain. In MATLAB, this is simply done by counting the sample data under 50 dB.

3.8.2 Second version of data acquisition

Similar to the first testing version, the signal analysis of second version was also divided into different stages. The following is the list of the programming stages:

1. Data collection
2. Normalization
3. Significant position recognition algorithm
4. Short-time Fourier transform

5. Magnitude hit count

The data collection and normalization stages of MATLAB programming for the second version were similar to the first stage hence, these will not be repeated in this section.

3.8.2.1 Significant position recognition algorithm

As shown in Figure 4.17 in Section 4.2.1, the SPRA is divided into 4 stages where each is indicated with the "POS" initial. The MATLAB algorithm can be simplified into the following 4 Figures as represented in Figures 3.47, 3.48, 3.49 and 3.50, where each flowchart shows how each POS was calculated.

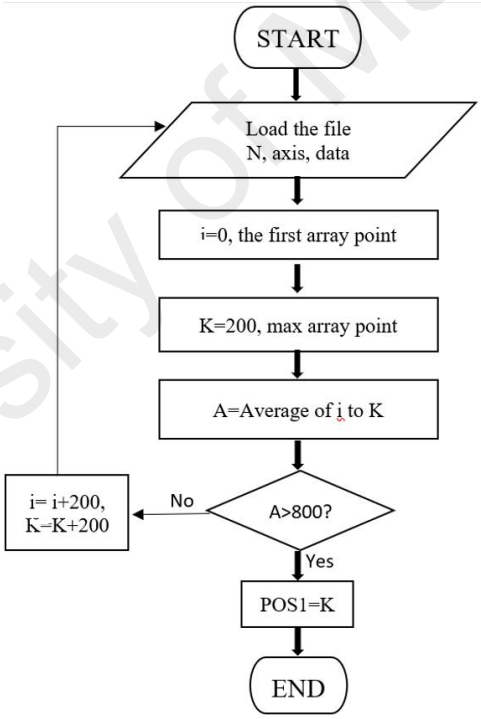

Figure 3.47: Flowchart of POS 1 SPRA

To indicate POS1, the algorithm would look for major amplitude fluctuations in the time domain of the z-axis. When the average amplitude change was more than 800, POS1 was found and selected.

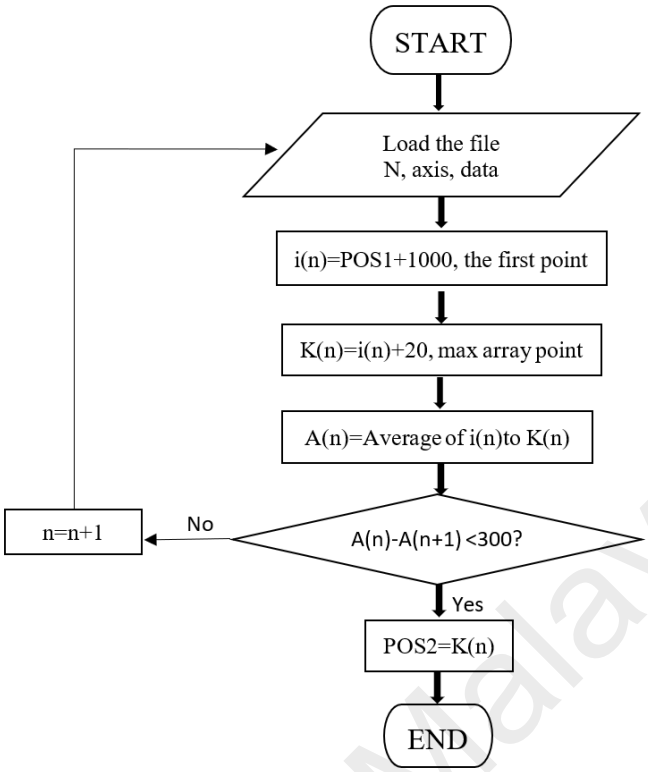

Figure 3.48: Flowchart of POS2 SPRA

As shown in Figure 4.13 Section 4.2, POS2 was the ending point of standing up. Between POS1 and POS2 the z-axis plot amplitude fell rapidly. The algorithm as shown in Figure 4.48 would check the amplitude change every 20 points and compared the results of the neighbouring 20 points and since there was no major amplitude fluctuation, POS2 was marked.

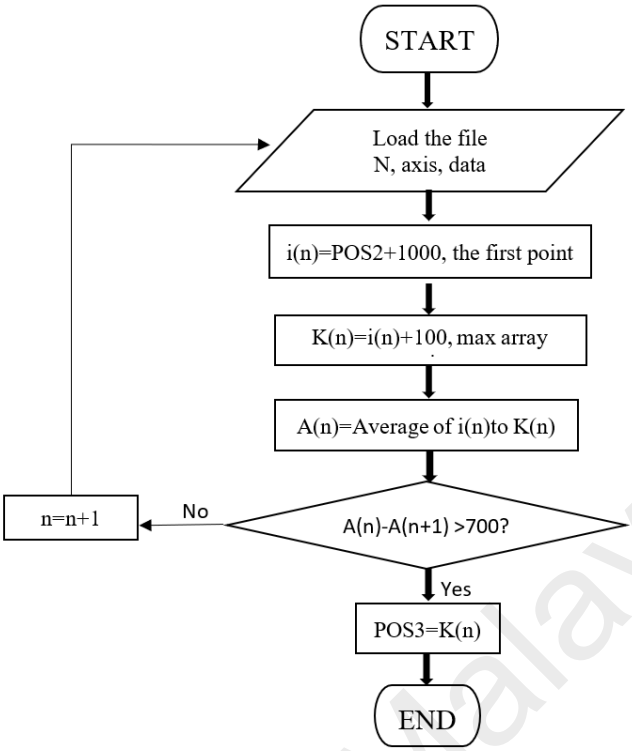

Figure 3.49:Flowchart of POS3 SPRA

Identifying POS3 was very similar to POS1. Between POS2 to POS3 the subject is remained standing and does not perform major movement . POS3 was calculated by measuring the magnitude fluctuations at each 100-sampling point and when the fluctuation was detected to be more than 700 units sample point was then marked as significant position change.

The points between POS3 and POS4 act opposite of POS1 to POS2 so the MATLAB programming was also similar. However, slight adjustment to the maximum amplitude was applicable to detect the change that was done to increase the reliability of the algorithm. Figure 3.50 shows the MATLAB programming flowchart of POS4 SPRA.

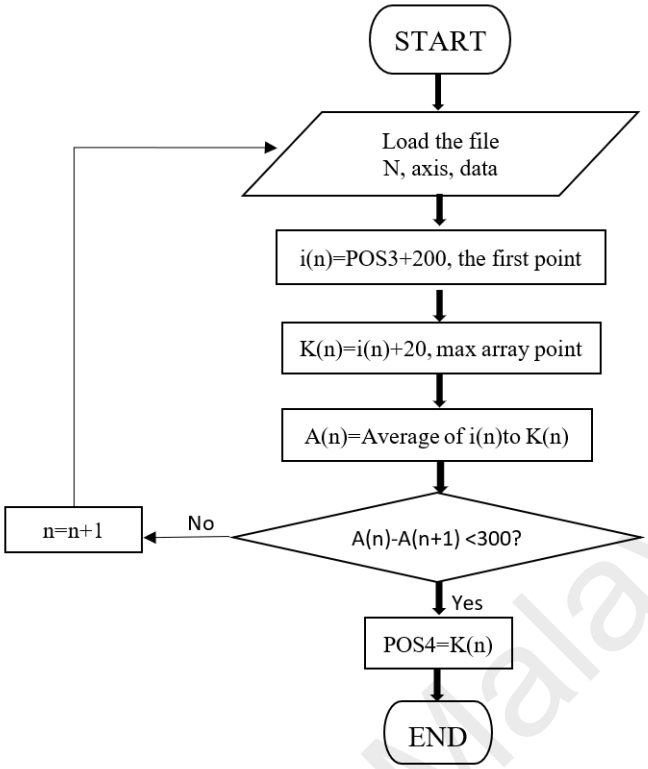

Figure 3.50: Flowchart of POS4 SPRA

3.8.2.2 Short-time Fourier transform

Short-time Fourier transform (STFT) is the essential part of the study due to the properties of VAG signals generated by the knees. By measuring the magnitude frequencies at each specific point of time, numerous information about the signal characteristic could be extracted. In this section, the methods used in MATLAB to convert the time domain signal into STFT were explored.

The STFT is a three-dimensional plot of time, frequency, and magnitude dimensions. MATLAB provides many types of plots for viewing 3D data and this study used the spectrogram plot to optimally show the results (sample can be seen in Figure 4.14). To perform STFT in MATLAB, the time domain signal was divided into several small sections and FFT was done in those sections. The humming window selected for FFT

was 600 samples. The following Figure 3.51 is the flowchart of STFT MATLAB programming.

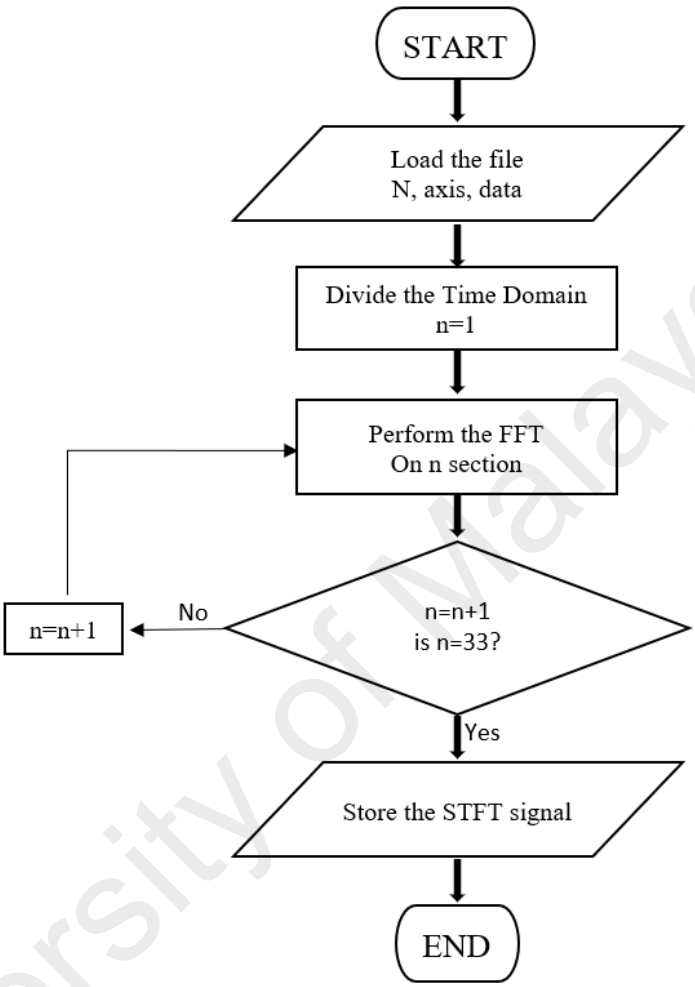

Figure 3.51: Flowchart of MATLAB STFT

3.8.2.3 Magnitude hit count

The magnitude hit count was done by considering the two limiters. SPRA was able to detect the duration where the sit-stand-sit test was performed by limiting the STFT between POS1 to POS4. SPRA was then able to calculate the speed ratio and limit the frequency range of STFT. The two limiting factors created a small window in between STFT and by measuring the frequency magnitude at this area, MHC can be evaluated.

As shown in Figure 4.15, the most optimal frequency magnitude range to measure the difference between OA and healthy knee is between 20 to 40 dB. In MATLAB programming, the number of magnitudes in this range (between the limiting windows) is counted and averaged. Figure 3.52 is the flowchart of MATLAB programming for MHC in the limited range.

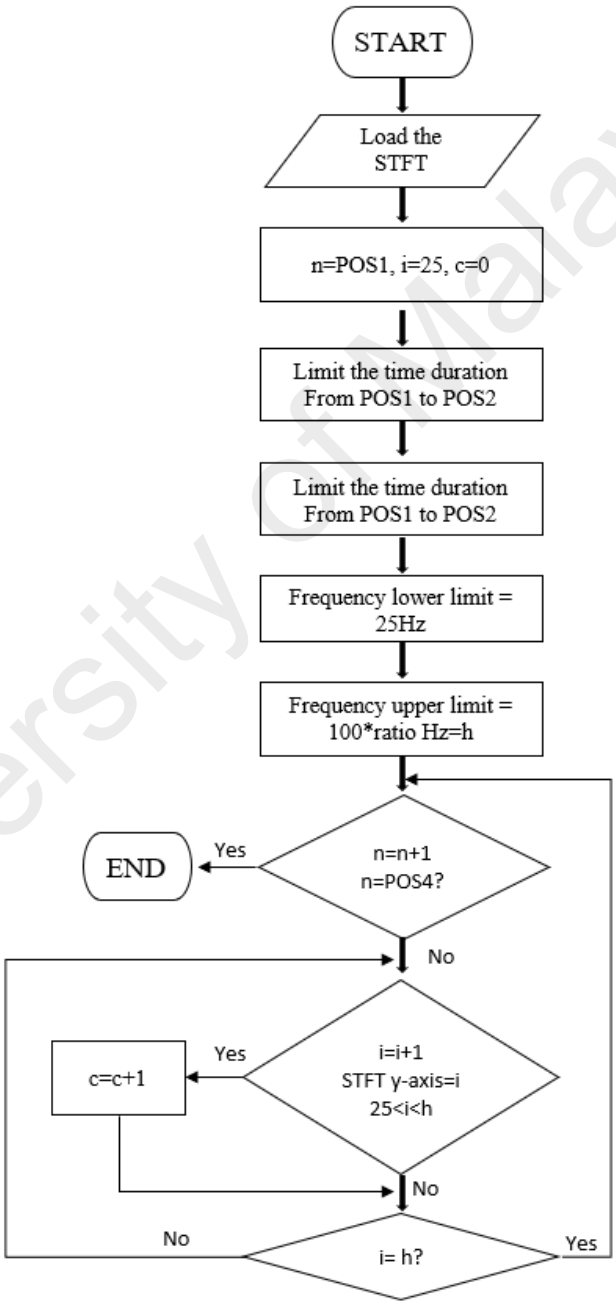

Figure 3.52: Flowchart of MATLAB MHC programming

CHAPTER 4: RESULTS AND DISCUSSION

4.1 FIRST VERSION OF PROTOTYPE

Figures 4.1 and 4.2 represent samples of normal knee and OA knee VAG signals respectively, taken using the sit-stand-sit method. From the z-axis, the positioning of the knee while standing up and siting down can be determined, stemming from patella pushing the sensor outward while standing up and pulling it inward while sitting down. As one can be observed from the z-axis of both figures, the subjects stood up in the time duration of 0 to 3 seconds then proceeded to sit down in the duration of 4 to 7 seconds. The data were captured at 1300 samples per second with 20 KHz ADC sampling rate. In the one-second rest between standing up and sitting down, the magnitude variation of z-axis decreased dramatically simplifying the detection of knee angle.

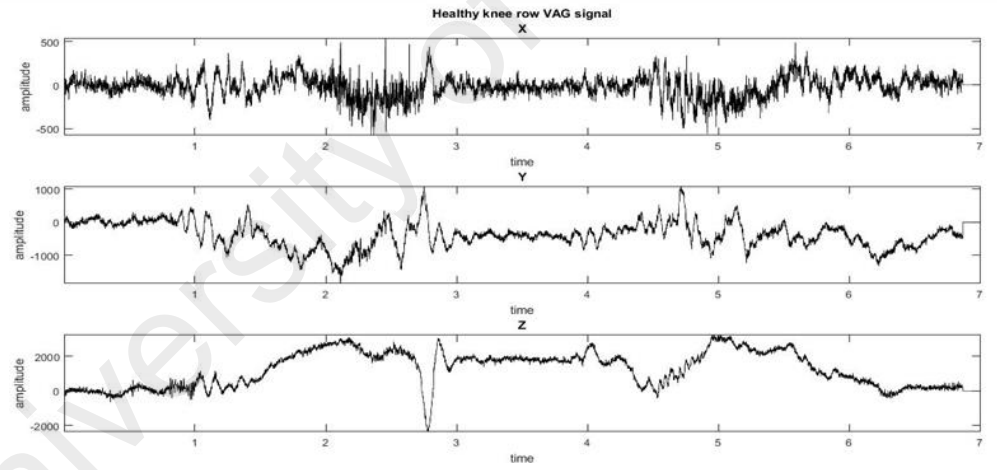

Figure 4.1: Three axis VAG signal taken from a healthy knee

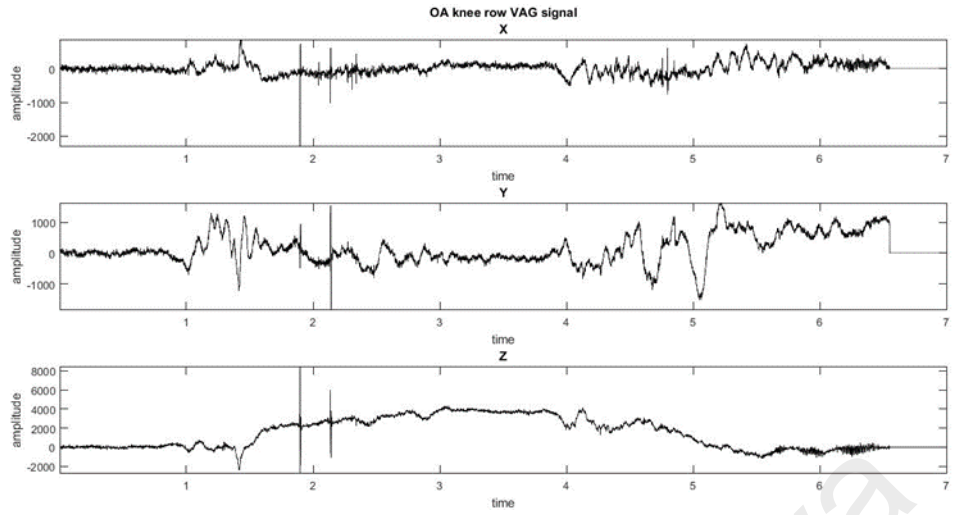

Figure 4.2: Three axis VAG signal taken from an OA knee

It should be noted that the data taken did not exactly follow the time interval procedure due to a minor human error in the process of capturing data. The data shown in Figures 4.1 and 4.2 were averaged to 0 amplitude to ease the analysis and comparison of data. In so doing would force all the signal axes to start from 0 amplitude.

All VAG signals taken from OA and healthy knees were then separated and averaged. Figure 4.3 presents the power spectrum density (PSD) of all averaged signals captured in the first version of data acquisition. The power spectral density (PSD), Pv(f),was used to estimate the power of fluctuations at a given frequency (f) and of the variations over a time scale of the order of "1/ f". A distinct separation of power density of healthy knee signals from OA knees can be observed in Figure 4.3. The power difference was set in between 4 Hz to 30 Hz frequency range. By utilising this significant difference, all the VAG signals obtained were filtered between 4 Hz to 30 Hz range. The band filtering procedure used was as follows: The signals were passed through the digital finite impulse respond (FIR) low pass filter with a cut-off frequency (fc) of 30 Hz on the 20th order filter. A lower limit of frequency, 30 Hz was selected as to remove the unwanted vibration produced by the movement. This lower filter limit was recommended and used by Krishnan (1997). The signals then were passed through

a FIR 20th order digital high pass filter with a cut-off fc of 4 Hz. The corresponding filtered signals after passing through filters are shown in Figures 4.4 and 4.5 for healthy and OA knees respectively.

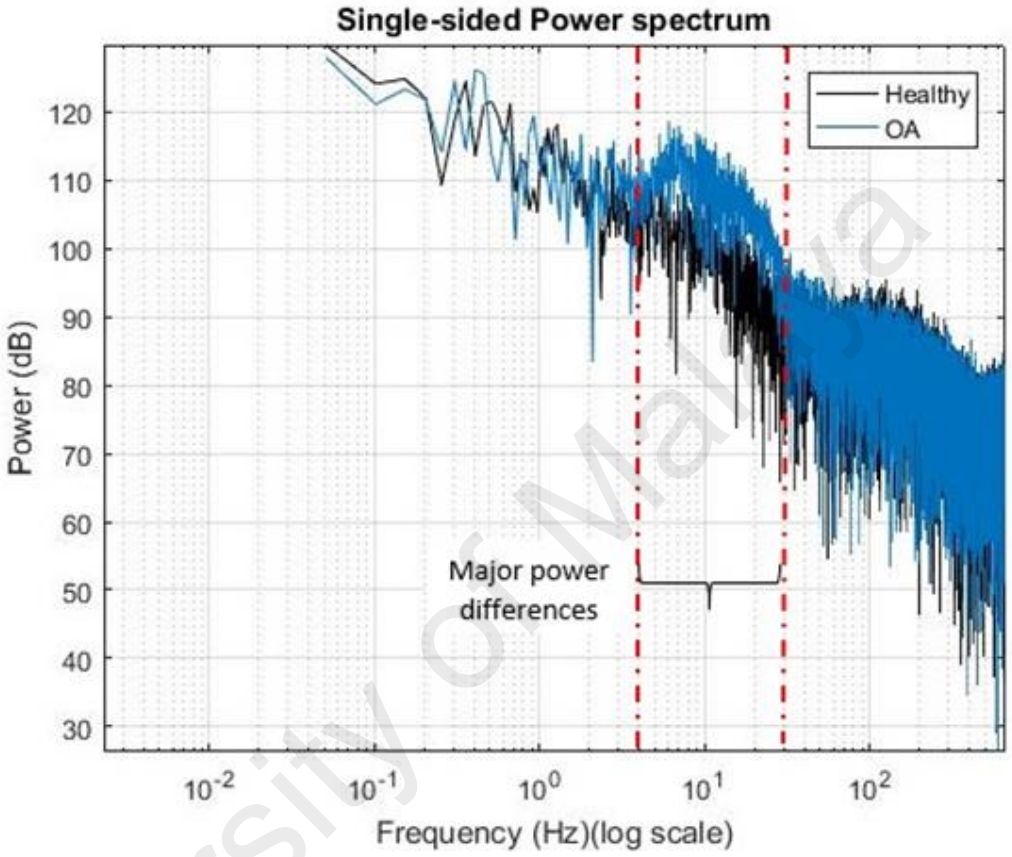

Figure 4.3: PSD of the mean of collected healthy and OA knee. Red dotted line indicated the range of power difference of OA and healthy knee

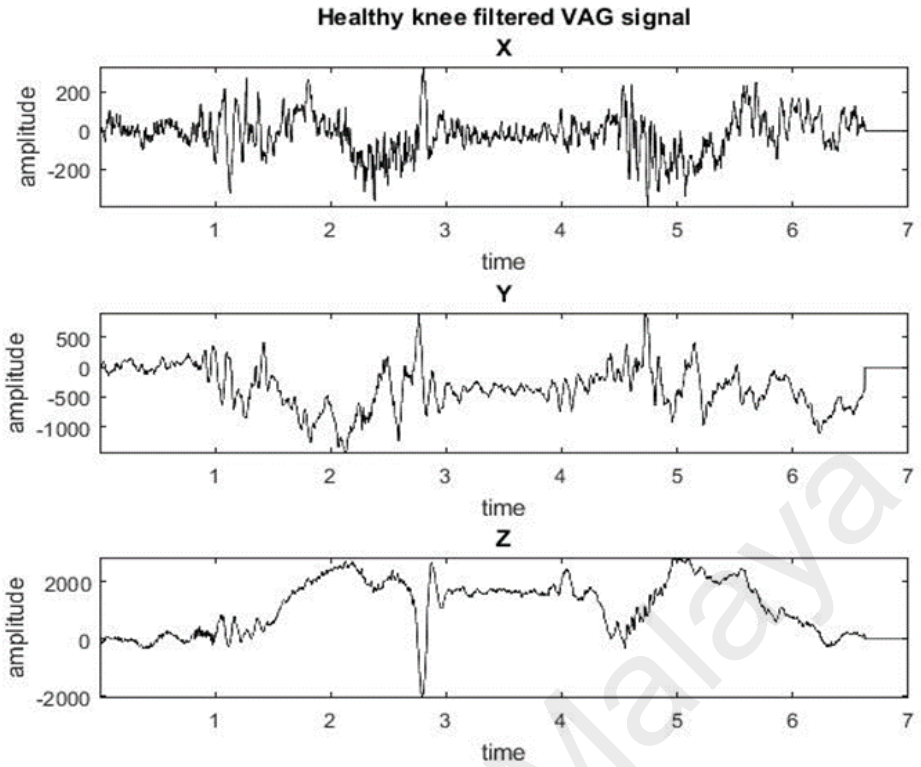

Figure 4.4: VAG of filtered Healthy knee vibration

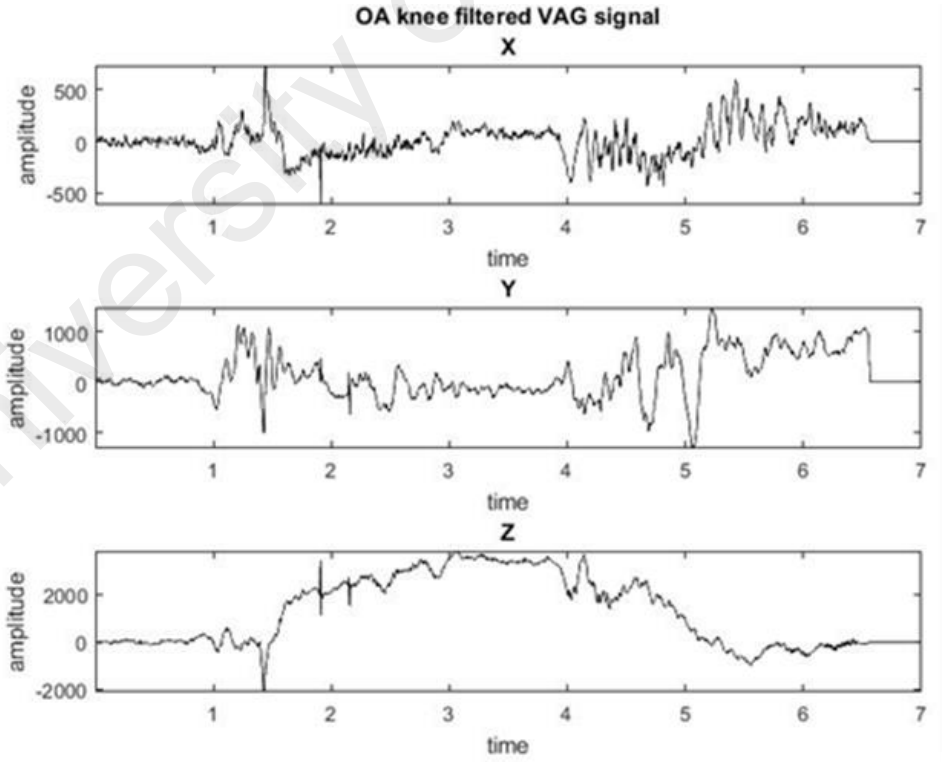

Figure 4.5: VAG of filtered OA knee vibration

The filtered VAG signals were then plotted in the frequency domain as it is shown in Figures 4.6 and 4.7, representing the healthy and OA knees respectively. The signal frequency ranges were then normalized to the Nyquist frequency for ease of calculations later in this chapter. From these plots, a major difference in the signal magnitude at a specific frequency for the healthy and OA knees could be observed. The most significant difference between OA and healthy knees, as shown in Figures 4.6 and 4.7, was the frequency magnitude fluctuation after 0.3 Nyquist frequency. The frequency fluctuation in the OA knee frequency domain was much higher than that of healthy knees'. This trend as well continued similarly for most of the other knee samples collected.

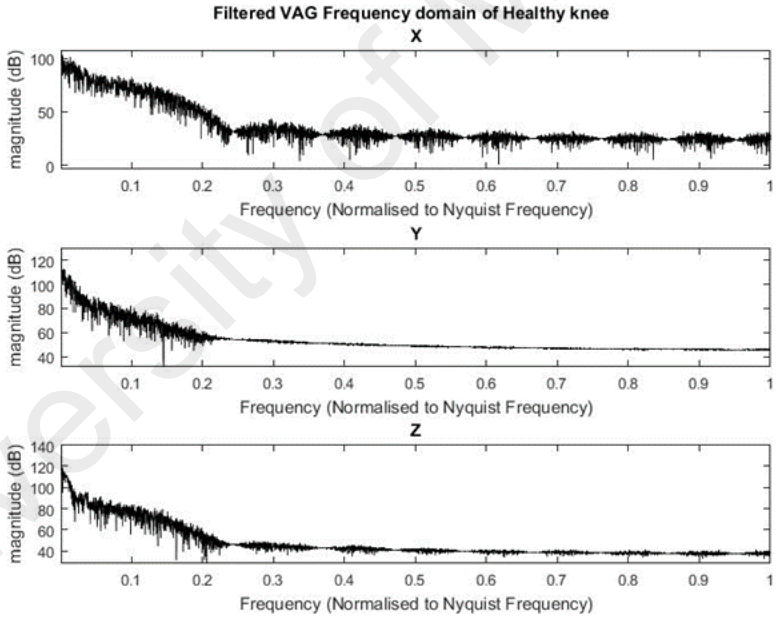

Figure 4.6: Nyquist Frequency domain of Healthy knee filtered VAG signal

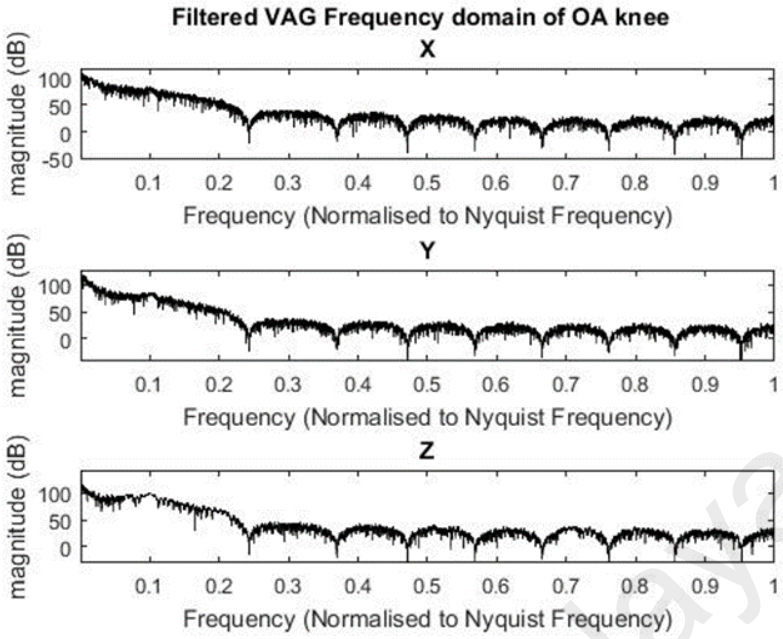

Figure 4.7: Nyquist Frequency domain of OA knee filtered VAG signal

Based on the plotting (Figures 4.6 and 4.7), a healthy knee VAG signal triggered much higher magnitude (more than 40 dB) in all three axes passing from 0.25 Nyquist frequency. However, unlike the healthy VAG signal (Figures 4.6), OA VAG signal contained lower magnitudes with a fluctuation to negative magnitude limit as it progressed (fluctuated between -10 dB to 20 dB).

4.1.1 Clinical Trial

The data collected from all OA and normal knee results were analysed based on their corresponding filtered Fourier transform. The collective results of all three axes (x, y, and z) could provide more accurate results through summarising. To provide a general summary, the number of frequency magnitude hits (FMH) was counted across all three axes. This process was then recorded and listed in Table 4.1. From data analysis, it was noted that OA knees had many points across the frequency interval which hit

magnitudes lower than 50 dB. By measuring the FMH, the number of magnitude hits was counted, and a comprehensive 3D graph was plotted as shown in Figure 4.8.

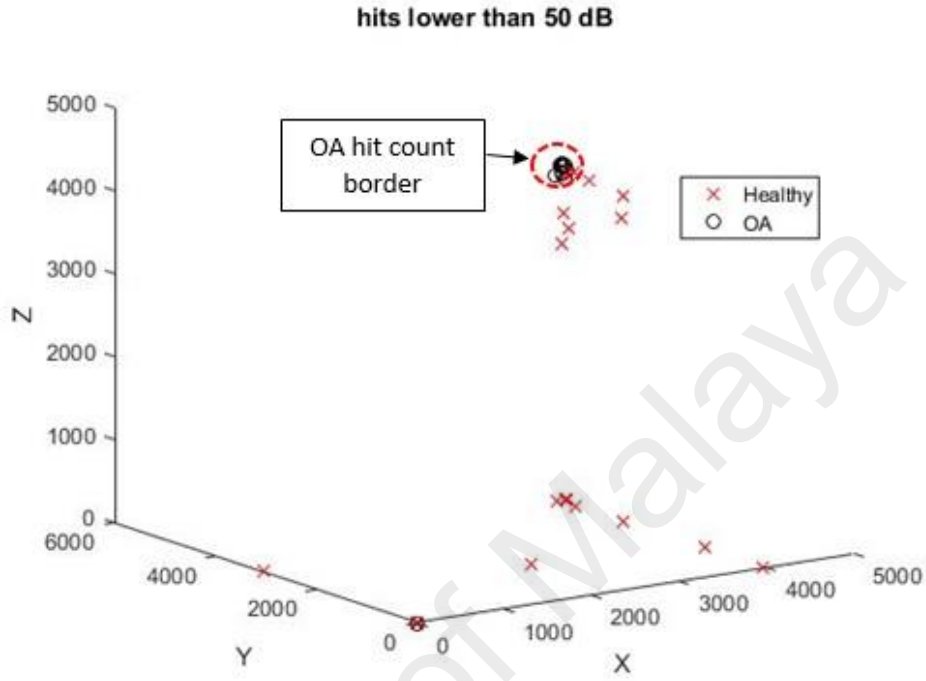

Figure 4.8: VAG FMH less than 50dB of all three axes

Table 4.1: FMH count of all test subjects

Data no.	OA FMH			Healthy FMH		
	X	Y	Z	X	Y	Z
1	1801	2318	1696	1	0	0
2	2059	2317	1583	1	0	0
3	2143	2154	1589	308	0	1
4	2293	2260	1616	2	0	0
5	2501	2576	1674	0	35	0
6	2107	2097	1268	0	0	0
7	2291	2087	1613	2	8	1
8	1996	2209	1138	0	0	0
9	2108	2230	1876	0	0	0
10	2014	2460	1606	1456	0	0
11	1289	1958	1243	1810	0	0
12	2155	1983	1684	2048	0	0
13	2275	2298	1721	29	0	0
14	2295	2451	1769	0	0	0
15	-	-	-	0	0	0
16	-	-	-	0	0	1556
17	-	-	-	6	0	0
18	-	-	-	76	128	0
19	-	-	-	0	0	0
20	-	-	-	4	44	0
21	-	-	-	4	44	1060
22	-	-	-	0	5	0
23	-	-	-	0	0	0
24	-	-	-	623	33	0
25	-	-	-	0	0	0
26	-	-	-	29	0	0
27	-	-	-	199	0	0
28	-	-	-	0	17	0
29	-	-	-	0	0	1
30	-	-	-	0	1	0
31	-	-	-	0	0	0
32	-	-	-	2107	0	0

As shown on Figure 4.8, the OA knees had much higher magnitude hit counts compared to the healthy ones. 10 out of 14 OAs were concentrated at 3000 to 4000 hit limit in x and y axes, and between 4000 to 5000 hit counts in the z-axis limit. Due to the majority of OA hits placed at that specific limit, a border sphere was drown to indicate the OA border limit with its centre placed at point 4000 of all axes expanding with a radius of 1000 points. The normal knees however, had a much wider variety in the

number of hit counts. More specifically, they consisted of much lesser z-axis hit counts relative to OA knees.

Overall, the total accuracy in the classification of OA of healthy knee was 86.95%. The accuracy rating was calculated based on the number of OA knees FMH counts beyond the OA border limit which had been previously defined. Table 4.2 demonstrates how the calculation was done to calculate the accuracy rating.

Table 4.2: Accuracy calculation of the first data Acquisition version

	OA FMH limit	Average of OA FMH	Healthy FMH limit	Average of Healthy FMH	Number of FMH overlap	Accuracy
X-axis	1289 to 2501	2094.78	0 to 2048	272.03	4	91.30%
Y-axis	1958 to 2576	2242.71	0 to 128	9.844	1	97.83%
Z-axis	1138 to 1876	1576.86	0 to 1556	81.844	1	97.83%
Total	1138 to 2576	1971.45	0 to 2048	121.24	6	**86.95%**

4.1.2 Problems encountered

Many obstacles were encountered especially during the testing on the subjects and signal processing. Tests done on the subjects strictly relied on the Arduino built in timer to perform the 7-second sit-stand-sit test. The Arduino timer however, was very unstable for long duration tasks. Due to its instability, the sample size of each test was varied relative to other tests. Sample size differences could directly affect sample frequencies as well as the maximum frequency limit after FFT. The use of FFT on the nonlinear and periodic signals could also remove essential features in the signal.

The sensor bands used to mount the sensor and execute the test could not sit properly on the knees while the test was performed. While the subjects were standing up or

sitting down, the sensor bands were lifted up from the knee. This had resulted to unreliable readings and void information.

4.2 THE SECOND VERSION OF PROTOTYPE

Majority of the issues addressed in the first stage were resolved in the second stage for both hardware and signal processing which will be explained later in this section.

As described in Chapter 3, two distinct tests were administered on the subjects; the stairs test and sit-stand-sit test on both knees simultaneously. Figures 4.9 and 4.10 show the raw data captured from the healthy right and left knees respectively whilst Figures 4.11 and 4.12 show the OA KLG grade 3 raw data. As can be seen in these figures, the modified sit-stand-sit sequence (explained in Figure 3.23) can be traced at z-axis plot based on the amplitude changes. Tracking the sit-stand-sit test through z-axis is very important in signal analyses of the second version of prototype as to pinpoint the positions where the knee rotation change has occurred. This will help to determine the knee bend speed while the subject is performing the test.

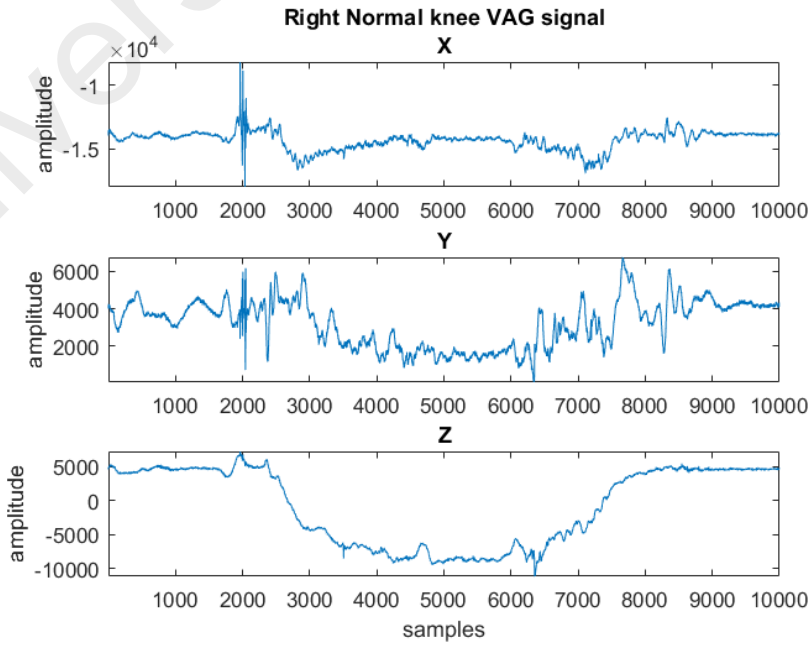

Figure 4.9: Raw VAG signal of Right Healthy knee

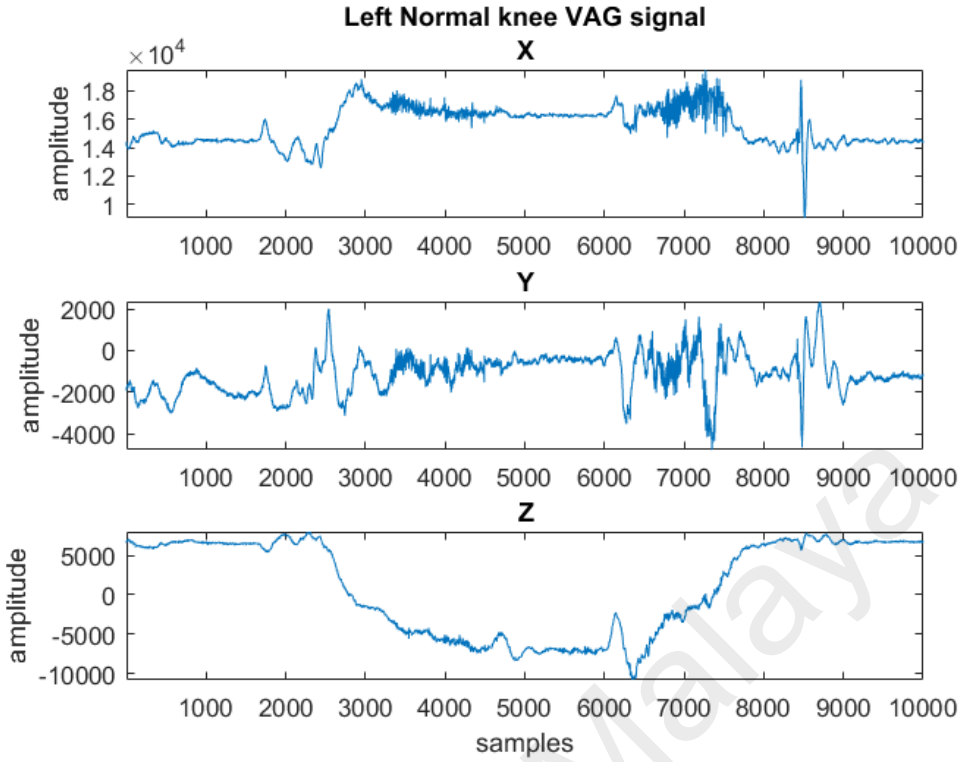

Figure 4.10: Raw VAG signal of Left Healthy knee

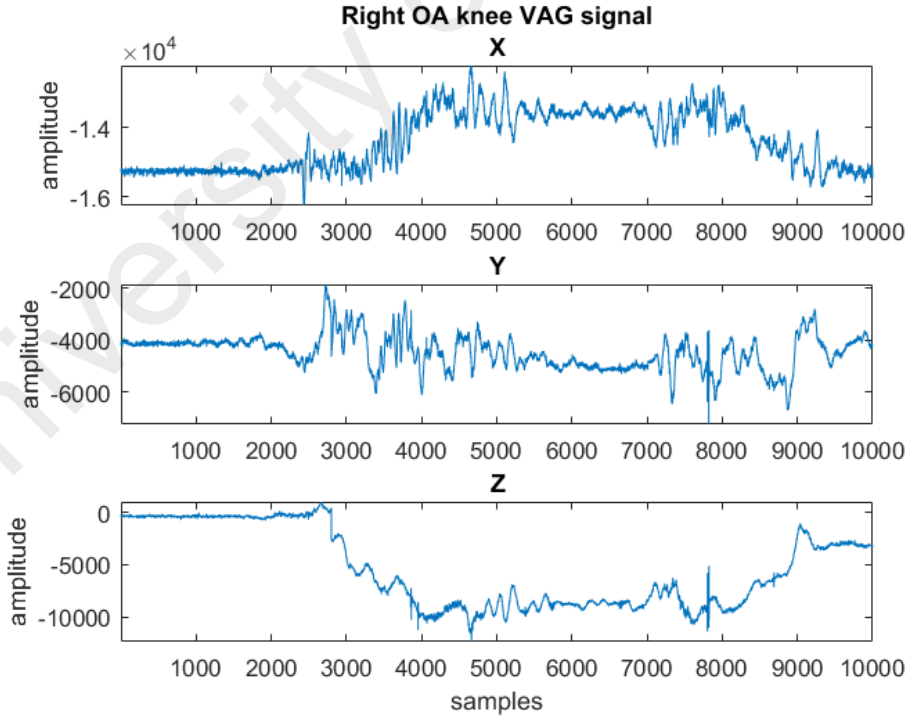

Figure 4.11: Raw VAG signal of Right OA knee

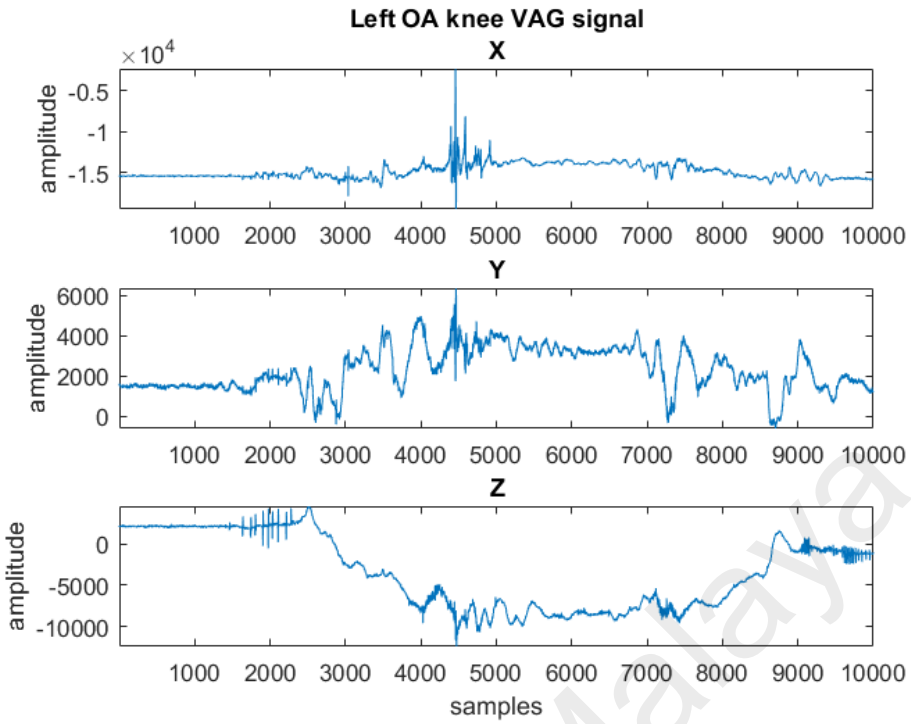

Figure 4.12: Raw VAG signal of Left OA knee

One of the signal processing novelties of this second version of prototype is the signal processing method used and the motion gesture recognition tool created based on z-axis plot. The z-axis of the accelerometer was able to detect the minor upward position changes of the knee. Using this feature, we were able to accurately detect when the subject stood up and sat down based on the z-axis value changes. Signal processing was done in time and frequency domains by creating motion gesture recognition tool and feeding the rotation speed ratio obtained from this tool into the magnitude analysis algorithm. The magnitude analysis algorithm used short-time Fourier transform (STFT) to analyse the specific magnitude of the signal at a unique range limit specified by the sit-stand-sit test speed ratio. By using this method, both speed and vibration of the knee were analysed with a very reliable system in analysing and tracking the progress of OA.

A healthy knee's cartilage on femur, patella and tibia has a much smoother surface in comparison to an OA knee. Based on this characteristic, the proposed method of approach to perform feature extraction is as follows:

The smoother surface of healthy knee cartilage was able to create more consistent frequency over the long duration while the sit-stand test was performed. Longer duration of a certain frequency would result in higher magnitude (dB). However, for OA patient's cartilage, the surface was uneven. The uneven surface would most often produce higher frequencies, and that in turn, translates to higher magnitude (dB) at higher frequencies and lower magnitude (dB) at lower frequencies relative to healthy knee.

Figure 4.13 shows the significant position recognition algorithm (SPRA) detecting the rotation changes of the knee bend. In short, the SPRA was able to detect the significant position changes of the knee angle and mark them for knee rotation speed calculation.

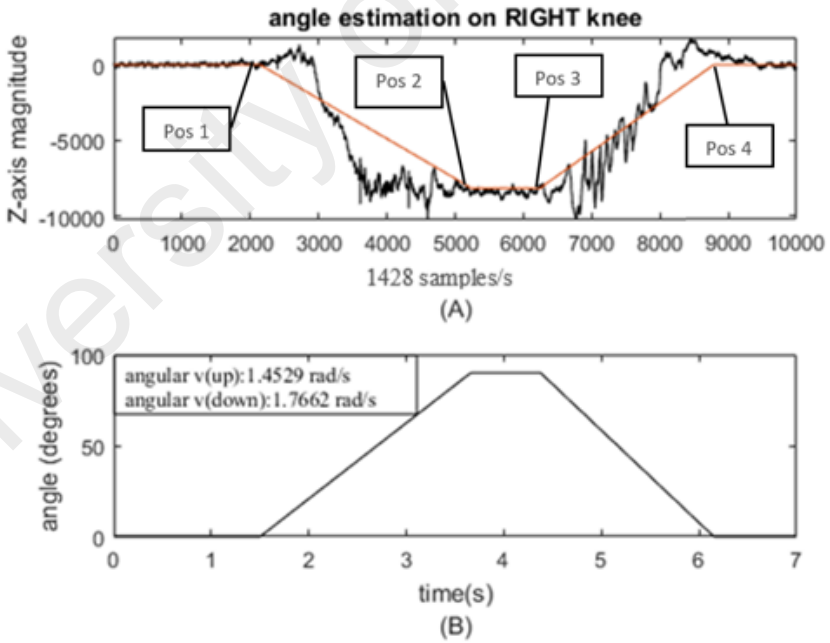

Figure 4.13: Knee angle speed estimation (B) done on the Z-axis (A)

Based on Figure 3.25 the expected total sit-stand-sit test speed was approximately 4rad/s. However, as can be seen in Figure 4.13, the total angular speed for this specific sample was estimated at 3.2191 rad/s. The angular speed can vary from one subject to

another depending on their physical well-being. In order to determine the error ratio, the following formula was created:

$$speedratio = \frac{actualspeed}{4} \quad (4.1)$$

The speed ratio was able to accurately demonstrate the difference between the subject's total speed and ideal total speed (4 rad/s). The ratio can vary wildly (0<ratio<2). This ratio later was used in determining the range of STFT magnitude hit count. Figure 4.14 (A) shows the significant points called POS1, POS2, POS3, and POS4. These points indicate the initial point of rotation change on the knee:

- POS1 indicates the start of the knee movement while subject started to stand up.
- POS2 indicates the initial point where the subject was fully standing.
- POS3 indicates the initial point where the subject start sitting motion.
- POS4 indicate the fully seated position.

The significant position recognition algorithm (SPRA) was designed to pinpoint the significant position with minor errors. The algorithm managed to identify each position one by one from POS1 to POS4 consecutively.

To analyse the time-frequency domain of VAG signals, a short time Fourier transform (STFT) was used to create a 3D time-frequency plot. However, to effectively extract the features of all three axes, performing root mean square (RMS) on all three axes would still retain their properties. Figure 4.14 shows the STFT of RMS of three axes for healthy (A) and OA (B) knees. Equation 4.2 presents the per sample root mean square (RMS) used to combine the axes:

$$RMS_{xyz}(n) = \sqrt{\frac{x(n)^2 + y(n)^2 + z(n)^2}{3}}, 0 \leq n \leq 10000 \qquad (4.2)$$

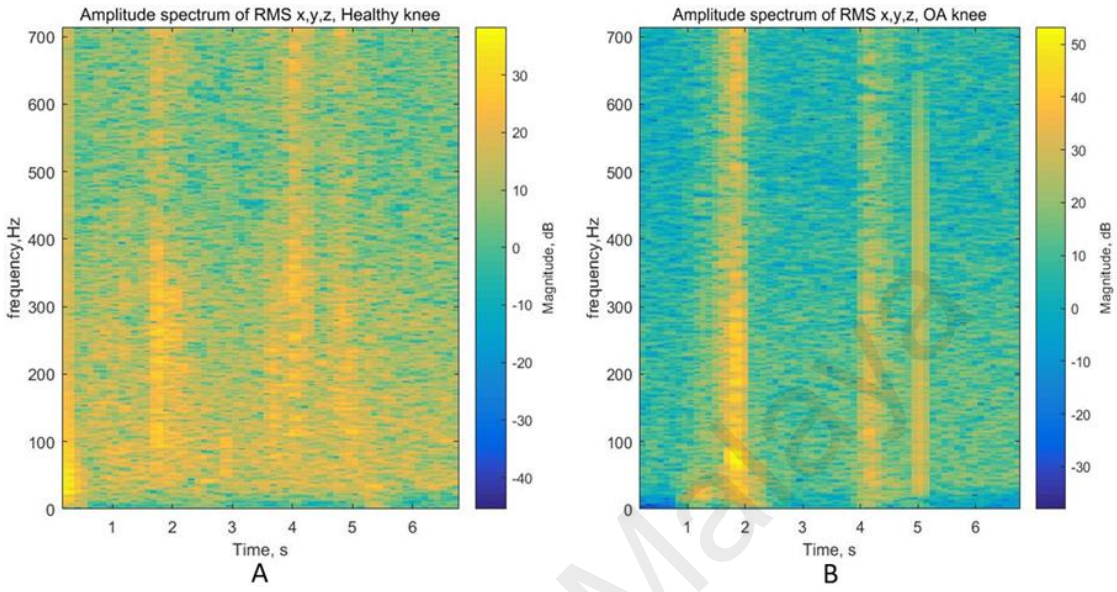

Figure 4.14: RMS x, y and z axis VAG signals of healthy knee (A) and OA knee (B)

Indicating factor to determine the difference between OA and healthy knees is the magnitude difference in specific frequency range depending on the speed ratio. This was done by measuring the number of maximum magnitudes passing through specified magnitude limit (magnitude hit) at each instance of standing up and sitting down.

The frequency range limit was determined from Equation 4.3. As it is stated in the equation, the frequency was directly proportional to the rotational speed and the speed of sit-stand-sit test increased the maximum frequency of the vibration and it increased linearly.

$$f_{limit} = V_{ratio} \times f, \qquad f_{limit} \propto V_{ratio} \qquad (4.3)$$

At each instant of time, the maximum magnitude of the VAG signal could vary at different frequency ranges. A specific magnitude range is required to determine the magnitude hit count (MHC). To seek for the suitable magnitude range limit, one subject

from the healthy knee control group and one subject from the OA control group were selected and the most repeated magnitude during the whole duration of sit-stand-sit test, in each frequency range was calculated. As can be observed in Figure 4.15, the magnitude of healthy knees at lower frequency was substantially higher than OA knees between 20 to 40 dB for the first 100 Hz confirming the proposed method explained earlier to differentiate the characteristics between the OA and healthy knees. However, no major difference could be detected at higher frequencies.

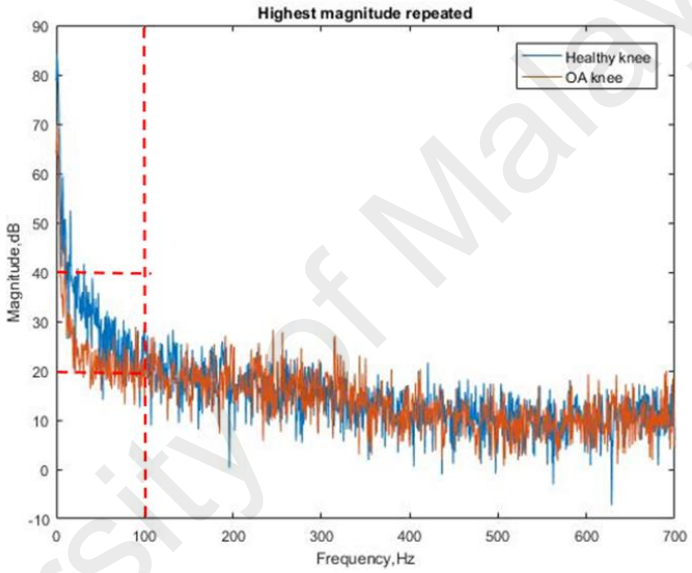

Figure 4.15: Highest magnitude repeated during the test in all range of frequency

Based on Figure 4.15, it could be estimated that the number of magnitude hit for healthy knees in the magnitude range limit of 20 to 40 dB would be a little bit lower compared to the OA knees. By applying the magnitude range limit to the STFT frequency limit, an average magnitude hit rate could be obtained.

Figure 4.16 shows the frequency limit (A) of the STFT of a normal knee sample and the number of magnitude hit at 20 dB (B). The number of magnitude hit was averaged by the duration of the sit-stand-sit test due to varying speeds and the total duration of the test depended on the subjects.

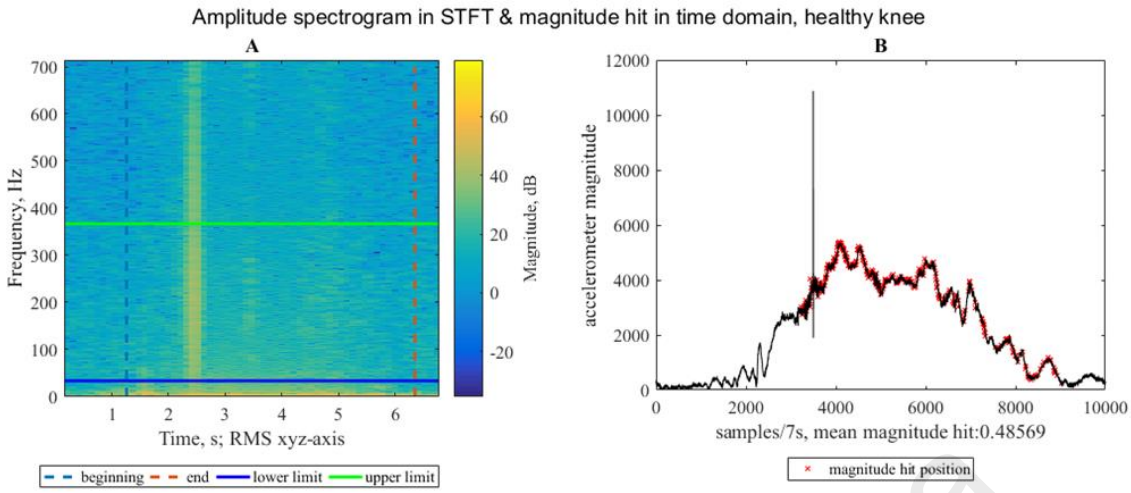

Figure 4.16: Magnitude hit measurement on the limited STFT (A) and in time domain (B)

The lower frequency on all subjects was limited to 25 Hz as frequencies lower than 25 Hz can only carry information about physical body movements which are peripheral to this study. The upper limit of the frequency however, was limited to just depending on the subjects' movement speeds which was calculated using Equation 4.3.

4.2.1 Clinical Trial

The magnitude hit test was performed on the control group to verify the reliability of the method. Several varying conditions were performed for the best possible results. The varying conditions were the frequency limit width, maximum magnitude hit, and magnitude hit range limit. To focus on a specific magnitude range, lower limit will help in identifying the most suitable magnitude limit. Figure 4.17 shows the results of comparing the OA and healthy knee control group in different magnitude hit limits. The mean magnetic hit between OA and healthy knees for both left and right knees shows that 20 dB magnitude limit between the two types of knees was much wider resulting in a more accurate classification of the OA and healthy knees. However, at 40 dB, most VAG signals captured could not be detected in STFT and only showed invalid values.

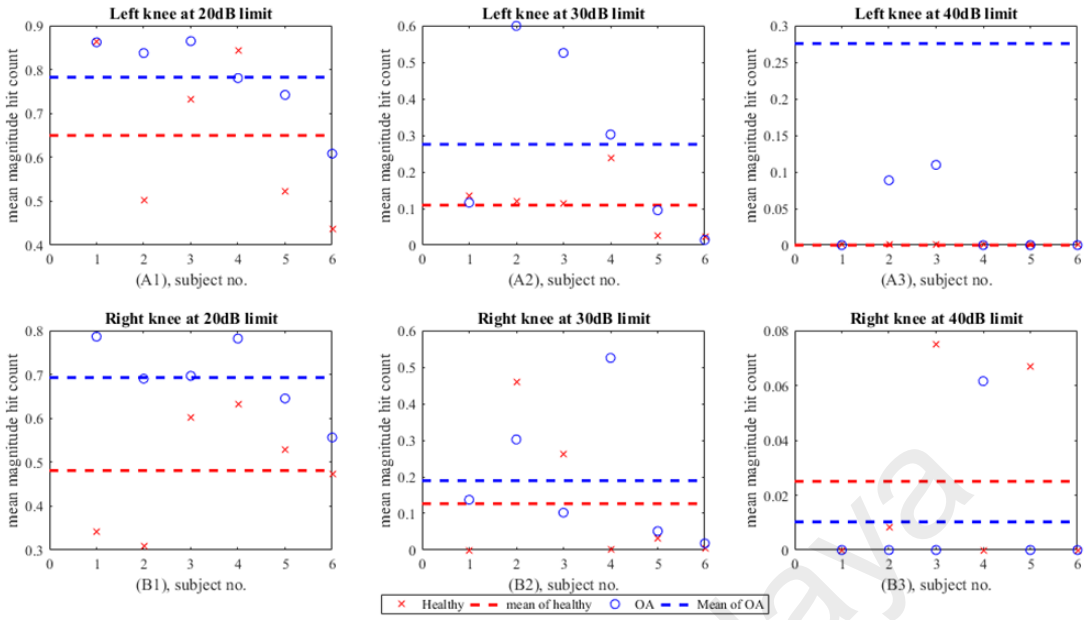

Figure 4.17: Averaged Magnitude Hit count between OA and healthy knee at 20dB (A1 & B1), 30dB (A2 & B2) and 40dB (A3 & B3) magnitude hit limit

By considering the optimal frequency and magnitude hit limit, the same configuration was applied to the testing group which contained 40 knee samples (20 OA and 20 healthy). Table 4.3 shows that the mean magnitude hit as well as the sit-stand-sit speed ratio performed by each subject. As shown there was a major MHC difference between the OA and healthy knees. The range of difference between the MHCs is shown in Figure 4.18.

Table 4.3: MHC of the health and OA knee in test group

No.	Healthy		OA		
	MHC	**Speed ratio**	**MHC**	**Speed ratio**	**KLG**
Left					
1	0.4938	1.3916	0.8763	1.1113	2
2	0.6915	1.2773	0.8271	1.0806	2
3	0.5292	1.2070	0.8838	1.3271	3
4	0.6268	1.1785	0.7587	1.0176	3
5	0.7249	1.1106	0.8520	0.9782	2
6	0.6814	1.2002	0.8892	0.9815	3
7	0.7592	0.8950	0.8881	0.9612	2
8	0.7792	0.9695	0.8657	0.9700	3
9	0.5598	1.1657	0.8617	0.9703	4
10	0.7425	1.1043	0.5692	0.9383	4
Right					
11	0.5359	1.3916	0.6486	1.1113	3
12	0.4157	1.2773	0.6278	1.0806	3
13	0.4140	1.2070	0.6851	1.3271	3
14	0.6105	1.1785	0.7066	1.3014	2
15	0.6272	1.1106	0.8033	1.1708	2
16	0.6814	1.2002	0.9175	0.8728	3
17	0.6574	0.8950	0.9289	0.9612	2
18	0.6873	1.2426	0.8629	0.9700	2
19	0.4954	1.1657	0.8782	0.7767	4
20	0.6997	0.8237	0.6054	0.9383	4

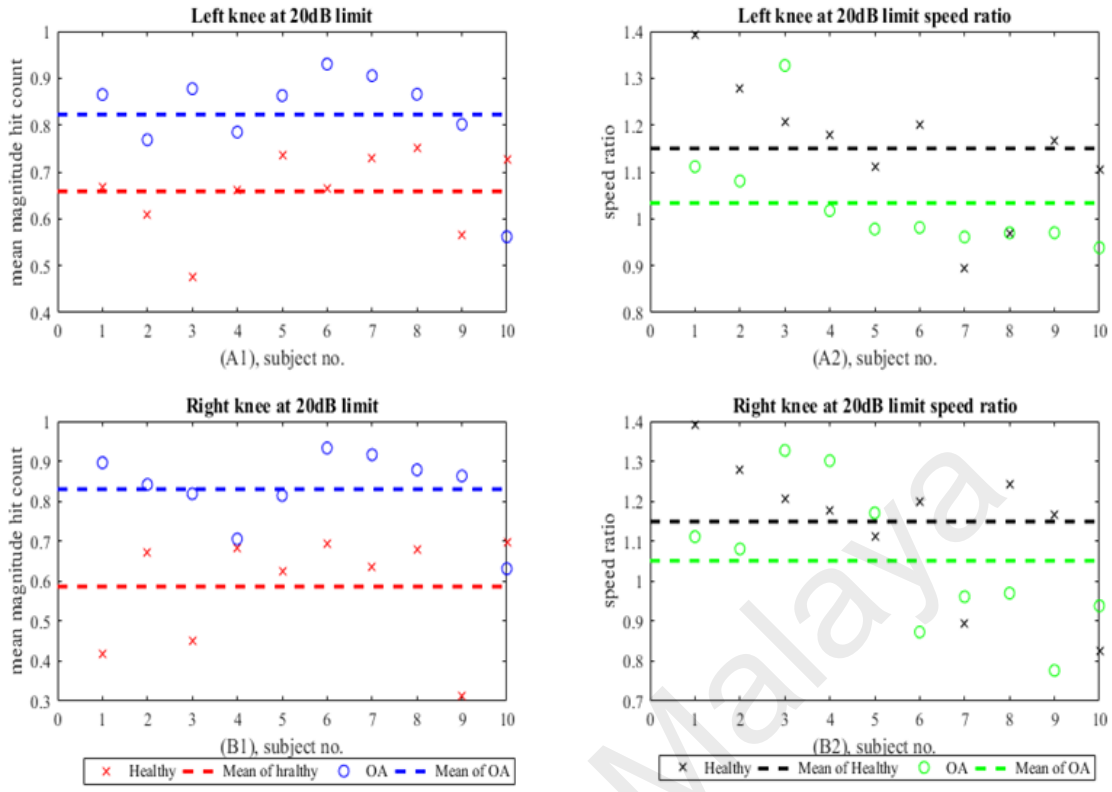

Figure 4.18: MHC of OA and healthy knee test group (A1 & B1); the sit-stand-sit test speed ratio of each subject (A2 & B2)

Based on Table 4.3, Figure 4.18, along with the OA and healthy knee MHC difference found in the 'control groups' (Figure 4.17), the MHC range limit was defined to identify the unique difference range limit between OA and healthy knees as shown in Table 4.4. By using the range limit, the overlap between OA and healthy MHC could be obtained and considered as error.

Table 4.4: MHC range of OA and healthy knee

type	Left MHC	Right MHC	No of error
OA	0.7587 to 0.8892	0.7066 to 0.9289	1
Healthy	0.4938 to 0.7425	0.4240 to 0.6997	3

The classification accuracy was calculated by evaluating the total number of overlaps. Classification accuracies of the left and right knees and the total classification accuracy are provided in Table 4.5. This study was able to achieve much higher

accuracy and reliability in comparison with previously conducted studies. The accuracy achieved was approved as a satisfactory limit by the UMMC physicians.

Table 4.5: Classification Accuracy

Type	Number of overlaps	Total number of samples	Accuracy
Left	2	40	95%
Right	3	40	90%
Total	5	80	92.5%

4.3 STAIR CLIMBING TEST

As it was explained earlier in section 3.4 the stair test faced many issues and during data acquisition stage, it was ignored as most data were corrupted. However, in future studies, a more comprehensive data acquisition using this method of testing may provide valuable results since the pressure on the knee is much higher while the subject climbs the stairs compared to the sit-stand-sit test. Figure 4.19 shows a sample of the raw VAG signal taken from an OA patient performing the stair test. As per every step the subject took, there was a sudden increase in x-axis magnitude particularly. This indicates that moving up or down the stairs is a one-direction movement of the knee which can put more pressure on specific points of knee joint.

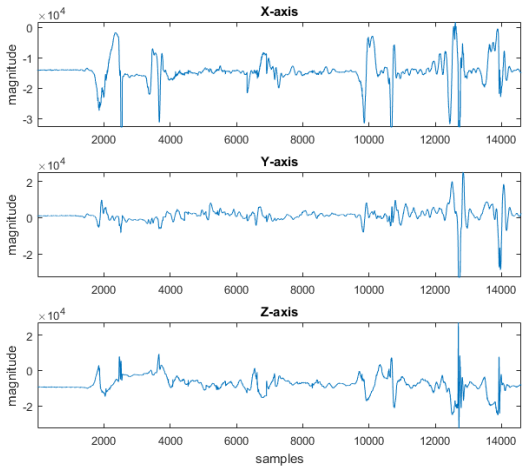

Figure 4.19: Sample of stair test done on an OA patient's left leg

4.4 SUMMARY

A feasibility study on the non-invasive detection of OA using triaxial accelerometer was administered in two versions of prototypes. The first version explored the possibility of using the accelerometer and method of testing on the patients while the second version improved upon the first stage and resolved all the issues on hardware, software, and signal processing.

The first stage used a single accelerometer mounted on a sensor band designed to be placed under the knee band. The modified knee band was then worn by the subjects. The subjects were then asked to perform the sit-stand-sit test. A signal analysis was done by filtering the signal and performing FFT. Overall, the final results of the first stage testing were unsatisfactory due to lack of information obtained from the signals and it could only achieve a classification accuracy of 86%.

For the second version, the testing participants were divided into the testing group or control group. Most of the signal analyses were done on the control group in order to obtain reliable results. Then, the same signal processing method was used on the testing group. Two accelerometers were used in the second test and each was placed on both knees to record the VAG signals of both knees simultaneously. To analyse the VAG signals, the STFT was used where it was filtered based on the subject's speed while performing the test. This method unveiled promising results with a total of 92.5% classification accuracy.

CHAPTER 5: CONCLUSION

Although many tests and research were done on feasibility study of non-invasive OA detection, this research took a Novel approach in detection OA by considering the both time domain and frequency domain and taking advantage of the human error. A unique testing method was introduced which opened many new opportunities for further research and discoveries.

Use of STFT in analysis of knee vibration using capacitive tri-axial accelerometer, exhibits great results in identifying and classifying the OA knee from healthy knee and proves the validity of the proposed method earlier. The cartilage on the knee joint provides smooth lubricated surface for the knee to move easily. This will cause vibration in low magnitude at lower frequencies; however, in OA knees the fluctuation and deformity of the knee bones will lead to much higher magnitude vibration frequencies at lower frequencies and vice versa. Past studies faced many issues regarding utilisation of knee vibration in detection of OA. Krishnan's research in year 2000 by using time and frequency modelling (TFDM) was only able to achieve 68% accuracy. Several other researches done as well could only achieve slightly higher accuracy rating. Following are the list of researches done and signal processing method used:

- Rangayyan et al., 2013, using Fractal analysis could achieve classification accuracy of 74.6%.
- Rangayyan et al., 1997, Using CC-RA could achieve classification accuracy of 75.6%.
- Umapathy et al., 2006, Using WPD-LDB could achieve classification accuracy of 76.4%.

- Cai et al., 2013, Using Matching pursuit could achieve classification accuracy of 88.76%.

This study has shown the utilization of this property in STFT is accurate (with accuracy of 92.5%) and applicable in non-invasive diagnosis of the knee OA. This study as well has shown higher magnitudes of the knee vibration frequency on the left knee in comparison with the right knee for both OA and healthy knees which marks the beginning of the development of the knee OA.

The method is not limited only to be applied on the knee OA. As most OAs carry the same property. Further developments in this field may help in non-invasive early detection of any type of OA as well as providing important information about characteristics of the OA for better treatment of the diseases.

5.1 FUTURE STUDIES

The discoveries in this research were just a mile stone for great and highly reliable non-invasive OA detection tool. Many more researches need to be dine in this field to consider all the possibilities.

Data mining is the most important step to create reliable database. By Following the explained testing method, more VAG samples must be collected categorised based on the main contributing factors to the OA. Such as categorisation based on weight and gender. Furthermore, this research can greatly take advantage of AI in OA pattern recognition to be used with large database.

In this research, not much attention was given to the stair climbing tests due to time constraints, However, even with limited data gathered, The OA knee major difference in frequency fluctuation compared to normal knee. More investigation in this area is needed to proof the feasibility of this testing method for non-invasive OA detection

REFERENCES

Abramson, S. B., & Yazici, Y. (2006). Biologics in development for rheumatoid arthritis: Relevance to osteoarthritis. *Advanced Drug Delivery Reviews, 58*(2), 212-225. doi:https://doi.org/10.1016/j.addr.2006.01.008

Abraham, A. M., Goff, I., Pearce, M. S., Francis, R. M., & Birrell, F. (2011). Reliability and validity of ultrasound imaging of features of knee osteoarthritis in the community. BMC Musculoskeletal Disorders, 12, 70. http://doi.org/10.1186/1471-2474-12-70

Al-Ghamd, A. M., & Mba, D. (2006). A comparative experimental study on the use of acoustic emission and vibration analysis for bearing defect identification and estimation of defect size. *Mechanical Systems and Signal Processing, 20*(7), 1537-1571. doi:https://doi.org/10.1016/j.ymssp.2004.10.013

Annette, W., Otto, R., & Lars, L. (2010). Surgery for knee osteoarthritis in younger patients. *Acta Orthopaedica, 81*(2), 161-164. doi:10.3109/17453670903413186

Atlas, S. J., & Deyo, R. A. (2001). Evaluating and Managing Acute Low Back Pain in the Primary Care Setting. *Journal of General Internal Medicine, 16*(2), 120-131. doi:10.1111/j.1525-1497.2001.91141.x

Baydar, N., & Ball, A. (2001). A comparative study of acoustic and vibration signals in detection of gear failures using wigner–ville distribution. *Mechanical Systems and Signal Processing, 15*(6), 1091-1107. doi:http://dx.doi.org/10.1006/mssp.2000.1338

Baydar, N., & Ball, A. (2003). Detection of gear failures via vibration and acoustic signals using wavelet transform. *Mechanical Systems and Signal Processing, 17*(4), 787-804. doi:http://dx.doi.org/10.1006/mssp.2001.1435

Brenner, G. A., Darby, S. (2004). Risk of cancer from diagnostic X-rays: estimates for the UK and 14 other countries. *Lancet,* 363(9406), 345-351. doi: 10.1016/s0140-6736(04)15433-0

Buckwalter, J. A. (2003). Sports, joint injury, and posttraumatic osteoarthritis. *J Orthop Sports Phys Ther, 33*(10), 578-588. doi:10.2519/jospt.2003.33.10.578

Callaghan, J. (2003). *The Adult Knee* (Vol. 1): Lippincott Williams & Wilkins.

Choudhury, A., & Tandon, N. (1998). A Theoretical Model to Predict Vibration Response of Rolling Bearings to Distributed Defects Under Radial Load. *Journal of Vibration and Acoustics, 120*(1), 214-220. doi:10.1115/1.2893808

Choudhury, A., & Tandon, N. (2000). Application of acoustic emission technique for the detection of defects in rolling element bearings. *Tribology International, 33*(1), 39-45. doi:https://doi.org/10.1016/S0301-679X(00)00012-8

Cohen, L. (1995). *Time-frequency analysis* (Vol. 778): Prentice Hall PTR Englewood Cliffs, NJ:.

Collins, J. E., Deshpande, B. R., Katz, J. N., & Losina, E. (2016). Race- and Sex-Specific Incidence Rates and Predictors of Total Knee Arthroplasty: Seven-Year Data From the Osteoarthritis Initiative. *Arthritis Care Res (Hoboken), 68*(7), 965-973. doi:10.1002/acr.22771

Cooper, C., Snow, S., McAlindon, T. E., Kellingray, S., Stuart, B., Coggon, D., & Dieppe, P. A. (2000). Risk factors for the incidence and progression of radiographic knee osteoarthritis. *Arthritis Rheum, 43*(5), 995-1000. doi:10.1002/1529-0131(200005)43:5<995::aid-anr6>3.0.co;2-1

Davis, J., Eaton, C. B., Lo, G. H., Lu, B., Price, L. L., McAlindon, T. E., Driban, J. B. (2017). Knee symptoms among adults at risk for accelerated knee osteoarthritis: data from the Osteoarthritis Initiative. *Clin Rheumatol, 36*(5), 1083-1089. doi:10.1007/s10067-017-3564-2

Eaton, C. B., Sayeed, M., Ameernaz, S., Roberts, M. B., Maynard, J. D., Driban, J. B., & McAlindon, T. E. (2017). Sex differences in the association of skin advanced glycation endproducts with knee osteoarthritis progression. *Arthritis Res Ther, 19*(1), 36. doi:10.1186/s13075-017-1226-z

Faisal, A., Ng, S.-C., Goh, S.-L., & Lai, K. W. (2017). Knee cartilage segmentation and thickness computation from ultrasound images. Med Biol Eng Comput. doi:10.1007/s11517-017-1710-2

Ferri, F. (2016). Ferri's Clinical Advisor 2016. *Osteoarthritis.* Retrieved from https://www.clinicalkey.com

Gelber, A. C., Hochberg, M. C., Mead, L. A., Wang, N. Y., Wigley, F. M., & Klag, M. J. (2000). Joint injury in young adults and risk for subsequent knee and hip osteoarthritis. *Ann Intern Med, 133*(5), 321-328.

Gray, H. (2000). *Anatomy of the human body*. New York: Bartleby.com,.

Hawker, G. A., Stewart, L., French, M. R., Cibere, J., Jordan, J. M., March, L., Gooberman-Hill, R. (2008). Understanding the pain experience in hip and knee osteoarthritis--an OARSI/OMERACT initiative. *Osteoarthritis Cartilage, 16*(4), 415-422. doi:10.1016/j.joca.2007.12.017

Hemelrijck, D., V., Busse, G., Solodov, I., & Anastasopoulos, A. (2008). *Emerging Technologies in NDT*: A.A. Balkema.

Hinterwimmer, S., Krammer, M., Krotz, M., Glaser, C., Baumgart, R., Reiser, M., & Eckstein, F. (2004). Cartilage atrophy in the knees of patients after seven weeks of partial load bearing. *Arthritis Rheum, 50*(8), 2516-2520. doi:10.1002/art.20378

Ismail, M. N., Chee, S. S., Nawawi, H., Yusoff, K., Lim, T. O., & James, W. P. (2002). Obesity in Malaysia. *Obes Rev, 3*(3), 203-208.

Kauffman, T. L., & Bolton, M. (2007). Chapter 16 - Muscle weakness and therapeutic exercise *Geriatric Rehabilitation Manual (Second Edition)* (pp. 107-113). Edinburgh: Churchill Livingstone.

Kellgren, J. H., & Lawrence, J. S. (1957). Radiological assessment of osteo-arthrosis. *Ann Rheum Dis, 16*(4), 494-502.

Krishnan, S., Rangayyan, R. M., Bell, G. D., & Frank, C. B. (2000). Adaptive time-frequency analysis of knee joint vibroarthrographic signals for noninvasive screening of articular cartilage pathology. *IEEE Trans Biomed Eng, 47*(6), 773-783. doi:10.1109/10.844228

Krishnan, S., Rangayyan, R. M., Bell, G. D., Frank, C. B., & Ladly, K. O. (1997). Adaptive filtering, modelling and classification of knee joint vibroarthrographic signals for non-invasive diagnosis of articular cartilage pathology. *Med Biol Eng Comput, 35*(6), 677-684.

Liu, K., Luo, X., Yang, S., Cai, S., Zheng, F., & Wu, Y. (2014). *Classification of knee joint vibroarthrographic signals using k-nearest neighbor algorithm.* Paper presented at the 2014 IEEE 27th Canadian Conference on Electrical and Computer Engineering (CCECE).

Mascaro, B., Prior, J., Shark, L. K., Selfe, J., Cole, P., & Goodacre, J. (2009). Exploratory study of a non-invasive method based on acoustic emission for assessing the dynamic integrity of knee joints. *Medical Engineering & Physics, 31*(8), 1013-1022. doi:http://dx.doi.org/10.1016/j.medengphy.2009.06.007

McCoy, G. F., McCrea, J. D., Beverland, D. E., Kernohan, W. G., & Mollan, R. A. (1987). Vibration arthrography as a diagnostic aid in diseases of the knee. A preliminary report. *J Bone Joint Surg Br, 69*(2), 288-293.

Park, H.-J., Kim, S. S., Lee, S.-Y., Park, N.-H., Park, J.-Y., Choi, Y.-J., & Jeon, H.-J. (2012). A practical MRI grading system for osteoarthritis of the knee: Association with Kellgren Lawrence radiographic scores. *European Journal of Radiology, 82*(1), 112-117. doi:10.1016/j.ejrad.2012.02.023

Peng, Z. K., & Chu, F. L. (2004). Application of the wavelet transform in machine condition monitoring and fault diagnostics: a review with bibliography. *Mechanical Systems and Signal Processing, 18*(2), 199-221. doi:https://doi.org/10.1016/S0888-3270(03)00075-X

PIPiezoTechonology. (2014). Piezoceramic Components. Retrieved from https://www.piceramic.com/en/products/piezoceramic-components/

Polikar, R. (2007). *The wavelet tutorial* (2 ed.). Rowan University.

Prior, J., Mascaro, B., Shark, L.-K., Stockdale, J., Selfe, J., Bury, R., Goodacre, J. A. (2010). Analysis of high frequency acoustic emission signals as a new approach for assessing knee osteoarthritis. *Ann Rheum Dis, 69*(5), 929-930. doi:10.1136/ard.2009.112599

Rabenda, V., Manette, C., Lemmens, R., Mariani, A. M., Struvay, N., & Reginster, J. Y. (2007). Prevalence and impact of osteoarthritis and osteoporosis on health-related quality of life among active subjects. *Aging Clin Exp Res, 19*(1), 55-60.

Rangayyan, R. M., Krishnan, S., Bell, G. D., Frank, C. B., & Ladly, K. O. (1997). Parametric representation and screening of knee joint vibroarthrographic signals. *IEEE Transactions on Biomedical Engineering, 44*(11), 1068-1074. doi:10.1109/10.641334

Rangayyan, R. M., & Yunfeng, W. (2008). *Screening of knee-joint vibroarthrographic signals using parameters of activity and radial-basis functions.* Paper presented at the 2008 Canadian Conference on Electrical and Computer Engineering.

Richards, J. (2008). *Biomechanics in Clinic and Research* (1st ed.): ELSEVIER.

Roemer, F. W., van Holsbeeck, M., & Genant, H. K. (2005). Musculoskeletal ultrasound in rheumatology: A radiologic perspective. *Arthritis Care & Research, 53*(4), 491-493. doi:10.1002/art.21318

Samson, D. J., Grant, M. D., Ratko, T. A., Bonnell, C. J., Ziegler, K. M., & Aronson, N. (2007). Treatment of primary and secondary osteoarthritis of the knee. *Evid Rep Technol Assess (Full Rep)*(157), 1-157.

Schiphof, D., Boers, M., & Bierma-Zeinstra, S. M. (2008). Differences in descriptions of Kellgren and Lawrence grades of knee osteoarthritis. *Ann Rheum Dis, 67*(7), 1034-1036. doi:10.1136/ard.2007.079020

Scruby, C. B. (1987). An introduction to acoustic emission. *Journal of Physics E: Scientific Instruments, 20*(8), 946.

Shark, L. K., Chen, H., & Goodacre, J. (2011). Knee acoustic emission: A potential biomarker for quantitative assessment of joint ageing and degeneration. *Medical Engineering & Physics, 33*(5), 534-545. doi:http://doi.org/10.1016/j.medengphy.2010.12.009

Sharma, L., Song, J., Felson, D. T., Cahue, S., Shamiyeh, E., & Dunlop, D. D. (2001). The role of knee alignment in disease progression and functional decline in knee osteoarthritis. *Jama, 286*(2), 188-195.

Song, J., Gilbert, A. L., Chang, R. W., Pellegrini, C. A., Ehrlich-Jones, L. S., Lee, J., Dunlop, D. D. (2017). Do Inactive Older Adults Who Increase Physical Activity Experience Less Disability: Evidence From the Osteoarthritis Initiative. *J Clin Rheumatol, 23*(1), 26-32. doi:10.1097/rhu.0000000000000473

Suszynski, M. (2016). Understanding Primary and Secondary Osteoarthritis. *Osteoarthritis.* Retrieved from http://www.everydayhealth.com/arthritis/osteoarthritis

Tamil, E. B. M., Kamarudin, N. H., Salleh, R., & Tamil, A. M. (2008). A Review on Feature Extraction & Classification Techniques for Biosignal Processing In N. A. Abu Osman, F. Ibrahim, W. A. B. Wan Abas, H. S. Abdul Rahman, & H.-N. Ting (Eds.), *4th Kuala Lumpur International Conference on Biomedical Engineering 2008: BIOMED 2008 25–28 June 2008 Kuala Lumpur, Malaysia* (pp. 107-112). Berlin, Heidelberg: Springer Berlin Heidelberg.

Tan, C. K., Irving, P., & Mba, D. (2007). A comparative experimental study on the diagnostic and prognostic capabilities of acoustics emission, vibration and spectrometric oil analysis for spur gears. *Mechanical Systems and Signal Processing, 21*(1), 208-233. doi:https://doi.org/10.1016/j.ymssp.2005.09.015

Tanaka, N., & Choudhury, A. (1999). A review of vibration and acoustic measurement methods for the detection of defects in rolling element bearings. *Tribology International, 32*(8), 469-480.

Tehranzadeh, J., Ashikyan, O., & Dascalos, J. (2003). Magnetic resonance imaging in early detection of rheumatoid arthritis. *Semin Musculoskelet Radiol, 7*(2), 79-94. doi:10.1055/s-2003-41342

Trebacz, H., & Zdunek, A. (2006). Three-point bending and acoustic emission study of adult rat femora after immobilization and free remobilization. *Journal of Biomechanics, 39*(2), 237-245. doi:10.1016/j.jbiomech.2004.10.040

Umapathy, K., & Krishnan, S. (2006). Modified local discriminant bases algorithm and its application in analysis of human knee joint vibration signals. *IEEE Transactions on Biomedical Engineering, 53*(3), 517-523. doi:10.1109/TBME.2005.869787

Veerapen, K., Wigley, R. D., & Valkenburg, H. (2007). Musculoskeletal pain in Malaysia: a COPCORD survey. *The Journal of Rheumatology, 34*(1), 207-213.

Wakefield, R. J., Kong, K. O., Conaghan, P. G., Brown, A. K., O'Connor, P. J., & Emery, P. (2003). The role of ultrasonography and magnetic resonance imaging in early rheumatoid arthritis. *Clin Exp Rheumatol, 21*(5 Suppl 31), S42-49.

Wang, S. Z., Huang, Y. P., Saarakkala, S., & Zheng, Y. P. (2010). Quantitative assessment of articular cartilage with morphologic, acoustic and mechanical properties obtained using high-frequency ultrasound. *Ultrasound Med Biol, 36*(3), 512-527. doi:10.1016/j.ultrasmedbio.2009.12.005

Wierzcholski, k., ch. (2006). Friction forces for human hip joint lubrication at a naturally permeable cartilage *Applied Mechanics and Engineering, 11*(3), 515-527.

Zhang, Y., & Jordan, J. M. (2010). Epidemiology of Osteoarthritis. *Clinics in Geriatric Medicine, 26*(3), 355-369. doi:https://doi.org/10.1016/j.cger.2010.03.001

LIST OF PUBLICATIONS AND PAPERS PRESENTED

Golshan, F., & Lai, K, W. (2017). Vibroarthrography difference between left and right knee on OA and Healthy knees, *presented 2nd International Conference for Innovation in Biomedical Engineering and Life Sciences*, Penang, KL: ICIBEL, 289-294.

Golshan, F., Lai, K, W., Sajadpoor, S., Hum, Y, C., Murphy, B, P., & Jaafar, Z. (2017). A new approach to non-invasive detection of osteoarthritis using capacitive tri-axial accelerometers, *JMIHI*